

Communications of the Byurakan Astrophysical Observatory

2

Erevan 2019

Introduction

Editorial Board*

This issue of the Communications of BAO is dedicated to the 90th anniversary of **Prof. Marat Arakelian** - one of the prominent Byurakan astronomers, the author of famous **Arakelian galaxies**, which at present are target for many-sided studies with ground-based and space telescopes.

M. Arakelian is known as a distinguished specialist in the theoretical astrophysics and extragalactic astronomy. He has compiled and published the Catalog of 621 high-surface-brightness galaxies, has proved the extragalactic origin of quasars, has determined the space density of extragalactic objects, has proposed several methods for study of properties of extragalactic objects, has made a comparative analysis of properties of different types of galaxies, and with his Russian colleagues spectroscopically has observed and studied some 800 faint galaxies and quasars. Arakelian galaxies have been observed in many observatories in the USA, UK, USSR, and elsewhere in optical wavelengths, radio and X-rays. Especially interesting objects are Akn 120 and Akn 564 (both are strongly variable AGN in X-ray and optical wavelengths; Akn 564 is a Narrow-Line Seyfert 1 galaxy that strongly changes the intensities of its emission lines).

In the occasion of the jubilee, the International Conference “Active Galaxies and Quasars” took place during on 9-10 September 2019 in the Byurakan Astrophysical Observatory. This issue includes the proceedings presented at the International Conference. All the papers passed relevant peer-review.

* combao@aras.am

Marat Arakelian: Life and Scientific Activity

A. M. Mickaelian*

NAS RA Byurakan Astrophysical Observatory (BAO), Byurakan 0213, Aragatzotn Province, Armenia

Abstract

We review the life and scientific activity of one of the outstanding Armenian astronomers Marat Arakelian (1929-1983). Arakelian was one of the prominent Byurakan astronomers, the author of famous Arakelian galaxies, which at present are target for many-sided studies with ground-based and space telescopes. Arakelian is known as a distinguished specialist in the theoretical astrophysics and extragalactic astronomy.

Keywords: *active galaxies, AGN, Starburst Galaxies, quasars, Seyfert galaxies, LINERs*

Introduction

Prof. Arakelian is one of the prominent Byurakan astronomers, the author of famous **Arakelian galaxies**, which at present are target for many-sided studies with ground-based and space telescopes. Arakelian is known as a distinguished specialist in the theoretical astrophysics and extragalactic astronomy.



Life and Activities

Marat Arsen Arakelian was born on January 15, 1929, in Goris, Armenia, USSR. He studied at the Physical-Mathematical Department of the Yerevan State University (YSU) and graduated from

*aregmick@yahoo.com, Corresponding author

it in 1951, among the first students specialized on Astrophysics. He was directed to the Byurakan Astrophysical Observatory (BAO), where he worked first as assistant astronomer, and later as junior research associate. Soon he became a postgraduate student at the Leningrad State University (LSU, presently, St. Petersburg), finished the studies in 1955, and in 1956 successfully passed his Ph.D. thesis “*Spectrophotometric investigation of Algol*” under the supervision of Prof. O.A. Melnikov at the LSU.

In 1957-1959 Arakelian combines his work with senior teacher position at the Department of Astrophysics of the YSU. From 1960 to 1966 he was a junior researcher and lectured at the LSU. He was awarded the title of Associate Professor. Later on, since 1966 Arakelian again works at BAO and combines his research with a position of a lecturer at the Department of Astrophysics of the YSU. In 1967, he became a senior researcher at BAO and headed an important direction in the extragalactic astronomy.

Since 1967, Arakelian completely devoted himself to the research work and during a short period performed a fantastic productivity for those times, publishing 62 papers in 1968-1983, and giving important scientific results in almost each of these works!

In 1977, Arakelian defended his second Doctoral Degree thesis “*Spectral observations and statistics of galaxies with active nuclei*” at the Moscow State University (MSU) and became a Doctor of Sciences.

Arakelian combined his scientific work with pedagogical one as well. In 1982 he was elected the Chair of the Department of Astrophysics and Theoretical Physics of the Armenian State Pedagogical Institute after Kh. Abovian. Together with L. V. Mirzoyan, A. T. Kalloghlian, and H. M. Tovmassian, he was the co-author of the textbook “*Astronomy*” for secondary schools (three editions in 1970, 1971, and 1973, in Armenian). Arakelian has written an extended review on Clusters of galaxies in the book “*Problems of extragalactic astronomy*” (1981).

Arakelian has published about 80 papers in various astrophysical journals, including such prestigious journals, as Nature, Astronomical Journal, and Astrophysical Journal (one of the rare Byurakan astronomers to publish a paper in Nature), as well as in proceedings of several international conferences. He was the editor of the two proceedings books of the Byurakan meetings: “*The Non-Stable Stars*” (1956) and the IAU Symp. #29 “*Non-Stable Phenomena in Galaxies*” (1966).

Since 1973, Arakelian was a member of the International Astronomical Union (IAU), Commission #28 “*Galaxies*”.

M. A. Arakelian passed away very early, at the age of 54 years on January 20, 1983, in Moscow, when he was at the period of prosperity of his scientific activity.

Scientific Results and Achievements

We give here the most important results and achievements by Marat Arakelian.

1968, Study of the luminosity function and the stellar space density in the Solar neighborhood. The results were published in *Astrophysics*.

1968-1969, Study of the luminosity evolution of quasars based on the evolutionary effects associated with them. The results were published in *Astrophysics* (Астрофизика, 2 papers in 1969-1970), in *Soviet Astronomical Circular* (Астрономический циркуляр), and a summary of these works was published in the prestigious journal *Nature* in 1970 (vol. 225, p. 358-359).

1969-1970, Statistical study of flare stars in the solar vicinity. The results were published in *Communications of the Konkoly Observatory*, *Communications of BAO*, and were reported at the conference “*Non-periodic phenomena in variable stars*” in 1969.

1970, Derivation of the luminosity function of field galaxies (together with A. T. Kalloghlian). The results were published in *Soviet Astronomy* (Астрономический журнал).

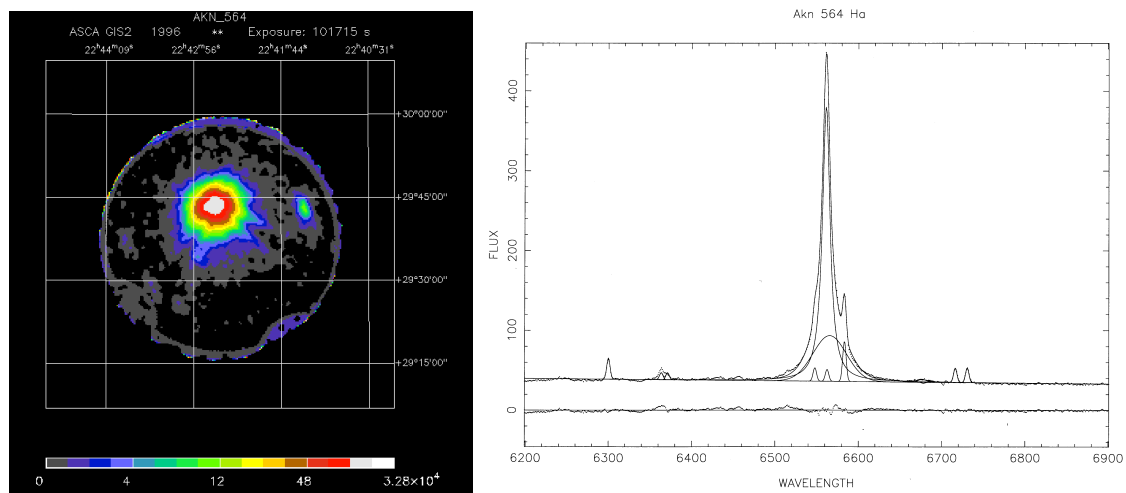
1970-1971, The proof of the extragalactic origin of quasars. The results were published in *Astrophysics* and *Вестник АН СССР* (*Bulletin of the USSR Acad. Sci.*).

1970-1973, Spectroscopic observations and studies of a few hundred Markarian galaxies and discovery of more than 40 new Seyferts among them (together with Russian astronomers E.A. Dibai and V.F. Esipov). The results were published in series of 8 papers in *Astrophysics* and 5 papers in the *Soviet Astronomical Circular*.

1972-1974, Analysis of the surface brightness of emission-line galaxies (including Seyfert and Markarian ones) and development of method for revealing galaxies with high surface brightness. The results were published in 3 papers in *Astrophysics*.

1973, Suggestion of a new method for definition of space density of extragalactic objects and estimation of the mean density of matter in the Metagalaxy. The results were published in *Astrophysics*.

1975, Compilation and publication of the catalogue of “Galaxies of high surface brightness” (named **Arakelian galaxies**, Akn), a list of 621 objects with surface brightness at least 22.0 magnitudes from an area of 1 sq. arcsec. The sample contained 4% of all galaxies in an area of with $\delta > -3^\circ$ and $|b| > 20^\circ$. Arakelian catalog became a source for many new AGN (*Communications of BAO, No. 47, p. 3-42, 1975*).



1975, Derivations of the luminosity function and space density of galaxies with UV continuum (Markarian galaxies). The results were published in *Soviet Astronomy*.

1975-1976, Spectroscopic observations and studies of Arakelian galaxies (galaxies with high surface brightness) and discovery of new Seyferts among them (together with E. A. Dibai and V. F. Esipov). The results were published in a series of 4 papers in *Astrophysics*, a paper in the *Soviet Astronomical Circular*, and were reported in the meeting “Stars and galaxies from observational points of view” in 1975.

1976-1977, Study of the dependence of the emission-line intensities of Markarian and Seyfert galaxies on their color index. The results were published in 2 papers in *Astrophysics*.

1977, Study of the distribution of the mean surface brightness of galaxies in the Coma cluster. The results were published in *Astrophysics*.

1977-1980, Study of the relation between the mean surface brightness and radio emission of galaxies, including Seyfert galaxies (together with R. A. Kandalyan). The results were published in 2 papers in *Astrophysics*.

1981, Study of the estimations of the kinetic energies of clusters of galaxies; the extent to which a kinetic energy estimate would be affected by a possible mass dependence of the velocity dispersion of galaxies in clusters was considered. It was concluded that in some cases the kinetic energy might be underestimated (together with A. G. Kritsuk). The results were published in *Astrophysics*.

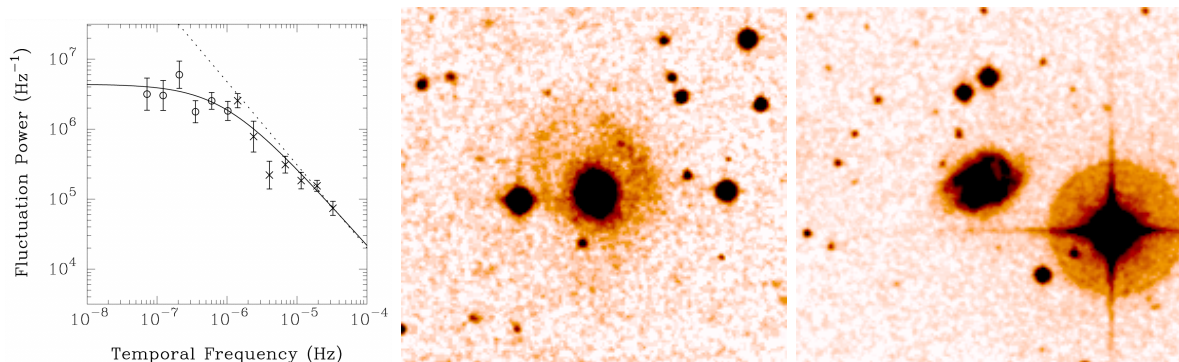
1980-1981, Radio (6cm) observations of Arakelian galaxies and publication of their accurate positions (together with USA astronomers G. Kojoian, D. F. Dickinson, R. Elliott, M. D. Bica). The results were published in the *Astronomical Journal*.

1981-1982, Comparative study and statistics of the surface brightness and morphological types of isolated and double galaxies (together with A. P. Mahtessian). The results were published in 2 papers in *Astrophysics*.

1981-1982, Study of Seyfert galaxies in clusters and Seyfert properties of the cluster galaxies (together with V. Yu. Terebizh). The results were published in the *Soviet Astronomical Circular* and *Soviet Astronomy Letters* (*Письма в Астрономический журнал*).

1983, Proposing a method for construction of the luminosity function of the components of double galaxies on the basis of an arbitrary sample of pairs of galaxies. The results were applied to the data of Karachentsev's Catalog of Isolated Pairs. The presence of a correlation between the absolute magnitudes of the components of pairs was confirmed. The results were published in *Astrophysics*.

1986, A method for the determination of the bivariate luminosity function utilizing an incomplete sample with an application to Seyfert galaxies. It was shown that the results of incomplete radio and X-ray surveys could be used for the determination of the bivariate luminosity functions, having both the distribution of luminosities of objects in the detected subsample and the distribution of apparent magnitudes in the surveyed sample. A paper was published in *Astrophysical Journal* after Arakelian's death.



Chronology of Marat Arakelian's life and activity

1929	Marat Arsen Arakelian was born on January 15 in Goris, Armenia, USSR
1946-1951	studies at the Phys.-Math. Department of the Yerevan State University (YSU)
1951	starting working at the Byurakan Astrophysical Observatory (BAO) (first as assistant astronomer, and later as junior research associate)
1953-1955	postgraduate student at the Leningrad State University (LSU)
1956	Ph.D. thesis " <i>Spectrophotometric investigation of Algol</i> " (supervisor: Prof. O. A. Melnikov)
1957-1959	senior teacher at the Department of Astrophysics of the YSU
1960-1966	junior researcher and lecturer at the LSU
1965:	Associate Professor at the LSU
1966-1983	work at BAO and lecturer at the Department of Astrophysics of the YSU
1967	senior researcher at BAO, head of a group
1968-1969	study of the luminosity evolution of quasars, a paper in <i>Nature</i> in 1970
1970-1971	the proof of the extragalactic origin of quasars
1970-1973	spectroscopic observations and studies of a few hundred Markarian galaxies (<i>together with E. A. Dibai and V. F. Esipov</i>)

1973	suggestion of a new method for definition of space density of extragalactic objects and estimation of the mean density of matter in the Metagalaxy
1973	member of the International Astronomical Union (IAU), Commission #28 "Galaxies"
1975	compilation and publication of the catalogue of "Galaxies of high surface brightness" (named <i>Arakelian</i> galaxies, Akn), a list of 621 objects
1975-1976	spectroscopic observations and studies of <i>Arakelian</i> galaxies (<i>together with E. A. Dibai and V. F. Esipov</i>)
1977	Doctoral thesis " <i>Spectral observations and statistics of galaxies with active nuclei</i> " at the Moscow State University (MSU)
1982	Chair of the Department of Astrophysics and Theoretical Physics of the Armenian State Pedagogical Institute after Kh. Abovian
1983	proposing a method for construction of the luminosity function of the components of double galaxies on the basis of an arbitrary sample of pairs of galaxies
1983	M. A. Arakelian passed away on January 20 in Moscow

Summary of publications

Here we give the summary of Marat Arakelian's all publications by journals or other editions, including the numbers and years. In total, there should be 76 publications, however some are missing in the list. Most important journals and editions are in bold.

Journal / edition	Number of publications	Years
Nature	2	1968, 1970
Astronomical Journal (AJ)	1	1981
Astrophysical Journal (ApJ)	1	1986
Astronomy Reports (Астрон. Ж.)	4	1959-1975
Astronomy Letters (ПАЖ)	2	1982
Reports USSR Acad. Sci., Series: Physics (ДАН СССР, серия Физика)	1	1968
Astrophysics (Астрофизика)	31	1968-1983
Bull. USSR Acad. Sci. (Вестник АН СССР)	2	1969, 1971
Communications of BAO	3	1970-1975
Communications of Konkoly Obs.	1	1969
Astronomical Circular (Астрон. Циркуляр)	8	1970-1981
BAAS	2	1980-1981
Proceedings of meetings	3	1969, 1976, 1978
Theses (PhD, Doctoral)	2	1956, 1977
Astronomy textbooks (in Armenian)	3	1970, 1971, 1973
Clusters of Galaxies (in Book)	1	1981
Editing of Proc. of Byurakan Symposia	2	1956, 1966
Total	69	1956-1986

Summary

Arakelian has compiled and published the catalog of 621 high-surface-brightness galaxies, has proved the extragalactic origin of quasars, has determined the space density of extragalactic objects, has proposed several methods for study of properties of extragalactic objects, has made a comparative analysis of properties of different types of galaxies, and with his Russian colleagues spectroscopically has observed and studied some 800 faint galaxies and quasars. Arakelian galaxies have been observed in many observatories in the USA, UK, USSR, and elsewhere in optical wavelengths, radio and X-rays. Especially interesting objects are Akn 120 and Akn 564 (both are strongly variable AGN in X-ray and optical wavelengths; Akn 564 is a Narrow-Line Seyfert 1 galaxy that strongly changes the intensities of its emission lines).

Many Arakelian galaxies are AGN or Starbursts and entered the Véron-Cetty & Véron (2010) catalogue, as well as many are X-ray sources and have been detected by ROSAT (Voges et al. 1999, 2000), and many are radio sources and have been detected by NVSS (Condon et al. 1998), FIRST (Helfand et al. 2015) and other surveys. Many spectra of Arakelian galaxies have been observed by SDSS (Aguado et al. 2019) and are subject of appropriate classification for activity types.

References

- Aguado D. S., Romina A., Andrés A., et al. 2019, ApJS, 240, id. 23
- Condon J., Cotton W., Greisen E., et al. 1998, AJ, 115, 1693
- Helfand D. J., White R., Becker R. H., 2015, ApJ, 801, id. 26
- Véron-Cetty M. P., Véron P., 2010, A&A, 518, A10
- Voges W., Aschenbach B., Boller T., et al. 1999, A&A, 349, 389
- Voges W., Aschenbach B., Boller T., et al. 2000, MPE, Garching. The ROSAT Faint Source Catalogue

List of research papers by Marat Arakelian (1956-1986)

- Arakelian, M. A. 1956, Spectrophotometric investigation of Algol, PhD Thesis
- Dolidze, M. V.; Arakelyan, M. A. 1959, The T-Association Near ρ Ophiuchi, SvA 3, 434 (AZh 36, 444)
- Arakelian, M. A. 1961, Application of the Probability Method to the Determination of Absorption - Line Profiles, SvA 4, 945 (AZh 37, 1012)
- Arakelian, M. A. 1968, Determining the Luminosity Function and Star Density in the Neighborhood of the Sun, PhD Thesis 13, 190
- Arakelian, M. A. 1968, Luminosity function and stellar density in the neighborhood of the Sun, Ap 4, 256 (Afz 4, 617)
- Arakelian, M. A. 1968, Distances, Space Distribution and Luminosity Function of Quasi-stellar Objects, Nature 219, 595
- Arakelian, M. A. 1969, Curve of growth for an expanding atmosphere, Ap 5, 32 (Afz 5, 75)
- Arakelian, M. A. 1969, Evolutionary effects associated with quasi-stellar radio sources. I, Ap 5, 226 (Afz 5, 461)
- Arakelian, M. A. 1969, Nature of evolutionary effects connected with quasi-stellar radio sources. II, Ap 5, 308 (Afz 5, 603)
- Arakelian, M. A.; Kalloglyan, A. T. 1970, The Luminosity Function of Field Galaxies, SvA 13, 953 (AZh 46, 1215, 1969)
- Arakelian, M. A.; Ivanov, V. V.; Tovmasyan, G. M. 1969, Physics of stars, nebulae and galaxies (Symposium at Byurakan, 1968 Sep 16-20), VeSSR 3, 125
- Arakelian, M. A.; Dibai, E. A.; Esipov, V. F. 1970, Spectra of Markarian galaxies. I, Ap 6, 14 (Afz 6, 39)
- Arakelian, M. A.; Dibai, E. A.; Esipov, V. F.; Markaryan, B. E. 1970, Spectra of Markarian galaxies. II, Ap 6, 189 (Afz 6, 357)

- Arakelian, M. A. 1970, The spatial distribution and luminosity function for quasistellar radio sources, *Ap* 6, 291 (Afz 6, 531)
- Arakelian, M. A. 1970, Evolution of the luminosity of quasars, *ATsir* 552, 1
- Arakelian, M. A.; Dibaj, Eh. A.; Esipov, V. F.; Markarian, B. E. 1970, New Seyfert-type objects in the second Markarian's list, *ATsir* 568, 1
- Arakelian, M. A.; Dibaj, Eh. A.; Esipov, V. F.; Markarian, B. E. 1970, New Seyfert-type objects in the third Markarian's list, *ATsir* 568, 2
- Arakelian, M. A. 1970, Evidence of Radio Luminosity Evolution of Quasi-stellar Radio Sources, *Nature* 225, 358
- Arakelian, M. A. 1970, On the statistics of flare stars in the solar vicinity, *SoByu* 41, 56
- Arakelian, M. A. 1971, On the distances of quasi-stellar radio sources, *VeSSR* 11, 26
- Arakelian, M. A.; Dibai, E. A.; Esipov, V. F.; Markaryan, B. E. 1971, Spectra of Markarian galaxies. III, *Ap* 7, 102 (Afz 7, 177)
- Arakelian, M. A. 1971, Quasistellar radio sources and optical quasistellar objects, *Ap* 7, 269 (Afz 7, 457)
- Arakelian, M. A.; Dibai, E. A.; Esipov, V. F. 1972, Spectra of Markarian galaxies. IV, *Ap* 8, 17 (Afz 8, 33)
- Arakelian, M. A.; Dibai, E. A.; Esipov, V. F. 1972, Spectra of Markarian galaxies. V, *Ap* 8, 106 (Afz 8, 177)
- Arakelian, M. A.; Dibai, E. A.; Esipov, V. F. 1972, Spectra of Markarian galaxies. VI, *Ap* 8, 197 (Afz 8, 329)
- Arakelian, M. A. 1972, Estimates of the surface brightness of selected Markarian galaxies. I, *Afz* 8, 473
- Arakelian, M. A. 1972, Relationship between the gradient of the surface brightness and other characteristics of Seyfert galaxies, *Ap* 8, 368 (Afz 8, 624)
- Arakelian, M. A.; Dibaj, Eh. A.; Esipov, V. F. 1972, On the spectrum of the Markarian galaxy 388, *ATsir* 717, 7
- Arakelian, M. A.; Dibaj, Eh. A.; Esipov, V. F. 1972, New Seyfert-type objects from the IIIrd and IVth lists of galaxies with UV-continuum, *ATsir* 722, 3
- Arakelian, M. A. 1973, Estimate of the mean density of matter in the Metagalaxy, *Ap* 9, 84 (Afz 9, 151)
- Arakelian, M. A.; Dibai, E. A.; Esipov, V. F. 1973, Spectra of Markaryan galaxies. VII, *Ap* 9, 180 (Afz 9, 319)
- Arakelian, M. A.; Dibai, E. A.; Esipov, V. F. 1973, Spectra of Markaryan galaxies. VIII, *Ap* 9, 183 (Afz 9, 325)
- Arakelian, M. A. 1974, Surface brightness of galaxies with emission lines, *Ap* 10, 321 (Afz 10, 507)
- Arakelian, M. A. 1975, Luminosity function and space density of galaxies with an ultraviolet continuum, *SvA* 18, 432 (*AZh* 51, 730, 1974)
- Arakelian, M. A. 1975, Galaxies of high surface brightness, *SoByu* 47, 3

- Arakelian, M. A. 1975, Classification of the Central Regions of 711 Galaxies, SoByu 47, 43
- Arakelian, M. A.; Dibai, E. A.; Esipov, V. F. 1975, Spectral observations of galaxies with high surface brightness. I, Ap 11, 8 (Afz 11, 15)
- Arakelian, M. A.; Dibai, E. A.; Esipov, V. F. 1975, Spectral observations of galaxies with high surface brightness. II, Ap 11, 254 (Afz 11, 377)
- Arakelyan, M. A.; Dibai, E. A.; Esipov, V. F. 1976, Spectral observations of high-surface-brightness galaxies. III, Ap 12, 122 (Afz 12, 195)
- Arakelian, M. A. 1976, Dependence of the emission-line intensity of Markaryan galaxies on color index, Ap 12, 366 (Afz 12, 559)
- Arakelian, M. A.; Dibai, E. A.; Esipov, V. F. 1976, Spectral observations of high-surface-brightness galaxies. IV, Ap 12, 456 (Afz 12, 683)
- Arakelian, M. A.; Dibaj, Eh. A.; Esipov, V. F. 1976, New Seyfert-type objects, ATsir 914, 7
- Arakelian, M. A. 1976, Some results of spectral observations of galaxies of high surface brightness, sgov meet 297
- Arakelian, M. A. 1977, Mean surface brightness and radio emission of galaxies, Ap 13, 130 (Afz 13, 245)
- Arakelian, M. A. 1977, Dependence of the emission line intensities of Seyfert galaxies on the color index, Ap 13, 241 (Afz 13, 427)
- Arakelian, M. A. 1977, The distribution of the mean surface brightnesses of galaxies in the Coma cluster, Ap 13, 386 (Afz 13, 651)
- Arakelian, M. A. 1978, Markarian Galaxies in the Vicinity of the Coma Cluster, IAU S79, 274
- Kojoian, G.; Dickinson, D. F.; Arakelian, M. A. 1980, Centimeter Wavelength Observations of Arakelian Galaxies, BAAS 12, 822
- Arakelian, M. A.; Kandalyan, R. A. 1980, Mean Surface Brightnesses and Radio Emission of Seyfert Galaxies, Ap 16, 383 (Afz 16, 663)
- Arakelian, M. A.; Magtesyan, A. P. 1981, Mean Surface Brightnesses of Isolated and Double Galaxies, Ap 17, 28 (Afz 17, 53)
- Arakelian, M. A.; Terebizh, V. Y. 1981, Seyfert Galaxies in the Abell Cluster, ATsir 1188, 1
- Arakelian, M. A. 1981, III. Clusters of galaxies, pea conf 83
- Kojoian, G.; Dickinson, D.; Arakelian, M. A.; Bica, M. D. 1981, Six-Centimeter Survey of Arakelian Galaxies, BAAS 13, 522
- Kojoian, G.; Elliott, R.; Bica, M. D.; Arakelian, M. A. 1981, Accurate optical positions of Arakelian galaxies, AJ 86, 820
- Arakelian, M. A.; Kritsuk, A. G. 1981, On estimating the kinetic energies of clusters of galaxies, Ap 17, 384 (Afz 17, 709)
- Arakelian, M. A.; Terebizh, V. Iu. 1982, Cluster galaxies with Seyfert properties, SvAL 8, 72
- Arakelian, M. A.; Magtesyan, A. P. 1982, Spectrophotometry of Four Galaxies of High Surface Brightness, SvAL 8, 181 (PAZh 8, 334)
- Arakelian, M. A. 1983, Statistics of morphological types of isolated galaxies and components of pairs, Ap 19, 375 (Afz 19, 665)

Arakelian, M. A. 1983, Distribution of apparent magnitudes and luminosities of double galaxies, ApJ 19, 379 (Afz 19, 673)

Arakelian, M. A. 1986, A Proposed Method for the Determination of the Bivariate Luminosity Function Utilizing an Incomplete Sample with an Application to Seyfert Galaxies, ApJ 301, 92

BL Lacertae Objects: A Short Review

B. Kapanadze^{*1,2,3}

¹Ilia State University, Colokashvili Av. 3/5, Tbilisi, Georgia, 0162

²E. Kharadze National Astrophysical Observatory, Mt.Kanobili, Abastumani, Georgia, 0803

³INAF, Osservatorio Astronomico di Brera, Via E. Bianchi 46, 23807 Merate, Italy

Abstract

BL Lacertae objects (BLLs) constitute a class of active galactic nuclei (AGNs) with extreme observational features explained by non-thermal radiation from a relativistic jet nearly pointed along the observer's line-of-sight. Their spectral energy distribution (SED), extending over 17-19 orders of the frequency, is of non-thermal origin and shows a typical two-humped structure. The lower-energy component, ranging from the radio to X-rays, is explained via synchrotron radiation emitted by ultra-relativistic electrons/positrons/protons, to be initially accelerated via the Blandford-Znajek mechanism or magneto-hydrodynamic processes in the vicinity of a central supermassive black hole. Afterwards, the particles should undergo further acceleration to ultra-relativistic energies by means of different mechanisms (first and second-order Fermi processes, relativistic magnetic reconnection, shear acceleration, jet-star interaction etc.) locally, in the jet emission zone. Our intensive X-ray spectral study of TeV-detected, high-energy-peaked BLLs (HBLs) often show the signatures of an effective second-order Fermi (stochastic) acceleration close to the shock front, while the processes related to the first-order Fermi acceleration are relatively rarely presented. The TeV-undetected HBLs and low-energy-peaked BLLs (LBLs) mostly do not show the signatures of efficient stochastic acceleration in their jets. Concerning the higher-energy component, the most frequently considered scenario incorporates an inverse Compton (IC) scattering of synchrotron photons by their "parent" electron-positron population (synchrotron self-Compton model, SSC). However, this simple scenario sometimes is challenged by uncorrelated X-ray and TeV variability, more easily explained by multizone SSC, external Compton (EC) and hadronic scenarios.

Keywords: (*galaxies:*) *BL Lacertae objects: general*

1. INTRODUCTION

Galaxies are generally divided into active and inactive, depending on the appearance of a central "engine". Active galactic Nuclei (AGNs), one of the most luminous sources in the universe, are galaxies with a strong and variable non-thermal emission, believed to be the result of accretion of mass onto a supermassive black hole lying in the center of the galaxy. They present unique observational signatures that cover the full electromagnetic spectrum over 15–19 of magnitude in frequency. The origin, internal structure and the nature of physical processes underlying the observed properties of AGN are among of the open problems in astrophysics.

AGNs are characterized by a rich phenomenology and, consequently, they are divided into several classes:

- Quasars
- Seyfert galaxies
- Radio galaxies
- Blazars

*bidzina.kapanadze@iliauni.edu.ge

Table 1. Major blazar monitoring programs and samples

Program/Sample (1)	Frequencies/Bands (2)	Homepage (3)
Swift-XRT	X-ray 0.3-10 keV	http://www.swift.psu.edu/monitoring/
Swift-BAT	X-ray/ γ -ray 15-150 keV	https://swift.gsfc.nasa.gov/results/transients/
Swift-UVOT	optical-UV	https://www.swift.ac.uk/analysis/uvot/
Fermi-LAT	100 MeV–300 GeV	http://www.asdc.asi.it/fermi3fgl/
FACT	TeV	http://www.fact-project.org/
TUORLA	Optical R -band	http://users.utu.fi/kani/1m/index.html
OVRO	15 GHz	http://www.astro.caltech.edu/ovroblazars/
UMRAO	4.8, 8, 15 GHz	https://dept.astro.lsa.umich.edu/datasets/umrao.php
STEWART	Optical	http://james.as.arizona.edu/~psmith/Fermi/
SMARTS	Optical	http://www.astro.yale.edu/smarts/glast/
MAXI	X-ray 2–20 keV	http://maxi.riken.jp/top/index.html
RXTE-ASM	X-ray 1.5–12 keV	http://xte.mit.edu/ASM_lc.html
RXTE-PCA	X-ray 2–60 keV	https://heasarc.gsfc.nasa.gov/docs/xte/learning_center/pca.html
PERKINS	Optical	https://www.bu.edu/blazars/VLBaproject.html
GASP/WEBT	Optical	http://www.oato.inaf.it/blazars/webt/
CATALINA SKY SURVEY	Optical	http://nesssi.cacr.caltech.edu/catalina/Blazars/Blazar.html
MOJAVE	15 GHz	http://www.physics.purdue.edu/MOJAVE/allsources.html
KAIT	Optical	http://brando.astro.berkeley.edu/kait/agn/
ROBOPOL	Optical	http://robopol.org/
POLIMA	Optical	http://www.astrossp.unam.mx/blazars/
KANATA	Optical	http://adsabs.harvard.edu/abs/2011PASJ...63..639I
TeV CAT	TeV	http://tevcad.uchicago.edu/
TANAMI	8.4, 22GHz	http://pulsar.sternwarte.uni-erlangen.de/tanami
F-GAMMA	2-200GHz, IR, optical	http://www.mpifr-bonn.mpg.de/div/vlbi/fgamma/fgamma.html
METSAHOVI	22, 37 GHz	http://www.metsahovi.fi/quasar/
MARMOT	86 GHz, optical	http://www.astro.caltech.edu/marmot
SMA Calibrator Database	86, 300, 350 GHz	http://sma1.sma.hawaii.edu/callist/callist.html
ALMA Calibrator Database	90, 100, 230,340 GHz	https://almascience.eso.org/alma-data/calibrator-catalogue

- Quasi-stellar objects

Blazars form the most violently variable class of active galactic nuclei (AGNs), with timescales ranging from a few minutes (in the keV–TeV energy range) to several years (radio to optical frequencies), variable radio–optical polarization, compact radio-structure and superluminal motion of some components and very broad continuum extending over the radio to the very high-energy (VHE, $E > 100$ GeV) γ -ray energy ranges. Moreover, the bolometric luminosity occasionally can reach a level of 10^{48} ergs $^{-1}$ during the strong outbursts (see Falomo & et al. (2014)). Blazars are divided into two sub-classes:

- BL Lacertae Objects (BLLs)
- Flat-spectrum radio quasars (FSRQs)

Additionally, BL Lacertae sources (BLLs) are characterized by featureless spectra, to be produced by a beamed non-thermal emission of the relativistic jet pointed to the observer. The prototype of these sources, BL Lacertae ($\alpha=22^h02^m43.29^s$, $\delta=+42^\circ16'39.98''$ (2000)) was originally discovered and classified as an irregularly variable star by Hoffmeister (1929). After almost 40 years, its counterpart was detected by MacLeod & Andrew (1968). There were the detections of similar objects with high optical polarization, high variability and featureless, power law-shaped optical spectral continuum next years. This led to the recognition of a separate group of the extragalactic objects hosted by elliptical galaxies and sharing some characteristics of quasars (Strittmatter & et al. (1972)). The observational peculiarities of BLLs was later included in the coherent picture that foresees a relativistic jet viewed at a small angle as the main responsibility of all multi-wavelength BLL characteristics (Blandford & Rees (1978) and references therein).

In this paper, we review some observations properties of BLLs provide the discussion about the underlying physical mechanisms. In Section 2, we list the basic major monitoring programs and catalogues, containing BLLs. The spectral energy distribution and emission mechanisms are described in Section 3. The statistics of BLL redshifts are provided in Section 4. The internal BLL structure and superluminal motions are treated in Section 5. Section 6 is devoted to the X-ray spectra and particle

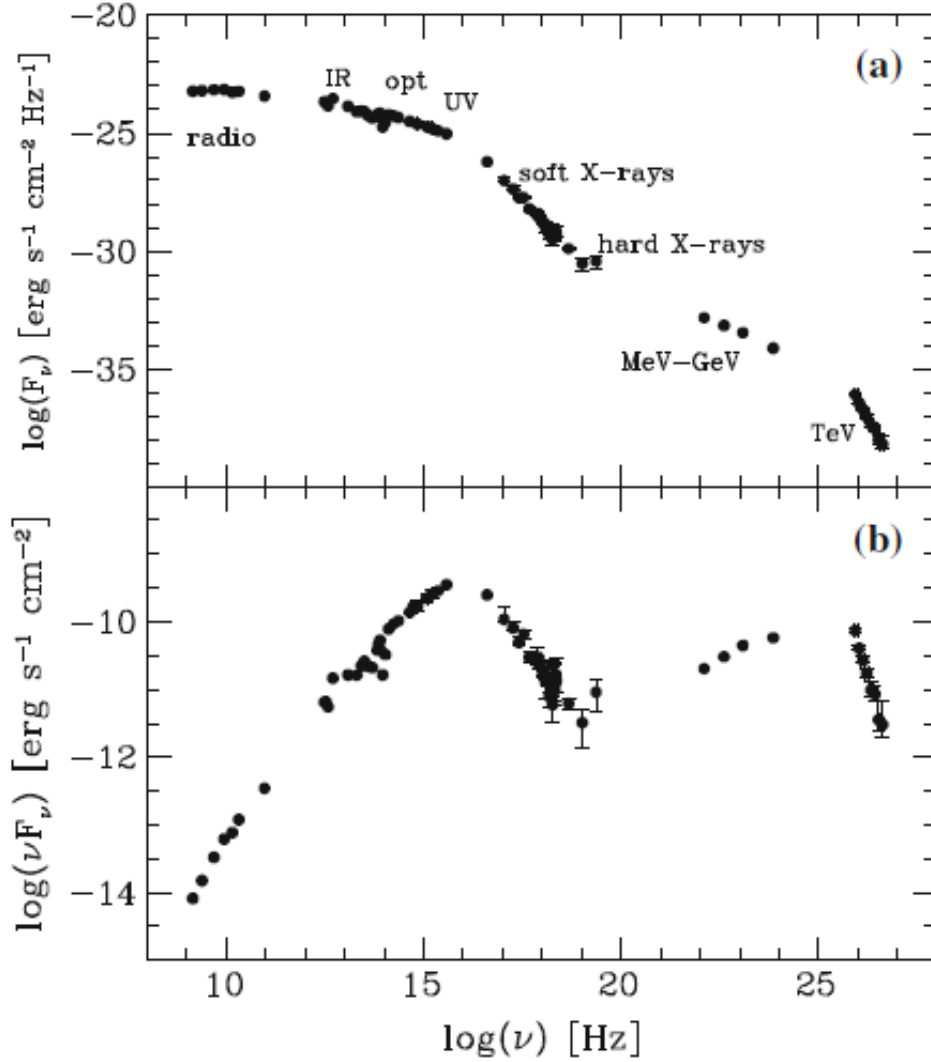


Figure 1. Broad-band spectrum of PKS 2155-304 ($z=0.116$) in the $\log \nu$ - F_ν (panel(a)) and $\log \nu$ - $\log \nu F_\nu$ (panel (b)) representations (adapted from Treves et al. 2014). The latter emphasizes the frequencies at which most of the power is emitted.

acceleration processes in BLL jets. Finally, the flux variability of BLLs are discussed in Section 7, and give the summary of our review in Section 8.

2. Catalogues and Major Monitoring Programmes

There is a number of the Multifrequency (MWL) catalogues and surveys which contain BLLs. Namely,

- Roma BZCAT – Multi-frequency Catalogue of Blazars, 5th edition (Massaro & et al. (2015))
- 4FGL – the fourth Fermi Large Area Telescope catalog of gamma-ray sources (Abdollahi & et al (2019); previous versions: 1FHL, 2FHL, 3FHL, 1FGL, 2FGL, 3FGL)
- Veroncat – Veron Catalog of Quasars and AGN, 13th Edition; contains 133336 quasars, 1374 BLLs objects and 34231 other AGNs (Veron-Cetty & Veron (2010))
- 1ES – Einstein Slew Survey (0.1-2 keV, 1992; previous versions: 1E, 2E; (Elvis et al. 1992): a catalog of 819 sources detected within the *Einstein Slew Survey* program of the X-ray sky.

- Gaia – Catalogue of Gaia Sources (Evans et al. 2018, optical G-band, the second release)
- PBC – Palermo Swift-BAT hard X-ray catalogue obtained from the analysis of data acquired during the first 39 months of the Swift mission (15-150 keV energy range, Cusumano & et al. (2010))
- 1RXS – ROSAT All-Sky Survey Bright Source Catalogue derived from the all-sky survey performed during the first half year (1990/91) of the ROSAT mission (Voges & et al. (1999); previous versions: RBS, RX, 2RE)
- PKS — Parkes Survey of Southern Radio Sources, containing the 8400 MHz flux densities for 1194 southern radio sources (Wright & et al. (1991))
- 10C – the 10th Cambridge Survey (10C) of radio-sources at 15.7 GHz using the Arcminute Microkelvin Imager Large Array, operated by the Cavendish Astrophysics Group at the University of Cambridge (Davies et al. 2011; previous versions: 1C-9C)
- SHBL – the multi-frequency sedentary survey is a flux-limited, statistically well-defined sample of highly X-ray dominated BLLs, which includes 150 sources (Giommi & et al. (2005))
- 2XMM – Second XMM-Newton X-ray source catalogue (0.1-12 keV, 2009; <https://xmmssc-www.star.le.ac.uk/Catalogue/2XMM/>; previous version: XMMSL1)
- EGR – a catalog of point γ -ray sources detected by the EGRET detector on the Compton Gamma Ray Observatory (Casandjian & Grenier (2008))
- PG — Palomar-Green Catalogue: a large area CCD survey for low surface brightness galaxies (Gregory & et al. (1996))
- GB6 — 6th Green Bank Catalogue compiled by means of the Green Bank 4.85 GHz survey performed with the NRAO seven-beam receiver on the 91-m telescope during 1986 November and 1987 October (Gregory & et al. (1996); previous versions: GB1–GB5, 87GB)
- 1H – the catalog of X-ray sources detected during the NRL Large Area Sky Survey (LASS) with the HEAO-1 satellite (Wood & et al. (1984)).
- TXS – Texas survey of discrete radio sources between -35.5 deg and 71.5 deg declination, which was carried out at 365 MHz with the Texas Interferometer during 1974–1983 (Douglas & et al. (1996)).
- JVAS – Jodrell-Bank VLA Astrometric Survey: a catalogue of 800 compact radio sources in the declination range 35 – 75 deg (5 GHz; Patnaik & et al. (1992))
- S5 – the 5-GHz strong source survey between declinations 70° and 90° using the MPI 100-m telescope, containing 476 sources with flux densities above 50 mJy (Kuehr & et al. (1981); previous versions: S4, 1Jy).
- OHIO – catalogues of radio sources (OJ, OM, etc. , depending on the source’s position; 1964-1975; Rinsland & et al. (1975))
- B2 – the second Bologna Survey, a list of 448 radio sources observed with the Bologna Northern Cross Telescope (408 MHz, 1970-1974; Fanti & et al. (1974))
- QSO - Catalogue of Quasi-Stellar Objects (B-band, Hewitt & Burbidge (1980))

The major BLL monitoring programs (in the radio, optical, X-ray etc. energy ranges) are listed in Table 1 along with the corresponding websites. Note that many of these programs are still ongoing, while the expired ones are characterized by rich, publicly available data archives.

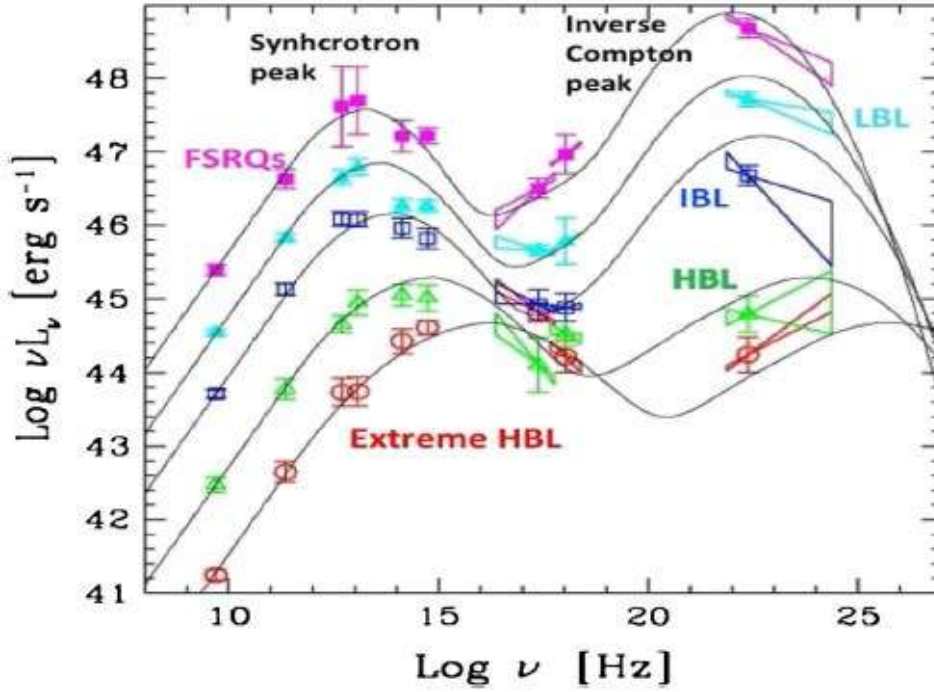


Figure 2. Broadband SEDs of the different BLL groups.

3. Spectral Energy Distribution and Emission Mechanisms

The optical spectra of BLLs are prominent for the absent or very weak spectral lines (belonging to host galaxy), and a similar situation is observed also in other spectral ranges. In the $\log \nu - \log \nu F_\nu$ plane, the broadband SED of BLLs shows two different components of a non-thermal origin (Figure 1):

- Lower-energy component extended from the radio to X-ray frequencies.
- Higher-energy component ranging from the X-ray up to very high-energy γ -rays.

Owing to the nonthermal, polarized nature of the lower-energy component, its origin is widely accepted as synchrotron emission of relativistic electrons (and, possibly, positrons and protons). On sub-parsec scales, jets should be pervaded by magnetic fields of the order of 0.1–10 Gauss that may have tangled geometries and cause particles — leptons or hadrons — to radiate through the synchrotron mechanism (Treves et al. 2014).

However, the origin of the higher-energy SED component is still less clear and there are two different “competing” scenarios. Namely,

- In the leptonic scenario, this is ascribed to inverse Compton (IC) scattering of lower energy photons off the (ultra)relativistic electrons. Consequently, the gamma-ray spectral shape is determined by the high-energy tail of the electron distribution and by the shape of the spectrum of the scattered photons, which can be either optical-to-soft-X-ray synchrotron photons (synchrotron self-Compton, SSC) or photons external to the jet, like those from the accretion disk, broadline region and dust torus (external Compton, EC; see Böttcher (2007)).
- In hadronic models, both primary electrons and protons are accelerated to ultra-relativistic energies, with protons exceeding the threshold for photo-pion production on the soft photon field in the emission region. While the low-frequency emission is still due to synchrotron emission from primary electrons, the high-energy emission is dominated by proton synchrotron emission, neutral pion decay photons, synchrotron and Compton emission from secondary decay products of

Table 2. The ranges of spectral parameters in HBLs during 1997–2016 (adapted from Kapanadze et al. 2018b).

Source	z	a	Γ	b	E_p
Mrk 421	0.031	1.34(0.02)-3.02(0.06)	1.68(0.02)-2.75(0.03)	0.06(0.02)-0.64(0.06)	0.002(0.001)-22.39(2.02)
Mrk 501	0.034	1.39(0.06)-2.05(0.05)	1.54(0.02)-2.22(0.04)	0.12(0.01)-0.56(0.11)	0.49(0.03)-101.6(23.7)
1ES 1959+650	0.048	1.46(0.05)-2.37(0.03)	1.71(0.02)-2.22(0.01)	0.12(0.04)-0.98(0.12)	0.12(0.04)-12.80(0.75)
PKS 2155–304	0.116	2.04(0.02)-2.75(0.02)	2.51(0.02)-2.81(0.02)	0.11(0.02)-0.80(0.15)	0.02(0.01)-0.89(0.10)
PG 15553+113	>0.4	2.17(0.07)-2.21(0.03)	2.09(0.03)-2.21(0.02)	0.23(0.04)-0.63(0.08)	0.51(0.11)-0.73(0.11)
1ES 1011+496	0.212	1.72(0.04)-2.48(0.06)	1.94(0.05)-2.50(0.07)	0.10(0.04)-0.67(0.20)	0.13(0.04)-5.01(0.68)
H 1426+428	0.129	1.68(0.02)-1.97(0.02)	1.86(0.03)-2.22(0.11)	0.12(0.02)-0.49(0.10)	1.11(0.06)-21.95(0.60)
H 1515+660	0.701	1.27(0.10)-2.17(0.06)	1.58(0.07)-2.53(0.18)	0.12(0.08)-0.89(0.22)	1.34(0.67)-3.53(1.52)
PKS 2005–489	0.071	1.96(0.05)-3.12(0.02)	2.00(0.03)-3.14(0.04)	-0.23(0.06)-0.70(0.34)	0.36(0.20)-1.25(0.22)
PKS 0548–322	0.069	1.53(0.07)-1.87(0.05)	1.49(0.03)-2.40(0.14)	0.14(0.03)-0.52(0.11)	1.77(0.21)-4.13(0.47)
1ES 0120+340	0.272	1.39(0.20)-1.94(0.14)	1.69(0.19)-1.94(0.14)	0.33(0.22)-1.28(0.38)	1.46(0.24)-3.31(0.44)
1ES 1218+304	0.184	1.89(0.05)-2.25(0.06)	1.97(0.06)-2.25(0.06)	0.39(0.11)-0.46(0.06)	0.63(0.08)-1.32(0.16)
1ES 2344+514	0.044	1.36(0.08)-1.87(0.11)	1.72(0.01)-2.27(0.04)	0.36(0.19)-0.83(0.33)	1.35(0.36)-6.03(0.89)
RBS 30	0.095	1.83(0.06)-1.89(0.05)	-	0.36(0.19)-0.68(0.15)	1.24(0.11)-1.44(0.29)
1ES 1421+582	0.638	1.91(0.07)-1.98(0.10)	1.77(0.10)-2.22(0.18)	0.37(0.17)-0.59(0.30)	1.22(0.33)-1.42(0.30)
1ES 0033+595	0.467	0.93(0.05)-1.60(0.16)	-	0.36(0.07)-0.93(0.07)	3.59(0.85)-6.47(0.95)
1ES 1727+502	0.055	1.76(0.06)-2.12(0.08)	1.90(0.05)-2.39(0.08)	0.28(0.14)-0.65(0.18)	0.81(0.14)-1.37(0.19)
RGB J0710+591	0.125	1.62(0.06)-1.73(0.06)	1.60(0.04)-1.85(0.02)	0.17(0.11)-0.23(0.13)	6.22(0.85)-6.70(0.93)
1ES 1101–232	0.186	1.64(0.08)-2.04(0.02)	1.95(0.09)-1.99(0.10)	0.17(0.03)-0.40(0.05)	0.76(0.06)-3.50(0.33)
1ES 0229+200	0.140	1.45(0.10)-1.60(0.10)	1.43(0.06)-1.45(0.06)	0.31(0.08)-0.44(0.21)	4.22(0.47)-5.54(0.65)
1ES 0502+675	>0.3	1.63(0.11)-1.91(0.06)	-	0.28(0.13)-0.70(0.20)	1.28(0.18)-2.17(0.26)
Mrk 180	0.045	1.60(0.06)-2.71(0.08)	1.96(0.05)-2.59(0.07)	0.17(0.12)-0.66(0.30)	0.29(0.07)-8.11(0.85)
RBS 1004	0.134	1.47(0.07)-1.74(0.07)	-	0.38(0.19)-0.96(0.23)	1.54(0.16)-4.26(1.57)
RBS 76	0.610	2.11(0.05)-2.30(0.09)	2.13(0.13)-2.29(0.09)	0.49(0.21)-0.79(0.13)	0.49(0.16)-0.79(0.13)
BZBJ1137–1710	0.601	1.39(0.11)-1.67(0.13)	1.48(0.15)-1.84(0.12)	0.75(0.24)-1.09(0.39)	1.42(0.58)-2.55(0.67)
RBS 1457	>0.5	1.47(0.12)-1.73(0.11)	1.75(0.17)-2.19(0.16)	0.74(0.28)-1.19(0.27)	1.52(0.46)-1.67(0.48)
1ES 1533+535	0.875?	2.00(0.09)-2.22(0.06)	-	0.34(0.18)-0.65(0.28)	0.47(0.11)-1.00(0.29)
BZBJ1341+3959	0.169	1.55(0.09)-1.64(0.07)	-	0.66(0.21)-0.70(0.14)	1.82(0.19)-2.20(0.38)
RBS 1366	0.236	1.72(0.15)-2.03(0.11)	1.90(0.09)	0.39(0.34)-0.88(0.59)	0.94(0.21)-2.08(1.24)
1ES 1440+122	0.163	1.80(0.20)-1.83(0.11)	2.15(0.18)	0.32(0.16)-1.36(0.57)	1.18(0.15)-1.93(0.52)
B3 2247+381	0.119	1.80(0.09)-2.43(0.06)	2.38(0.07)	1.22(0.13)-0.29(0.18)	0.19(0.02)-1.33(0.12)
BZBJ0832+3300	0.672	1.47(0.13)-1.52(0.07)	1.29(0.09)-1.81(0.09)	0.37(0.15)-0.87(0.31)	2.02(0.30)-4.45(0.52)

charged pions, and the output from pair cascades initiated by these high-energy emissions intrinsically absorbed by photon–photon pair production (see, e.g., [Mannheim \(1993\)](#) and references therein).

According to the position of the synchrotron SED peak position, BLLs are divided into four groups (see Figure 2):

- low-energy-peaked objects (LBLs) with the lower-energy peak at radio–IR frequencies
- Intermediate-energy-peaked objects (IBLs) peaking at optical frequencies
- High-energy-peaked objects (HBLs) with the synchrotron peak at UV–X-ray frequencies
- Ultra-High-energy-peaked objects (UHBLs) peaking at the frequencies corresponding to the energies $E > 10$ keV

Since the double-humped shape is present in all the aforementioned BLL groups, their relative intensities of the multifrequency emission differ significantly. According to [Fossati & et al. \(2008\)](#), the SED shape define a continuum of properties, whereby (a) the most luminous sources peaking at lower frequencies; (ii) the peak frequency of the gamma-ray component correlates with the peak frequency of the lower energy one; (iii) the luminosity ratio between the higher- and lower-energy components increases with bolometric luminosity, which is evident in Figure 2. Within the so-called blazar sequence scenario, BLLs are the sources with lower luminosities and higher characteristic synchrotron and inverse Compton frequencies. The parameters, governing this sequence, are the cooling efficiency of the relativistic particles, the accretion efficiency and ultimately the mass of the central black hole,

Table 3. The ranges of unabsorbed 0.3–2 keV and 2–10 keV fluxes (in units of 10^{-11} erg cm $^{-2}$ s $^{-1}$) of bright HBLs in different periods (adapted from Kapanadze et al. 2018).

Per.	$F_{0.3-2keV}^{min}$	$F_{0.3-2keV}^{max}$	$F_{2-10keV}^{min}$	$F_{2-10keV}^{max}$	References
Mrk 421					
1997 April – 2002 December	-	-	4.10	93.20	M04, R04
2005 March – 2008 June	15.17	261.82	3.50	312.35	K18a
2009 January – 2012 December	4.52	223.36	0.53	266.69	TW
2013 January–May	10.74	313.33	2.88	392.64	K16a
2013 November – 2015 June	19.72	166.72	4.37	140.93	K17a
1ES 1959+650					
1997 May– 2002 November	-	-	0.84	29.30	G02, P05, M08
2005 April – 2014 September	4.22	30.50	1.91	24.3	K16c
2015 August – 2016 August	11.17	34.67	6.17	50.58	K16b
Mrk 501					
1997 April 7 – 2007 April	-	-	3.02	52.40	M08
2014 March–October	7.21	33.19	6.04	53.20	K17b
PKS 2155-304					
1996 November – 2006 May	-	-	1.22	8.23	M08
2005 November – 2012 October	1.69	25.68	0.36	11.37	K14

while BLLs are accepted as the blazars having lower efficiencies and masses (Costamante & et al. (2001); Treves et al. 2014).

Note that HBLs undergo a large change in the position of the synchrotron SED peak E_p . For example, the nearby TeV-detected and X-ray bright source Mrk 421 showed $E_p < 0.002$ keV in 2011 May (i.e. in the optical band; Kapanadze & et al. (2018a)) and $E_p = 34_{-11}^{+22}$ keV in 2006 June (Tramacere & et al. (2009)), along with the tens of the spectra showing $E_p > 10$ keV (Kapanadze & et al. (2016), Kapanadze & et al. (2017a) Kapanadze & et al. (2018a), Kapanadze & et al. (2018b)). These cases show that Mrk 421 always was not an HBL source, but acts as an IBL or UHBL objects in low X-ray states and strong flares, respectively. A similar behaviour is observed also for many HBLs (see Table 2). The most extreme case was recorded for Mrk 501 during the dramatic X-ray flare in 1997 April when the position of the synchrotron SED peak moved from 0.94 keV to beyond 100 keV (i.e., to the γ -ray energies). While the presence of the synchrotron peak beyond 100 keV was firmly established during that unprecedented event, it could not be constrained from above because of lack of the *BeppoSAX* sensitivity beyond 100 keV (see Tavecchio & et al. (2001)).

Due to the positions of the lower-energy and higher-energy peaks, BLLs are bright X-ray (see Table 3 and Figure 3) and γ -ray sources. Namely, they represent the most frequently detected class of the extragalactic TeV sources (65 out of 82, see Table 4).

BLLs are one of the most frequently detected sources in the 100 MeV – 300 GeV with Fermi-LAT and form one of the most important constituents of the 4FGL catalogue. Namely, 3131 out of 5090 4FGL sources are blazars including

- 1116 BLLs
- 686 FSRQs
- 1330 blazar candidates of uncertain type

The MWL campaigns on bright sources (e.g. Mrk 4211, Mrk 501) showed that X-ray and VHE emission are generally highly correlated down to sub-hour timescales with no evidence of significant lags (Aharonian & et al. (2009), Fossati & et al. (2008), Alecsic & et al. (2015) etc.). This result provides a strong support to the one-zone SSC scenario, according to which both lower and higher energy BLL emissions are produced by a single electron population.

However, some MWL campaigns revealed the features which can not be explained within the one-zone SSC scenario. Namely, some BLLs showed

Table 4. List of the TeV-detected BLLs (<http://tevcat.uchicago.edu/>).

Source	Z	Type	Detection Year	Source	Z	Type	Detection Year
Mrk 421	0.031	HBL	1992	H 2356-309	0.165	HBL	2006
Mrk 501	0.034	HBL	1996	RX J0648.7+1516	0.179	HBL	2010
1ES 2344+514	0.044	HBL	1998	1ES 1218+304	0.182	HBL	2006
Mrk 180	0.045	HBL	2006	1ES 1101-232	0.186	HBL	2006
1ES 1959+650	0.048	HBL	1999	1ES 0347-121	0.188	HBL	2007
AP Librae	0.049	LBL	2010	RBS 0413	0.190	HBL	2009
TXS 0210+515	0.049	HBL	2019	RBS 0723	0.198	HBL	2014
1ES 2037+521	0.053	HBL	2016	1ES 1011+496	0.212	HBL	2007
1ES 1727+502	0.055	HBL	2011	MS 1221.8+2452	0.218	HBL	2013
PKS 1440-389	0.065	HBL	2012	PKS 0301-243	0.266	HBL	2012
PGC 2402248	0.065	HBL	2018	1ES 0414+009	0.287	HBL	2009
PKS 0548-322	0.065	HBL	2007	OJ 287	0.306	HBL	2017
BL Lacertae	0.069	IBL	2001	1RXS J023832.6-311658	0.322	HBL	2012
PKS 2005-489	0.071	HBL	2006	OT 081	0.322	LBL	2016
RGB J0152+017	0.080	HBL	2008	3C 66A	0.34	IBL	1998
1ES 1741+196	0.084	HBL	2011	PKS 0447-439	0.343	HBL	2009
SHBL J001355.9-185406	0.095	HBL	2010	KUV 00311-1938	0.61	HBL	2012
W Comae	0.102	IBL	2008	1ES 0033+595	-	HBL	2011
1ES 1312-423	0.105	HBL	2010	S2 0109+22	-	IBL	2015
PKS 2155-304	0.116	HBL	1999	RGB J0136+391	-	HBL	2012
B3 2247+381	0.119	HBL	2010	1ES 0502+675	-	HBL	2009
RGB J0710+591	0.125	HBL	2009	VER J0521+211	-	IBL	2009
1ES 0804+524	0.128	HBL	2008	1ES 0647+250	-	HBL	2011
H 1426+428	0.129	HBL	2002	S5 0721+71	-	IBL	2008
1ES 1215+303	0.131	HBL	2011	PG 1553+113	-	HBL	2006
RXJ1136.5+6737	0.134	HBL	2014	H 1722+119	-	HBL	2013
S3 1227+25	0.135	IBL	2015	HESS J1943+213	-	HBL	2010
1ES0229+200	0.140	HBL	2007	MAGIC J2001+435	-	IBL	2010
1RXS J101015.9-311909	0.143	HBL	2010	RGB J2243+203	-	HBL	2014
1ES 1440+122	0.163	HBL	2010	1ES 2322-409	-	HBL	2018

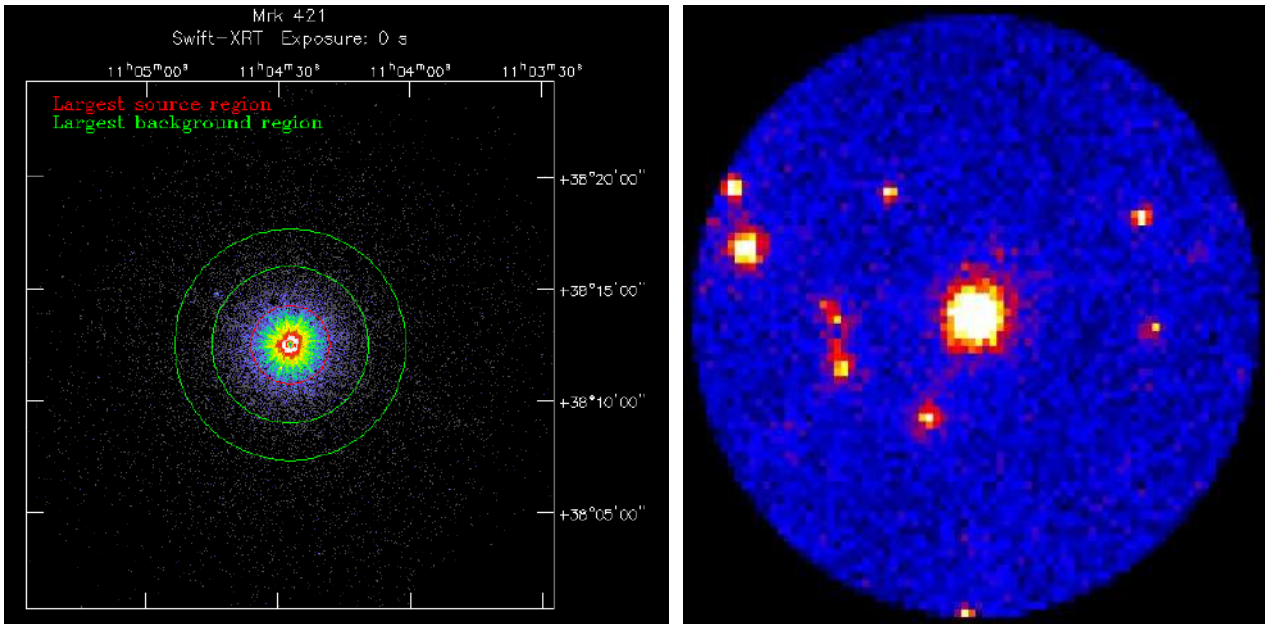


Figure 3. The 0.3–10 keV (Swift-XRT; left panel) and 300 MeV – 300 GeV (Fermi-LAT; right panel) images of Mrk 421.

- VHE flares without any visible X-ray counterpart (e.g., an “orphan” flare of 1ES 1959+650 in 2002 June; [Krawczynski & et al. \(2004\)](#)).
- X-Ray flares without VHE counterparts (e.g., in Mrk 421; [Blazejowski & et al. \(2005\)](#), [Kapanadze & et al. \(2017a\)](#))
- off-sets between X-ray and TeV flares with more than a day ([Blazejowski & et al. \(2005\)](#))
- More than a quadratic relation between the X-ray and VHE fluxes during some flares (in PKS 2155-304, [Aharonian & et al. \(2009\)](#); in Mrk 501, [Kapanadze & et al. \(2017b\)](#))
- Very fast (timescales of a few minutes) variability of some TeV blazars (see, e.g., [Albert & et al. \(2007\)](#)) poses severe problems for single-zone models due to the required extremely high bulk Lorentz factors ([Begelman et al. \(2008\)](#))

There are a few observational evidences of the IC emission in BLLs. For example, more than a squared relation between the optical and Fermi-band variability in some epochs in BL Lacertae ([Raiteri & et al. \(2013\)](#)). This feature can not explained within the one-zone SSC model, which predicting a quadratic relation between the synchrotron and IC emissions. Consequently, [Raiteri & et al. \(2013\)](#) suggested a requirement of additional seed photons of non-jet origin (e.g., from the dusty torus). Moreover, some authors reported an occasional detection of the γ -ray peak in the range between ~ 5 GeV and ~ 100 GeV in BL Lacertae, which was explained via the EC-upscatter of IR photons from dusty torus ([Ghisellini & Tavecchio \(2015\)](#)).

Hadronic models are particularly important for EHBLs with exceptionally hard VHE emission (up to ~ 10 TeV), which is very difficult to interpret the corresponding SED in the framework of the standard SSC model: extremely high Lorentz-factors of leptons and the reduction of the Klein-Nishina scattering cross-section necessarily entails soft spectra above 1 TeV ([Tavecchio \(2014\)](#)). Moreover, some HBLs exhibit very hard X-ray and MeV–GeV spectra, e.g., Mrk 501 and 1ES 1959+650 showed the photon index values within the range of 1.1–1.7, which is easier to explain within the hadronic scenarios ([Shukla & et al. \(2016\)](#), [Kapanadze & et al. \(2017b\)](#), [Kapanadze & et al. \(2018c\)](#)). Finally, an uncorrelated X-ray–VHE variability is “tolerated” by hadronic models (e.g., hadronic synchrotron mirror model, [Böttcher \(2005\)](#)).

On the other hand, there are some difficulties related to the use of hadronic models due to the reasons as follows:

- Requirement to accelerate protons to very high energies, together with the relatively low efficiency of the photo-meson and synchrotron proton emission generally implies higher magnetic fields and jet powers compared to leptonic models ([Böttcher \(2013\)](#)).
- It is very difficult to produce subhour flux variability within these models, since they require long cooling times ([Aleksic et al. 2015](#)).

4. BLL Redshifts

According to Roma-BZCAT, 1235 BL Lacs securely identified to date. The Redshifts are securely determined for 603 BLLs, ranging from from $z=0.020$ (NGC 2332; [Marcha & Caccianiga \(2013\)](#)) to $z=1.283$ (PKS 2131-021; [Drinkwater & et al. \(1997\)](#)). The distribution of the BLL redshift values and the observed ranges of the optical R-band magnitudes are provided in Figure 4.

103 BLLs have a tentative redshifts $z=0.07$ – 1.57 with $z>1$ for 11 sources and apparent optical R-band magnitudes of $R=14.7$ – 21.0 (see Table 3 for details). For the secure determination, we need to obtain deep optical spectra and identify absorption lines inherent to the host galaxy with higher confidence levels. Moreover, the redshifts are still unknown for another 677 BLLs whose ranges of the R-band magnitude are provided in Table 3. We see that these objects on average are fainter than the BLLs with the securely identified redshifts that prevents to obtain high-resolution optical spectra.

Among the BLLs with unknown redshifts, the most prominent is PG 1553+113, which a bright source ($R \sim 14$) and target of different multiwavelength campaigns, as well as a candidate object of

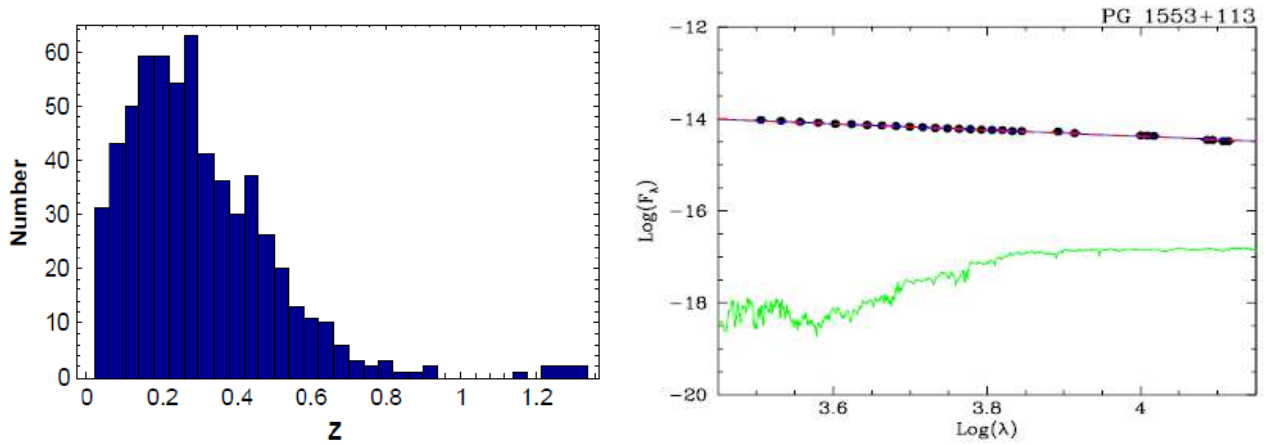


Figure 4. Redshift distribution of BLLs (left panel) and the UV–IR spectrum of PG 1553+113 (adapted from [Landoni & et al. \(2015\)](#))

Table 5. Major blazar monitoring programs and samples.

BLLs with Known Redshifts			BLLs with Unknown Redshifts		BLL Candidates	
z	Number	R -mag	Number	R -mag	Number	R -mag
≤ 0.05	25	8.0-16.5	10	14.0-15.0	0	14.0-15.0
0.05–0.10	50	9.8-17.5	29	15.0-16.0	1	15.0-16.0
0.10–0.20	138	12.8-18.9	89	16.0-17.0	5	16.0-17.0
0.30–0.40	92	15.0-21.6	123	17.0-18.0	8	17.0-18.0
0.4–0.6	119	15.5-20.8	183	18.0-19.0	14	18.0-19.0
0.6–0.6	25	16.5-20.8	150	19.0-20.0	20	19.0-20.0
0.8–1.0	7	15.0-20.0	40	20.0-21.0	3	20.0-21.0
> 1.0	3	17.6-19.2	4	21.0-23.0	1	21.0-22.0

having a binary central BH. Originally, it appeared in the Palomar-Green catalogue in 1986 and was proved to have featureless spectra in the near UV and optical bands (see, e.g., [Falomo et al. \(1993\)](#)). The spectroscopic observations with the 8-m VLT telescope also confirmed a featureless nature of the spectrum and derived a lower limit for the source of $z > 0.1$ based on the lack of absorption features from the starlight component ([Sbarufatti et al. \(2006\)](#)). The X-Shooter spectroscopy at the ESO-VLT confirmed the featureless nature of the spectrum on the wide spectral range 3200–15000 Angstroms (see Figure 3) and the redshift lower limit $z \gtrsim 0.3$ was estimated ([Landoni & et al. \(2015\)](#)).

Moreover, there are 88 BL Lac candidates which need further high-resolution spectral observations to exclude the presence of the emission lines with the equivalent width higher than 5 Angstroms (dividing line between BLLs and FSRQs; [Falomo & et al. \(2014\)](#)). Among these sources, the redshifts determined for 26 objects ($z=0.112$ – 0.598), while the tentative redshifts are provided for 10 sources ($z=0.085$ – 1.738).

There are incorrect redshift values in Roma-BZCAT:

- $z=0.007$ for 5BZG J0204+4005, while the correct value is $z=0.072$ ([Healey & et al. \(2008\)](#)).
- $z=1.34$ for 5BZB J0508+8432 (QSO B0454+844), although this is a lower limit to the redshift determined by [Healey & et al. \(2008\)](#) and no further redshift measurement has been performed.

Moreover, several most nearby objects are included incorrectly among BLLs in ROMA-BZCAT. Namely,

- 5BZG J1719+4858 (MCG+08-31-04) situated at $z=0.024$: there is no information about its BLL identification.
- 5BZG J1407–2701 (IC 4374) with $z=0.022$ which is a FSRQ source ([Russel & et al. \(2013\)](#)).
- 5BZG J1148+5924 (NGC 3894) situated at $z=0.011$: flat-spectrum weak-line radio galaxy (WLRG; [Bondi & et al. \(2001\)](#))

Table 6. Comparison between the redshifts of BLLs and FSRQs.

Parameter	BLLs	FSRQs
z_{\min}	0.02	0.07
z_{\max}	1.28	6.80
z_{mean}	0.29	1.44
$N_{z>1}(\%)$	3(0.002)	1269(67.5)

- 5BZG J0048+3157 (NGC 262, MRK 348) with $z=0.015$: in fact, this is a Seyfert 2 galaxy (Freitas & et al. (2018))
- 5BZG J1945–5520 (NGC 6812, $z=0.015$): no information about the BLL identification is available.
- 5BZG J1840–7709 (ESO 45–11) with $z=0.018$ is a LINER galaxy (Kollatschny & et al. (2008)).
- 5BZG J1336–0829 (NGC 5232) situated at $z=0.023$: no information about the BLL identification is available.
- 5BZGJ1407–2701 (PKS 1404–267, $z=0.022$) is a FSRQ source (Russel & et al. (2013)).

If we compare the securely determined redshifts of BLLs and FSRQs, the latter turn out to be significantly distant objects (see Table 4). Namely,

- The maximum redshift of BLLs is $z=1.28$ (5BZB J2134–0153), while FSRQs are found at the distances as high as $z=6.80$ (5BZQ J1556+3517), representing one of the most distant sources in the universe detected to date.
- The mean redshift of FSRQs is about 5-times larger than that of BLLs.
- A majority of FSRQs are detected at $z>1$, while only 3 out of 1235 BLLs are found at such distances.

However, the majority of the BLLs still do not have securely determined redshifts (as noted above), and the future deep spectral observations with large telescopes may change this statistics.

5. Internal Structure and Superluminal Motions

The innermost BLL region is still mostly unresolved by means of the direct observations, and we have to adopt its hypothetic structure as follows: there should be a central supermassive black hole (SMBH) of 10^8 Sollar masses, surrounded by the accretion disc (AD) “feeding” the central “engine”. Since the SMBH is spinning, it produces two opposite relativistic jets closely aligned to our line-of-sight (Blandford & Rees (1978) and references therein; see Figure 5). No observational evidences for the presence of broad/narrow line region is found, in contrast to other AGN classes. The existence of a dust torus around SMBH is also still controversial.

The SMBH masses of BLLs are evaluated using (i) relationship between BH masses and host luminosity (Woo & Urry (2002)); (ii) relationship between SMBH masses and stellar velocity dispersions (Falomo et al. 2003). The distribution of the SMBH masses obtained by means of the both methods are presented in Figure 6. As we see, the SMBH masses of several BLLs are estimated to be higher than $10^9 M_{\odot}$ on some occasion.

The mechanism of energy extraction and particle acceleration along the jet is not still completely understood. Two different scenarios of the BLL jet launching are generally considered:

- Blandford-Znajek mechanism (Blandford & Znajek (1977)) which is based on the Penrose effect – in accreting Kerr BH, magnetic field can be sustained by external currents. As such currents move along the horizon, the field lines are usually representing as originating from the event horizon and then being torqued by rotation. Consequently, there should be an outgoing electromagnetic flux of energy and momentum.

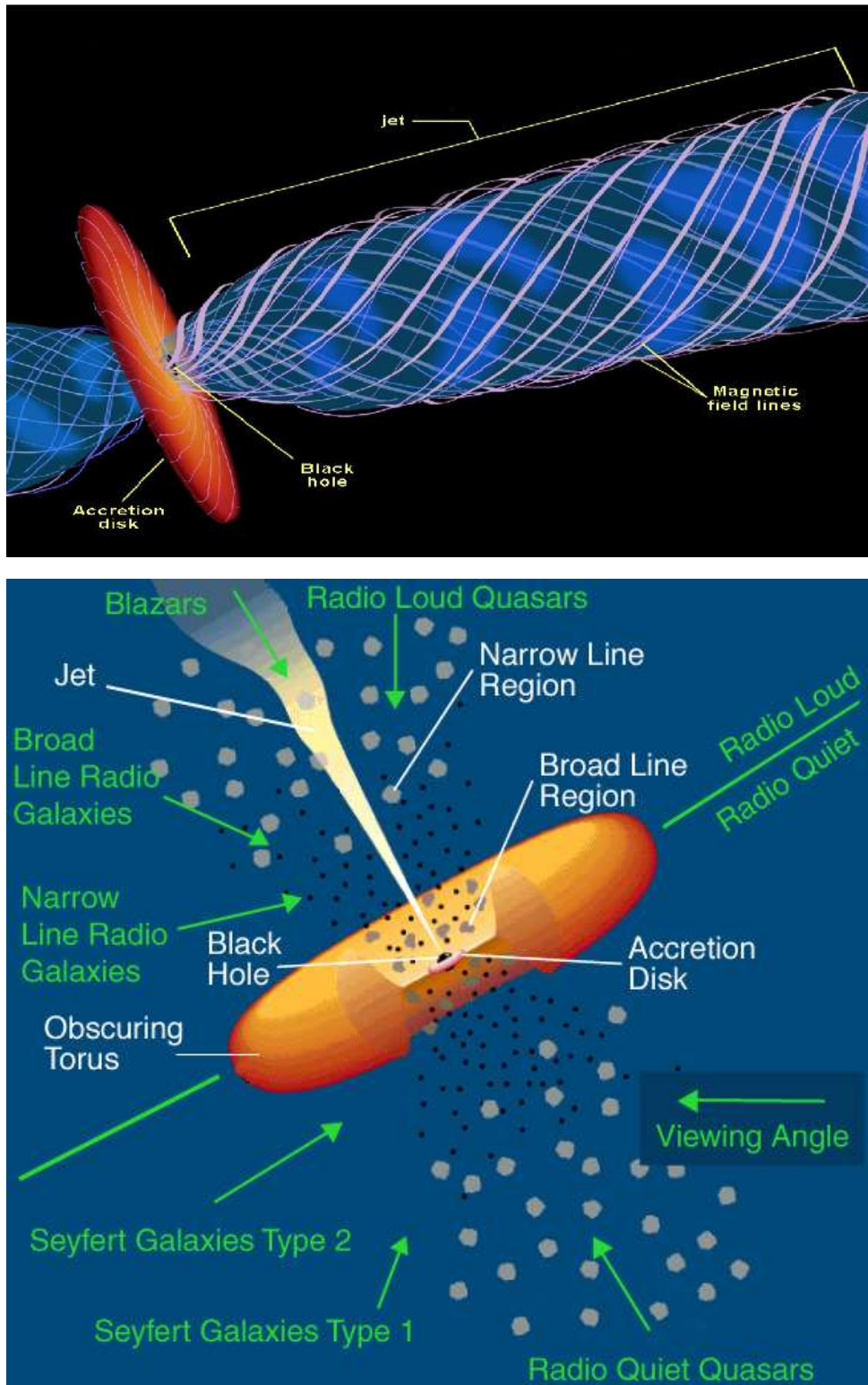


Figure 5. Hypothetic internal structure of a BLL source (www.universetoday.com/76443/astronomy-without-a-telescope-blazar-jets/)

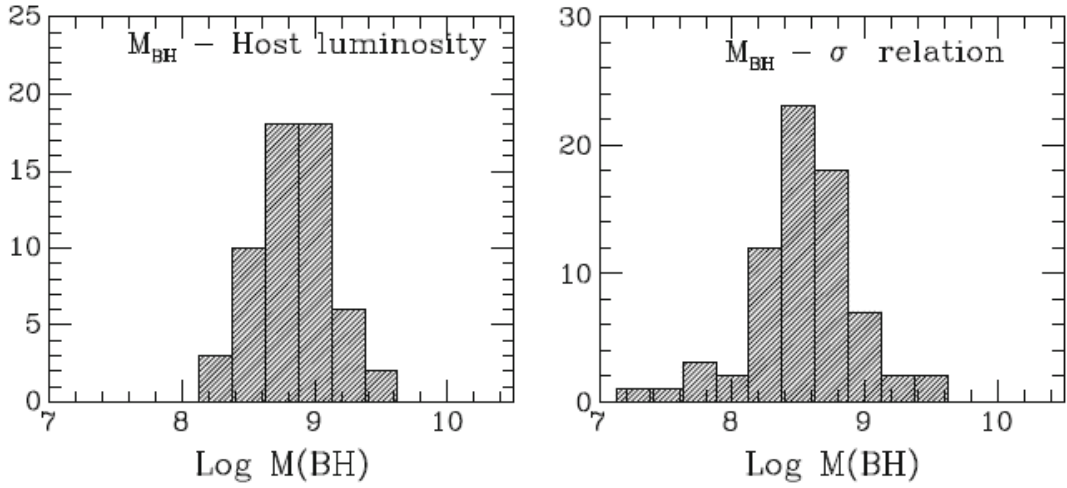


Figure 6. Distribution of BLL central BH β masses derived from different relations (adapted from Treves et al. 2014).

- Blandford-Payne mechanism (Blandford & Payne (1982)) – the BLL accretion disc should be threaded with magnetic field and torqued by its differential rotation. Consequently, it creates a magnetic coil that expels the accretion material and produces relativistic jets.

There is unanimous consensus on the fact that the extreme physical behavior of BLLs is related to the presence of a relativistic jet, which is closely aligned with the observer’s direction - the estimated angle between the jet axis and observer’s line-of-sight $\theta \lesssim 10$ deg (Begelman et al. (2008)). The highly relativistic kinematic regime and the small viewing angle produce a Doppler boosting of the observed emission as follows (Schneider (2006)):

$$F_{\text{obs}} = \delta^{3+\alpha} F_{\text{int}}, \quad (1)$$

where F_{obs} is the intrinsic emission generated in the jet emission zone; the Doppler factor

$$\delta = \frac{1}{\Gamma(1 - \beta \cos \theta)}, \quad (2)$$

with Lorentz factor

$$\Gamma = \frac{1}{\sqrt{1 - \beta^2}} \quad (3)$$

and $\beta = V/c$; V - the jet bulk speed; c - speed of light in vacuum. In the BLL jets, the hot plasma moves with the velocities $\Gamma \sim 10$ and can become as high as $\Gamma = 50$ during strong X-ray and γ -ray flares (Begelman et al. (2008)). On the other hand, a small viewing angle and high jet bulk speed lead to the observation of some radio components separation from the radio-core with the apparent velocity

$$V_{\text{app}} = \frac{V \sin \theta}{1 - \beta \cos \theta}, \quad (4)$$

which can be superluminal for the given angle θ , if

$$\beta > \frac{1}{\sin \theta + \cos \theta}. \quad (5)$$

Figure 7 presents an example of the superluminal motion of the IBL source 3C 66A with $V_{\text{app}} \approx 30c$ observed during 1992–1998, as well as the distribution of the superluminal V_{app} values obtained for BLLs with Very Large Baseline Interferometry (VLBI) observations.

As noted above, the observed flux increases highly due to the Doppler boosting and allows us to detect BLLs at significantly larger distances. On the other hand, their detection probability declines

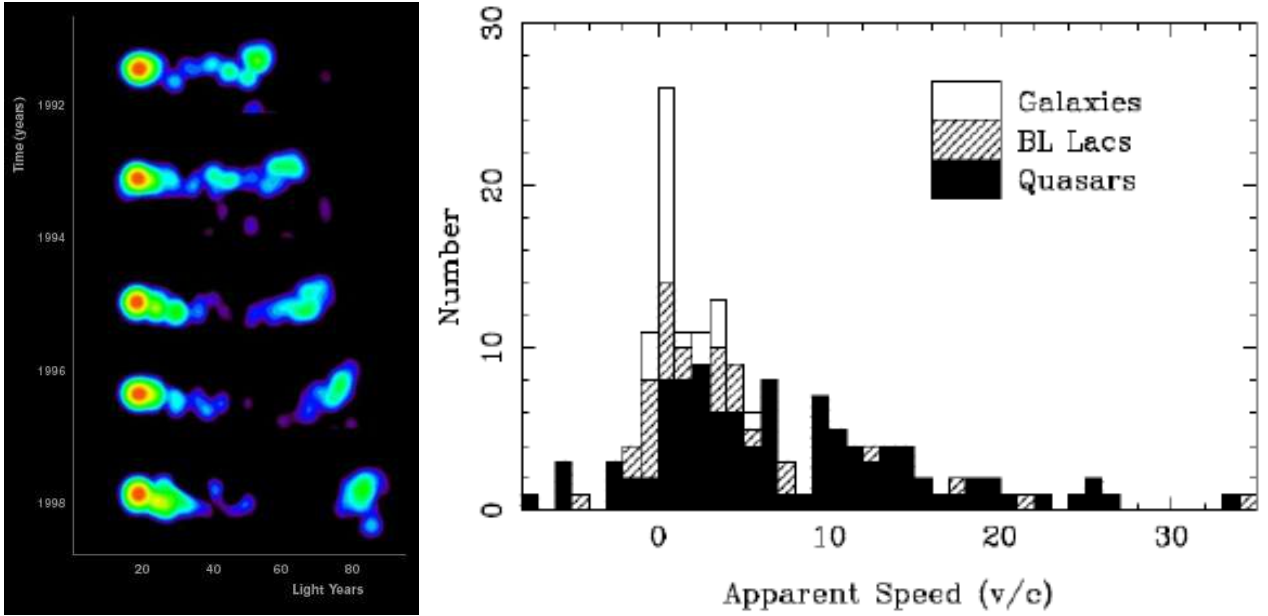


Figure 7. Superluminal motion of 3C 66A (left panel) and distribution of the superluminal motions observed for BLLs (right panel; adapted from Kellerman et al. 2003).

due to this effect – we can not reveal whether the particular elliptical galaxy possesses an BLL-type active nucleus if the angle between the jet axis and our line-of-sight is high enough. Consequently, it is impossible to evaluate an intrinsic number of the BLL sources in the universe and draw any firm conclusion whether an BLL-type AGN is one of the evolutionary stages of each elliptical galaxy.

6. X-Ray Spectra and Particle acceleration Processes in BLL jets

Generally, the X-ray spectra of BLLs are fitted with the theoretical models as follows:

- Simple power-law

$$F(E) = KE^{-\Gamma}, \quad (6)$$

with Γ , the photon index throughout the entire spectral range

- broken power-law

$$F(E) = \begin{cases} KE^{-\Gamma_1}, & E \leq E_{\text{br}} \\ KE_{\text{br}}^{\Gamma_2 - \Gamma_1} (E/1\text{keV})^{-\Gamma_2}, & E > E_{\text{br}}, \end{cases} \quad (7)$$

with E_{br} : break point for the energy in keV, Γ_1 : photon index for $E \leq E_{\text{br}}$, Γ_2 : photon index for $E > E_{\text{br}}$.

- log-parabolic model (Massaro & et al. (2004))

$$F(E) = K(E/E_1)^{-(a+b\log(E/E_1))}, \quad (8)$$

with E_1 , the reference energy; a , the photon index at the energy E_1 ; b , the curvature parameter; K , the normalization factor. The position and the height of the synchrotron SED peak are calculated as

$$\begin{aligned} E_p &= 10^{(2-a)/2b} \text{keV} \\ S_p &= 1.6 \times 10^{-9} K 10^{(2-a)^2/4b} \text{erg cm}^{-2} \text{s}^{-1} \end{aligned} \quad (9)$$

Note that the X-ray spectra of the HBL and EHBL sources show a good fit with the log-parabolic model (see Figure 8 and Table 2 for the value ranges of different spectral parameters). Such spectra can be produced by the electron population with the logparabolic energy distribution.

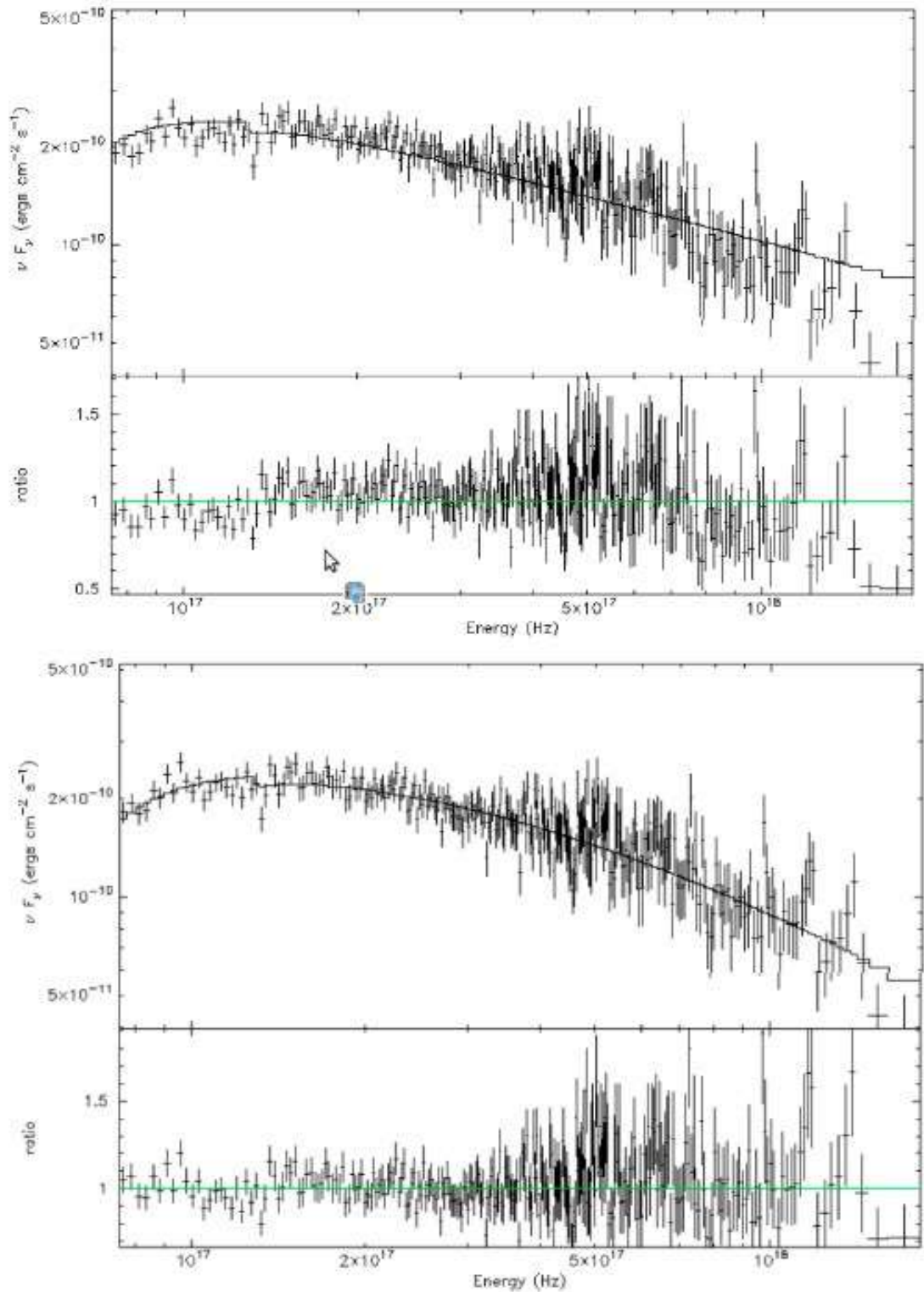


Figure 8. Simple power-law (upper panel) and log-parabolic (lower panel) fits of the spectrum derived from the Swift-XRT observation of Mrk 421 performed on 2009 March 24 (along with the distribution of the fit residuals with energy). We see that the fit with a simple power-law model produces a prominent trend in the residuals and is thus unsuitable for this spectrum. On the contrary, these residuals are distributed symmetrically around the value 1 in the case of the log-parabolic model, demonstrating a good fit of the model and the observed spectrum.

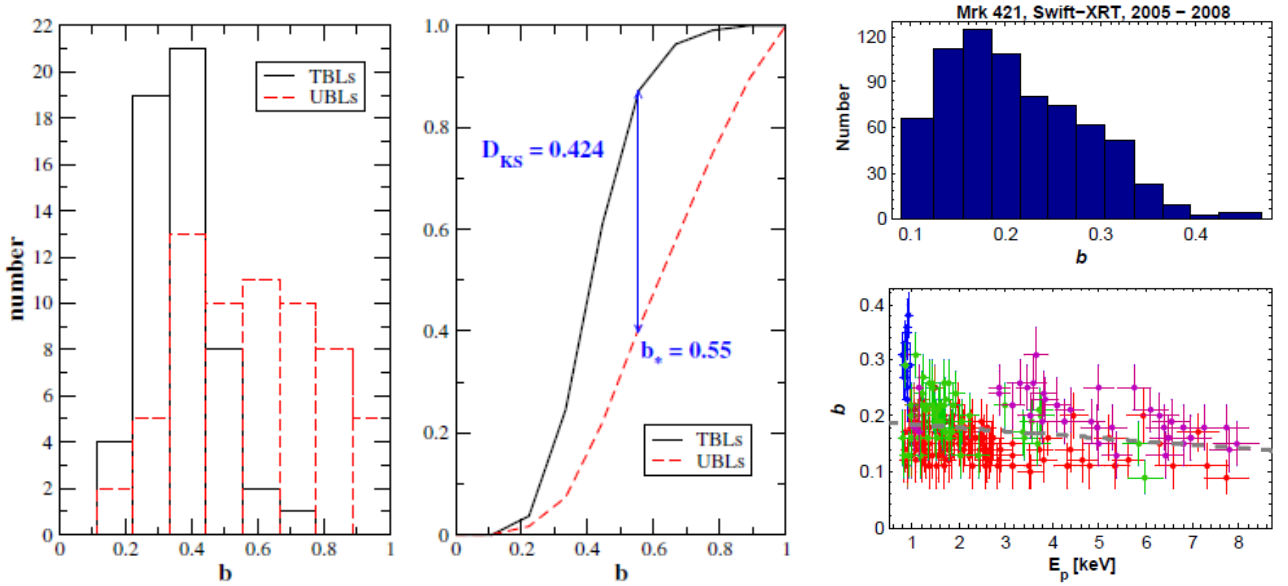


Figure 9. The distribution of the b parameter values derived for TBLs and UBLs: histogram (left panel) and cumulative normalized distribution (central panel; adapted from [Massaro & et al. \(2011\)](#)). Distribution of these values and the E_p - b anti-correlation for Mrk 421 from the Swift-XRT observations performed during 2005-2008 (right panels; adapted from [Kapanadze & et al. \(2018a\)](#)).

Generally, the energy spectrum of the BLL jet particles accelerated by some statistical mechanism, like that occurring in a shock wave, can be written as a power law ([Massaro & et al. \(2004\)](#)):

$$N(> \gamma) = N_0(\gamma/\gamma_0)^{-s+1}, \quad (10)$$

where $N(> \gamma)$ is the number of particles having a Lorentz factor higher than γ ; s is the spectral index of the distribution defined by:

$$s = -\frac{\log p}{\log \epsilon} + 1, \quad (11)$$

with p , the probability that a particle undergoes an acceleration step i in which it has an energy gain equal to ϵ . The latter parameter is generally assumed to be independent of the particle's energy:

$$\gamma_i = \epsilon \gamma_{i-1} \quad (12)$$

and

$$N_i = p N_{i-1} = N_0 p^i. \quad (13)$$

A log-parabolic energy spectrum can be established when the condition p is independent of energy is no more held and it can be described by a power-law relation as:

$$p_i = g/\gamma_i^q, \quad (14)$$

where g and q are positive constants. In the case $q > 0$, the probability for a particle to be accelerated is lower when its energy increases. Such a situation can occur in the jet region where the charged particles are confined by a magnetic field with a confinement efficiency decreasing for an rising gyration radius. Consequently, the probability of the particle's acceleration is lower when its energy increases, and the differential energy spectrum is given by

$$N(\gamma) \sim \gamma/\gamma_0^{-s-r \log \gamma/\gamma_0}, \quad (15)$$

with a linear relationship between the spectral index and curvature terms (s and r , respectively) as follows:

$$s = -r(2/q) \log g/\gamma_0 - (q-2)/2. \quad (16)$$

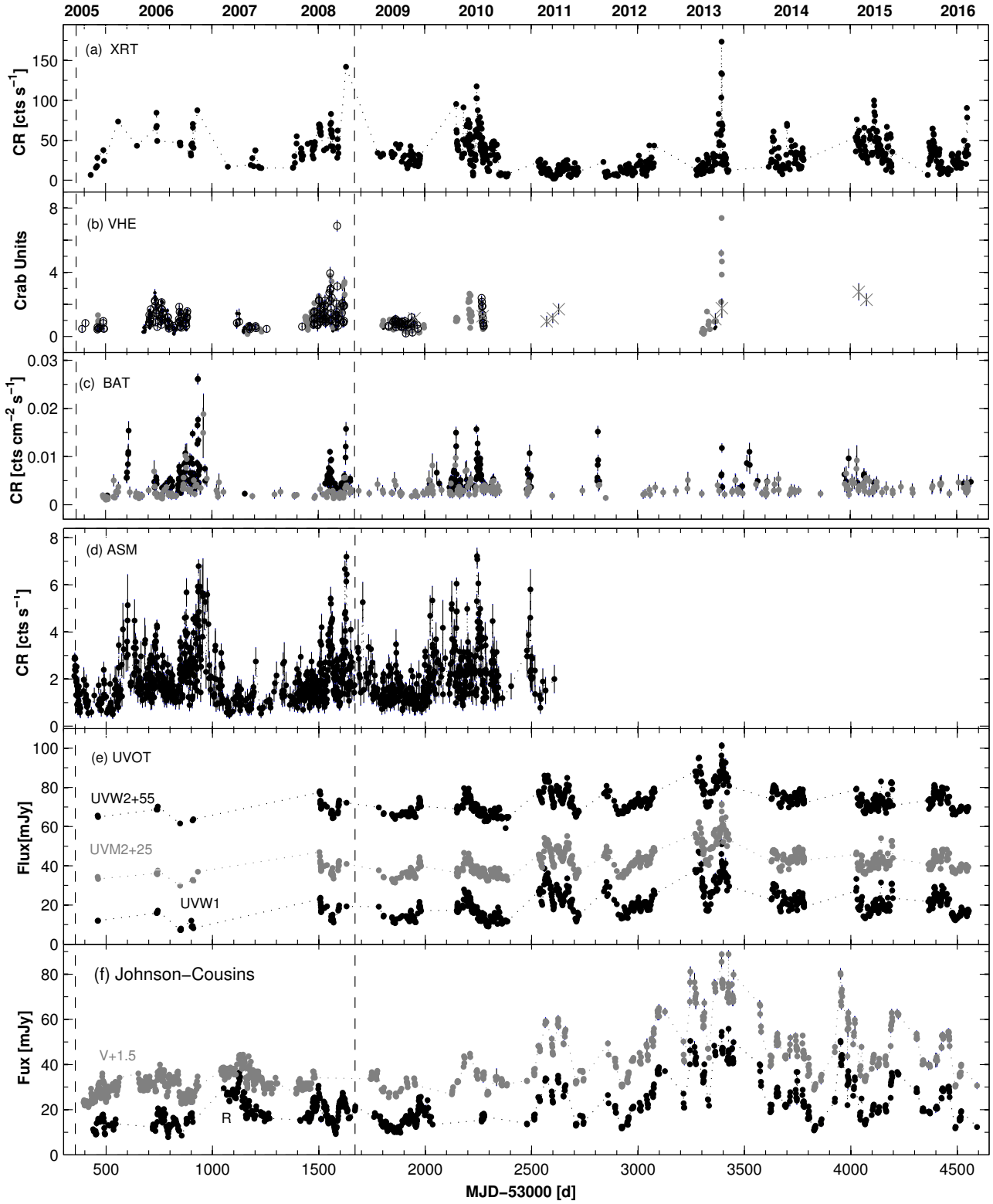


Figure 10. Historical light curves of Mrk 421 from the daily-binned MWL observations in 2005–2016 (adapted from [Kapanadze & et al. \(2018a\)](#)).

Note that a larger volume or a higher magnetic field can make more efficient the particle confinement. In this case one can also expect that energetic particle can reach higher energies.

The synchrotron emission produced by this distribution is given by

$$P_S(\nu) \propto (\nu/\nu_0)^{-(a+b\log(\nu/\nu_0))}, \quad (17)$$

with $a = (s - 1)/2$ and $b = r/4$, which can be derived using the aforementioned log-parabolic spectra

model. Equation (16) demonstrates, that there should be a linear a - b correlation in the case of the efficient first-order Fermi acceleration in the BLL jet. A positive is detected for nearby bright HBLs Mrk 421 and 1ES 1959+650 during the particular periods, using the densely-sampled observations performed with the X-Ray Telescope onboard the Swift satellite (Swift-XRT; Kapanadze & et al. (2017a), Kapanadze & et al. (2018a), Kapanadze & et al. (2018b), Kapanadze & et al. (2018c)). However, the detected a - b correlations were generally weak in each interval that can be explained due to the presence of the sub-samples having different slopes in the a - b plane, leading to a large scatter of the data points during the given period. Note that some sub-samples, corresponding to some X-ray flares, showed even a negative a - b trend, which is expected when $g > \gamma_0$, i.e., there were electron populations with a very low initial energy γ_0 in the emission zone.

Furthermore, the co-existence of the second-order Fermi (stochastic) acceleration also could weaken the a - b correlation, since this mechanism does not yield such a relation. The simulations of Katarzynski & et al. (2006) demonstrated that electrons can be accelerated at the shock front via the first-order Fermi process and continue gaining energy via the stochastic mechanism into the shock downstream region. Afterwards, the accelerating particle will be able to re-cross the shock front and repeat the aforementioned acceleration cycle. Consequently, such combined energization process will not yield a strong a - b correlation.

A shock acceleration is not the only statistical mechanism capable to produce a logparabolic energy distribution of charged particles. For example, the electron acceleration can occur in magnetohydrodynamical turbulence in which regions of magnetic field reconnection can develop in a very stochastic way (Massaro & et al. (2006)). The stochastic (second-order Fermi) acceleration is related to the presence of a momentum diffusion term in the Fokker-Plank equation (Tramacere & et al. (2011)). In this scenario, the diffusion term acts on the electron spectral shape, broadening the distribution via the inverse proportional relation between the curvature and diffusion terms:

$$r \propto \frac{1}{Dt}. \quad (18)$$

In the case of the efficient stochastic acceleration, an anticorrelation between the peak energy E_p and the curvature parameter b measured in the synchrotron SED is expected (Tramacere et al. 2009). However, the same correlation is expected also within the first-order Fermi mechanism, but the corresponding scatter plot is characterized by the slope which is different from that resulted in the case of the stochastic process. This circumstance explains a weak E_p - b anti-correlation, detected during the intense X-ray spectral study of nearby bright HBLs (see Kapanadze & et al. (2016), Kapanadze & et al. (2017a), Kapanadze & et al. (2017b), Kapanadze & et al. (2018a), Kapanadze & et al. (2018b), Kapanadze & et al. (2018c)); see Figure 9 for the corresponding example). The same studies also confirmed another expectation from the efficient stochastic acceleration: Massaro & et al. (2011) showed that the electrons in the jets of TeV detected HBLs (so-called TBLs) should undergo a more efficient stochastic acceleration than in those of the TeV-undetected HBLs (UBLs; see Figure 9). They demonstrated that the synchrotron SEDs are relatively broad (i.e. the curvature is smaller with $b \sim 0.3$) when the stochastic acceleration is more efficient while they are narrower ($b \sim 0.7$) in the opposite case (for UHBLs). The corresponding example, demonstrating a low spectral curvature for Mrk 421 in the ime interval 2005-2008 is presented in Figure 9.

According to Tramacere & et al. (2007), as the peak energy of the emission increases, the cooling timescale shortens and can compete with the acceleration timescales. Consequently, a positive $F_{0.3-10\text{keV}}-E_p$ correlation, i.e., a trend of shifting the synchrotron SED peak to higher energies with rising X-ray flux is expected and confirmed in the aforementioned our X-ray spectral studies.

Relativistic magnetic reconnection represents another efficient convertor of magnetic energy into bulk motion and operate efficiently in the highly-magnetized jet areas (see, e.g., Sironi & Spitkovsky (2014)). Although this mechanism provides a promising explanation for the long-wavelength (radio-to-optical) flares, its importance for higher-energy flares is still unclear and further intense simulations required.

Shear acceleration is a Fermi mechanism without shock, wherever scattering centers flow at different speeds, even if the flows are parallel (e.g., longitudinal shear across the jet radius). Consequently, particles are intercepted by the difference between the fast core of the jet and the slower exterior

(Rieger & Duffy (2016)). Note that the shear acceleration can overcome radiative and non-radiative losses and work efficiently, when the pre-accelerated seed particles are available. Consequently, it can continue to accelerate the particles already energized by the first- or second-order Fermi mechanisms. However, a shear acceleration acts slowly and can not be important for very fast X-ray – TeV flares (Tammi & Duffy (2009)).

7. Flux Variability

Flux variability of BLLs has been detected in most parts of the accessible electromagnetic spectrum, which is divided into different types according to their timescales (see, e.g., Gupta & et al. (2016)):

- Long term variability (LTV), incorporating the brightness changes on monthly–yearly timescales (see Figure 10): usually explained by adopting the shock-in-jet scenario (Marscher & Gear 1985 and references therein), which postulates that relativistic shocks in the jet cause particle acceleration and nonthermal emission, appearing as superluminal knots in VLBI maps. Relativistic shocks in the BLL jet can be triggered due to the intermittent variability in the physical properties in the innermost portion of the accretion disc. Such events may momentarily saturate the jet with extremely energetic plasma with much higher pressure than the steady jet plasma downstream. The high-energy plasma will sweep up slower moving material, forming a shock wave (Sokolov & et al. (2004)).
- Short term variability (STV), lasting from a few days to a few weeks. Such event be triggered by the collision between a relativistic shock wave traveling down the jet and a more slowly moving or stationary compression, e.g., the core seen in VLBI images of BLLs (Spada & et al. (2001)).
- Intraday variability (IDV) on timescales from several minutes to less than a day – can be produced by the shock interaction with the smallest-scale turbulent jet inhomogeneities with strongest magnetic fields (Marscher (2014); Mizuno & et al. (2014)), or by the instable processes in the SMBH vicinity and appearance of a "hot spot" on AD (Mangalam & Wiita (1993)). The latter should be easier detectable in lower brightness states when the variable emission is not overwhelmed by the huge emission produced at the shock front during the long-term flare. On the contrary, the IDVs detected in higher states can be explained more naturally within the shock-in-jet scenario.

Note that our detailed studies of Swift-XRT observations of nearby bright HBLs showed a dominance of the shock-in-jet scenario in triggering of 0.3–10 keV IDVS (Kapanadze & et al. (2016), Kapanadze & et al. (2017a), Kapanadze & et al. (2017b), Kapanadze & et al. (2018a), Kapanadze & et al. (2018b), Kapanadze & et al. (2018c)) shock-in-jet scenario. Note that our targets showed a series of the brightness halving and doubling events on timescales of a few hours. Such successive large brightness drop and rise events can be explained as a consequence of a shock passage through two inhomogeneous areas with strong magnetic fields, which are separated by a region with significantly weaker field and lower particle density (yielding the generation of fewer X-ray photons). The most extreme behaviour was observed during the giant X-ray outburst of Mrk 421 in 2013 April, with several events showing $\tau_d=1.2-7.2$ hr and $\tau_r=1.0-3.5$ hr (Kapanadze & et al. (2016)). The Variability character is generally erratic – BLLs change their amplitude, duration, maximum and minimum flux levels from flare to flare and can be characterized as a "red noise" - larger variability power at longer timescales.

The variability strength and timescales are highly dependent on subclass (LBL/IBL/HBL/UHBL): HBLs show the strongest and fastest variability in X-ray and TeV bands, while IBLs/LBLs are bright sources and undergo the strongest variability at the radio-optical and MeV–GeV frequencies. Note that MWL variability of the majority of BLLs are still poorly investigated.

8. Summary

- BLLs – an extreme classes of AGNs hosted by elliptical galaxies showing very wide range of distance: from $Z=0.02$ to beyond $Z=0.134$ with the distribution peak at $z \approx 0.28$. However, the intrinsic distribution peak may be quite different: there are 63% of BLLs with tentative or unknown redshifts, 88 BLL candidates and 227 blazars of uncertain type. Moreover, we can not evaluate the number of the undetected sources due to beaming effect or restricted instrumental capabilities. Consequently, it is impossible to draw any firm conclusion whether an BLL-type AGN is one of the evolutionary stages of each elliptical galaxy.
- The innermost structure of BLLs is still hypothetic since these regions are still unresolved via the direct observations. While the existence, properties and spatial scales are evaluated for the central SBBH, AD and two opposite jets, it is impossible to draw conclusion about the existence of BLR/NLR and dust torus, which are inherent to other AGN classes.
- BLLs represent one of the most extreme particle accelerators in the universe, showing an extreme range of broadband SED (up to 19 orders of frequencies, from radio to TeV) with two different non-thermal components. While the lower-energy one is firmly associated with the synchrotron emission of (ultra)relativistic charged particles gyrating in the jet magnetic field, there are different hypothetic mechanisms to be responsible for the appearance of the higher-energy SED component: one-zone SSC, multizone SSC, EC, or hadronic models. The intense MWL campaigns show that the model validity is variable from source to source and sometimes even one particular object requires different models from flare to flare.
- The most plausible for the initial particle acceleration scenarios invoke the Blandford-Znajek mechanism operating in the magnetospheres of the spinning Kerr SMBHs and the Blandford-Payne mechanism, related the magnetized accretion disc around SMBH. However, the keV–TeV observations of BLLs demonstrate a requirement of the further particle acceleration within the jet. The latter is explained via the first-order Fermi process operating at the relativistic shock front moving downstream the jet. Moreover, the signatures of the stochastic (second-order) Fermi acceleration are also frequently observed for bright TeV-detected BLLs, to be related to the repeated particle scatter on the turbulent magnetic irregularities.
- Another jet-related acceleration mechanisms can be at work (with different contribution to diverse spectral bands and flares on various timescales): shear acceleration and relativistic magnetic reconnection. However, these possibilities are still relatively poorly investigated.
- BLLs are strongly variable objects on timescales from years (and, possibly, decades-long change in baseline emission) down to the events observed within a few minutes. The variability strength and timescales are highly dependent on subclass and the MWL variations of the BLL majority is still poorly investigated.

References

- Abdollahi S., et al 2019, astro-ph/1902.10045v4
- Aharonian et al. 2009, A&A, 749, 502
- Albert J., et al. 2007, ApJ, 862, 669
- Alecsic J., et al. 2015, A&A, 22, 578
- Begelman M., Fabian A. C., Rees M. J., 2008, MNRAS, 384, L19
- Blandford R. D., Payne D. G., 1982, MNRAS, 883, 199
- Blandford R. D., Rees M. J., 1978, Pittsburgh Conf. on BL Lac Objects. Univ. Pittsburgh, Pittsburgh, PA, p. 328

- Blandford R. D., Znajek R. L., 1977, MNRAS, 433, 179
- Blazejowski M., et al. 2005, ApJ, 130, 630
- Bondi M., et al. 2001, MNRAS, 325, 1109
- Böttcher M., 2005, ApJ, 176, 621
- Böttcher M., 2007, ApSS, 95, 309
- Böttcher M., 2013, ApJ, 54, 768
- Casandjian J. M., Grenier I., 2008, A&A, 849, 489
- Costamante L., et al. 2001, A&A, 512, 371
- Cusumano G., et al. 2010, A&A, 48, 510
- Douglas J. N., et al. 1996, AJ, 1945, 111
- Drinkwater M J., et al. 1997, MNRAS, 85, 284
- Falomo R., et al. 2014, A&AR, 22, 37
- Falomo R., Bersanelli M., Bouchet P., Tanzi E. G., 1993, AJ, 11, 106
- Fanti C., et al. 1974, AJ, 18, 147
- Fossati G., et al. 2008, ApJ, 906, 677
- Freitas I. C., et al. 2018, MNRAS, 2760, 476
- Ghisellini G., Tavecchio F., 2015, MNRAS, 1060, 448
- Giommi P., et al. 2005, A&A, 385, 434
- Gregory P. C., et al. 1996, ApJS, 427, 103
- Gupta A. C., et al. 2016, MNRAS, 1127, 458
- Healey S., et al. 2008, ApJS, 97, 175
- Hewitt A., Burbidge G., 1980, ApJS, 57, 43
- Hoffmeister C., 1929, AN, 233, 236
- Kapanadze B., et al. 2016, ApJ, 102, 831
- Kapanadze B., et al. 2017a, ApJ, 103, 848
- Kapanadze B., et al. 2017b, MNRAS, 1655, 469
- Kapanadze B., et al. 2018a, ApJ, 66, 854
- Kapanadze B., et al. 2018b, ApJ, 68, 858
- Kapanadze B., et al. 2018c, MNRAS, 407, 480
- Katarzynski K., et al. 2006, A&A, 47, 453
- Kollatschny W., et al. 2008, A&A, 897k, 484
- Krawczynski H., et al. 2004, ApJ, 151, 601
- Kuehr H., et al. 1981, AJ, 854, 86

- Landoni M., et al. 2015, A&A, 126, 570
- MacLeod J. M., Andrew B. H., 1968, ApL, 1, 243
- Mangalam A. V., Wiita P. J., 1993, ApJ, 420, 406
- Mannheim K., 1993, A&A, 60, 269
- Marcha M. J. M., Caccianiga A., 2013, MNRAS, 430, 2464
- Marscher A. P., 2014, ApJ, 87, 780
- Marscher A. P., Gear W. K., 1985, ApJ, 114, 298
- Massaro E., et al. 2004, A&A, 413, 489
- Massaro E., et al. 2006, A&A, 861, 448
- Massaro E., et al. 2011, ApJ, L32, 742
- Massaro E., et al. 2015, Ap&SS, 75, 357
- Mizuno Y., et al. 2014, MNRAS, 3490, 439
- Patnaik A., et al. 1992, MNRAS, 655, 254
- Raiteri C., et al. 2013, MNRAS, 1530, 436
- Rieger F., Duffy P., 2016, ApJ, 34, 833
- Rinsland C. P., et al. 1975, AJ, 759, 80
- Russel H., et al. 2013, MNRAS, 530, 432
- Sbarufatti B., Treves A., Falomo R., et al. 2006, AJ, 132, 1
- Schneider P., 2006, in *Extragalactic Astronomy and Cosmology: An Introduction*, Springer, 188
- Shukla A., et al. 2016, A&A, 83, 591
- Sironi L., Spitkovsky A., 2014, ApJ, L21, 783
- Sokolov A., et al. 2004, ApJ, 725, 613
- Spada M., et al. 2001, MNRAS, 1559, 325
- Strittmatter P. A., et al. 1972, ApJ, 175L, 7
- Tammi J., Duffy P., 2009, MNRAS, 1063, 393
- Tavecchio F., 2014, MNRAS, 438, 3255
- Tavecchio F., et al. 2001, ApJ, 725, 554
- Tramacere A., et al. 2007, A&A, 521, 466
- Tramacere A., et al. 2009, A&A, 879, 501
- Tramacere A., et al. 2011, ApJ, 739, 66
- Veron-Cetty M. P., Veron P., 2010, A&A, 10, 518
- Voges W., et al. 1999, A&A, 389, 349
- Woo J.-H., Urry C. M., 2002, ApJ, 530, 579
- Wood K. S., et al. 1984, ApJS, 56, 507
- Wright A. E., et al. 1991, MNRAS, 330, 251

Water Ice in AGN and Starbursts

A.G.Yeghikyan* and A.L.Samsonyan†

NAS RA Byurakan Astrophysical Observatory, Byurakan 0213, Aragatzotn Province, Armenia

Abstract

Complex chemical species are easier formed in a solid phase, for example in a mixture of ices of water, carbon oxides, methane, ammonia, methanole and other, less abundant molecules. Ultraviolet photons in the range 5 - 13.6 eV and the charged particles with MeV-GeV energies serve as an energy source of reactions. Icy particles containing mentioned substances, can exist only in internal areas of the interstellar molecular clouds protected from influence of external ultraviolet radiation. However cosmic rays are capable to penetrate in clouds and to cause an irradiation of ices by means of secondary ultra-violet photons necessary for initiation of chemical reactions of complexisation. In this work a survivability of ices under harsh conditions of active galaxies is discussed. Preliminary model calculations show that abundances of ices depend not only on ionization parameters of the clouds but also on the shape of incident radiation that is on presence and level of hard ultraviolet and X-ray radiation. The last circumstance is directly related to the radiation of the accretion disk of galaxies with active nuclei and can be used to classify active galaxies, for example to distinguish starburst galaxies from those with active nuclei.

Keywords: *active galaxies, AGN, Starburst galaxies, IR spectra, water ice, UV radiation modeling, ice survivability*

1. Introduction

Water ice and polycyclic aromatic hydrocarbon (PAH) molecules are observed in the spectra of galaxies indicating the possibility of the formation of complex compounds, possibly involved in the synthesis of prebiomolecules. This is also supported by the results of laboratory experiments on the formation of heavy hydrocarbons (up to 30 carbon atoms) and amino acids due to irradiation of mixtures of ices with UV photons and energetic particles (Cottin et al., 2003), (Dworkin et al., 2004). UV radiation does not penetrate into the internal dense regions of molecular clouds, and it is in these areas that ice (ice mantle of dust particles) exists, which is believed to be responsible for the formation of very complex compounds (Tielens, 2005). The energy sources of the corresponding reactions in ices are the above-mentioned energetic particles in the MeV-GeV energy range (i.e. cosmic rays, CR), as well as the secondary UV radiation caused by them (in the range 6–13.5 eV). All of the above is true for active galaxies, where the observed ice and PAH content is directly related to the level of activity of galaxies (Yeghikyan, 2016), (Yeghikyan & Martirosyan, 2018). However, many of the details associated with the source/sources of hard radiation regulating the molecular content as well as the possibility of direct interaction between molecules and radiation, remain unclear.

The ices of the most common molecules and other carbon-containing compounds are observed in the spectra of normal galaxies in the form of characteristic bands. On the other hand, so far only absorption bands of 3.1 μm and 6.0 μm of water ice are visible in the spectra of active galaxies, for example, galaxies with starburst formation and galaxies with active nuclei (Boogert et al., 2015), (Imanishi et al., 2006), (Spoon et al., 2002). Often, absorption bands of 3.1 μm of ice appear in combination with a carbon dust absorption band of 3.4 μm and an emission band of 3.3 μm from PAH molecules.

*ayarayeg@gmail.com, Corresponding author

†anahit.sam@gmail.com

Ice plays an important role in the physics and chemistry of interstellar molecular clouds, including, as already noted, the formation of many complex compounds. Moreover, the formation of very complex chemical compounds containing tens of atoms is obviously difficult in a rarefied gas medium, while it is possible in the solid phase, even at low temperatures of the order of 5-10 K. The most famous example is the polycondensation of solid methane in experiments on the irradiation of solid methane with protons with energies of the order of 10 MeV with the formation of alkanes, alkenes and PAHs containing up to 30 carbon atoms (Kaiser, 1998, Kaiser & Roessler, 1997, Kaiser et al., 1997). The formation of complex compounds under the influence of UV radiation should also be indicated: according to experimental data irradiation of a mixture of ices (like water, carbon oxides, methanol, ammonium and methane) with photons with energies of about 10 eV leads to the appearance of a polycondensate containing, for example, up to 22 carbon atoms (Cottin et al., 2003), (Dworkin et al., 2004). The complex hydrocarbons observed in the experiments (Dworkin et al., 2004) are similar to natural bitumen (a mixture of aliphatic and aromatic hydrocarbons), which, interestingly, are considered as quite adequate analogues for reproducing the photometric characteristics of comets and surfaces of some asteroids (Moroz et al., 1998). It should also be emphasized that PAH and amino acid-related compounds are also formed in the above experiments (Cottin et al., 2003), (Dworkin et al., 2004).

To calculate the UV radiation inside the clouds of the circum-nuclear regions of active galaxies where narrow emission lines (so called Narrow Line Regions - NLRs) are formed, one can use the Cloudy computer program designed to model the ionization and physical-chemical structure of gas-dust clouds and described in Ferland et al. (2013).

This article is devoted to the description of some observational data and theoretical modeling of molecular clouds of active galaxies responsible for the existence of ices. The conditions under which that is possible can be interesting not only from the point of view of the possibility of the formation of various species, which in itself is important, but also as observational criteria, to distinguish galaxies with different levels of activity especially in circum-nuclear regions. Further, the observational data (Spitzer's archive) concerning ices in active galaxies are presented in Section 2, with the optical thicknesses of the absorption lines of water ice and silicates measured by us in the spectra, which were later transformed into column densities of ice and neutral hydrogen. The calculations of the radiation field with the given NLR parameters and various external conditions were implemented using Cloudy and discussed in Section 3. The calculations of the water ice content in dust particles are described and discussed in comparison with the observations in Section 4, and the conclusion is given in section 5.

2. Observational data

In this article we selected 22 galaxies from our list of active galaxies observed by the Spitzer observatory, whose spectra contain absorption bands of water ice and silicates (Table 1, see also Fig.1). The list of galaxies is given in Table. 1, together with the coordinates and possible classification. Optical thicknesses at the 6.0 μm , and 9.7 μm bands were measured according to the scheme proposed in (Spoon et al., 2002), (see also Fig. 2). In Table 2 optical thicknesses of water ice and neutral hydrogen are converted to the column densities according to (Hagen et al., 1983), (Bohlin et al., 1978), (Roche, 1984).

After determining the optical thicknesses of the ice (6.0 μm) and silicates (9.7 μm), the column densities of ice and neutral hydrogen can be calculated, respectively, by the relations (Hagen et al., 1983), (Roche, 1984), (Bohlin et al., 1978).

$$N(\text{ice}) = \frac{\tau(\text{ice})}{4.2 \cdot 10^{-20} \text{cm}^2 \cdot \text{molecules}^{-1}} \quad (1)$$

$$N(H) = \tau(\text{silicate}) \cdot 3.5 \cdot 10^{22} \text{cm}^2 \quad (2)$$

Table 1: A sample of 22 galaxies from the Spitzer archive, with optical thicknesses measured by us according to (Spoon et al., 2004)

Number	Name	RA	Dec	Type	Redshift	$\tau(ice)$	$\tau(silicate)$
1	IRAS06035-7102	90.72346	71.05331	AGN	0.0795	0.721	0.407
2	IRAS06206-6315	95.25333	-63.28978	AGN	0.0924	0.688	0.464
3	UGC5101	143.96521	61.35314	AGN	0.0394	0.627	0.320
4	IRASF09414+4843	146.176	48.48778	AGN	0.0553	0.875	0.522
5	IRAS10378+1109	160.12154	10.88825	AGN	0.1363	0.531	0.567
6	IRASF13279+3401	202.56346	33.77483	AGN	0.0213	0.815	0.143
7	Mrk273	206.1755	55.88697	AGN	0.0378	0.717	0.143
8	IRAS14348-1447	219.40946	-15.00683	AGN	0.0827	0.611	0.520
9	IRAS17068+4027	257.13383	40.39117	AGN	0.179	0.686	0.571
10	IC5298	349.00279	25.55675	AGN	0.0274	0.688	0.714
11	IRAS00199-7426	5.52921	-74.16158	Comp	0.0964	0.742	0.667
12	IRASF02417-0857	41.06071	-8.73914	Comp	0.0553	0.701	0.381
13	IRASF02437+2122	41.66304	21.58622	Comp	0.0233	0.850	0.208
14	IRAS04103-2838	63.08138	-28.50678	Comp	0.1175	0.876	0.902
15	IRAS04114-5117	63.18717	-51.1595	Comp	0.1246	0.757	0.714
16	IRASF08344+5105	129.51512	50.91917	Comp	0.0967	0.807	0.636
17	IRAS10494+4424	163.09829	44.14625	Comp	0.0921	0.877	0.700
18	IRAS13469+5833	207.16762	58.31442	Comp	0.1578	0.647	0.857
19	IRAS16487+5447	252.44533	54.70983	Comp	0.1038	0.711	0.455
20	IRAS17028+5817	255.92462	58.229	Comp	0.1061	0.851	0.750
21	IRAS20087-0308	302.84942	-2.99744	Comp	0.1057	0.803	0.500
22	IRAS23230-6926	351.51487	69.17231	Comp	0.1063	0.700	0.400

Table 2: The column densities of water ice and neutral hydrogen

Number	$\tau(ice)$	$\tau(sil)$	N(ice)	N(hydrogen)	N(ice)/N(hydrogen)
1	0.721	0.407	1.72E+019	1.42E+022	0.00121
2	0.688	0.464	1.64E+019	1.63E+022	0.00101
3	0.627	0.320	1.49E+019	1.12E+022	0.00133
4	0.875	0.522	2.08E+019	1.83E+022	0.00114
5	0.531	0.567	1.26E+019	1.98E+022	0.000637
6	0.815	0.143	1.94E+019	5.00E+021	0.00388
7	0.718	0.143	1.71E+019	5.00E+021	0.00342
8	0.611	0.520	1.46E+019	1.82E+022	0.000800
9	0.686	0.571	1.63E+019	2.00E+022	0.000817
10	0.688	0.714	1.64E+019	2.50E+022	0.000655
11	0.742	0.667	1.77E+019	2.33E+022	0.000757
12	0.701	0.381	1.67E+019	1.33E+022	0.00125
13	0.850	0.208	2.02E+019	7.26E+021	0.00279
14	0.876	0.902	2.09E+019	3.16E+022	0.000661
15	0.757	0.714	1.80E+019	2.50E+022	0.000721
16	0.807	0.636	1.92E+019	2.23E+022	0.000863
17	0.877	0.700	2.09E+019	2.45E+022	0.000853
18	0.647	0.857	1.54E+019	3.00E+022	0.000514
19	0.711	0.455	1.69E+019	1.59E+022	0.00106
20	0.851	0.750	2.03E+019	2.63E+022	0.000772
21	0.803	0.500	1.91E+019	1.75E+022	0.00109
22	0.700	0.400	1.67E+019	1.40E+022	0.00119

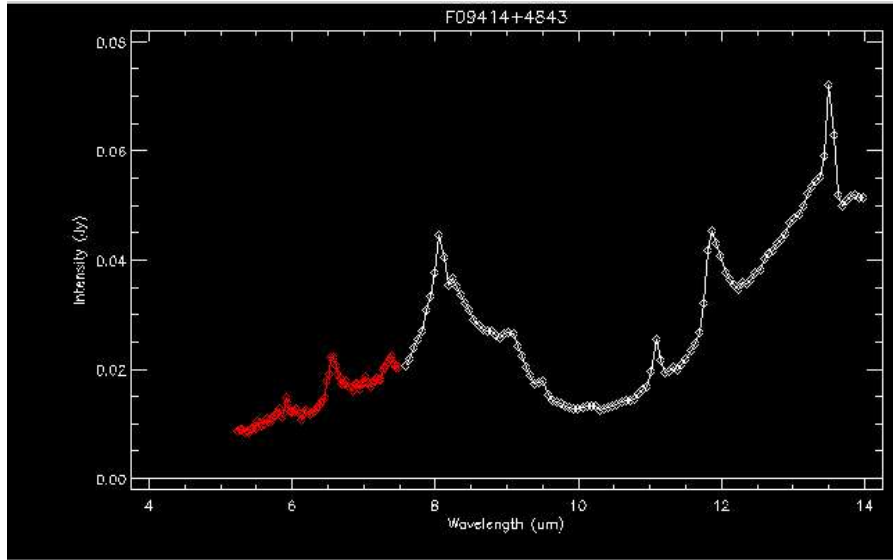


Figure 1: Absorption bands of water ice ($6.0 \mu\text{m}$) and silicates ($9.7 \mu\text{m}$) for active galaxy IRAS F 0494-4843

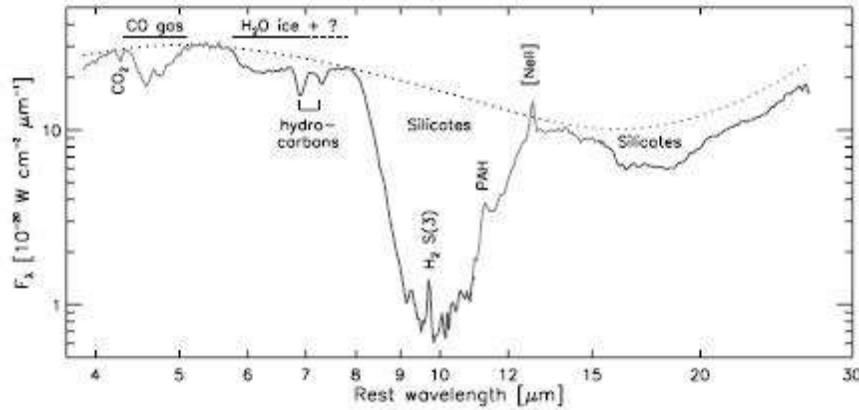


Figure 2: An example of a continuum drawing when measuring optical thicknesses according to (Spoon et al., 2004)

3. Constraining input values for column densities and ionization parameter

The data from Table 2 are analyzed in Fig.3, namely, the scattered values of $N(\text{ice})$ depending on $N(\text{H})$ values for 22 active galaxies are shown.

It turns out that the column densities of ice are between 1.3 and 2.2 (in units of 10^{19} cm^2) with $N(\text{H})$ values between 5 and 30 (in units of 10^{21} cm^2). The presence of ice in active galaxies, at least in the clouds of the near-nuclear regions, does not always depend on the type of activity, although it can be said that in Seyfert galaxies, ice survives worse than in galaxies with intense star formation or in merging galaxies. In this case, it is desirable to have a quantitative criterion for the survival of ice under the harsh conditions of active galaxies. It is clear that the ice content is sensitive to direct electromagnetic and corpuscular radiation, as well as to the physical parameters of the medium, for example, the gas and dust temperatures supported by these radiation. The conditions for the survival of ice can theoretically be clarified by means of numerical physicochemical models of interstellar gas-dust clouds with the correct description for the effects of radiation transfer, like in Cloudy code (see below).

First, we determine the total number of hydrogen ionizing quanta Q_H , which cause the recombination lines H_α and H_β in the gaseous nebulae of the NLR regions. In the SDSS spectra, the

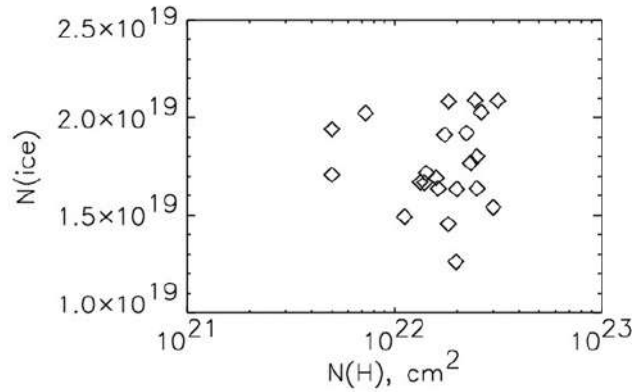


Figure 3: The $N(\text{ice})$ values depending on $N(\text{H})$ for 22 active galaxies from Table 2

$H_\alpha(6563\text{\AA})$ line is resolved from the [NII] lines 6548 and 6584 \AA . In the NLR, typical velocities in the medium are of the order of 400 km/s (Netzer, 2013), then the line widths can be estimated usually as $\Delta\lambda = \lambda \cdot z = \lambda \cdot v_{\text{ave}}/c = 8.8 \text{\AA}$. Other NLR parameters, characteristic sizes and concentration, were adopted, respectively, $r \sim 100 \text{ pc}$, and $n_e \sim 10 \sim 10^3 \text{ cm}^3$ (Netzer, 2013). Sometimes the so-called filling factor, which characterizes the raggedness of the medium, $f \sim 0.1$ or less. Next, we use $f \sim 1$. The distance to the galaxies was estimated by the redshift, $d = c \cdot z/H$, $H = 70 \text{ km/s/Mpc}$.

We use the standard photoionization model of the hydrogen cloud (a so-called case B at $T_e = 10^4 \text{ K}$), in which the recombination coefficient for all levels except the first is $\alpha_B = 2.59 \cdot 10^{-13} \text{ cm}^3 \text{ s}^{-1}$, and the effective recombination coefficients for the H_α and H_β lines are equal to $\alpha_{\text{eff}}(H_\alpha) = 1.17 \cdot 10^{-13}$ and $\alpha_{\text{eff}}(H_\beta) = 0.301 \cdot 10^{-13}$ (in units $\text{cm}^3 \text{ s}^{-1}$), respectively. Then, for Q_H we have (Osterbrock & Ferland, 2006)

$$Q_H = 4\pi d^2 \frac{F(H_\alpha)}{h\nu(H_\alpha)} \frac{\alpha_B}{\alpha_{\text{eff}}(H_\alpha)}, Q_H = 4\pi d^2 \frac{F(H_\beta)}{h\nu(H_\beta)} \frac{\alpha_B}{\alpha_{\text{eff}}(H_\beta)}. \quad (3)$$

Further, we determine the ionization parameter

$$U = \frac{Q_H}{4\pi r^2 n_H c}. \quad (4)$$

4. The radiation field inside the molecular cloud

It should be noted that only for photons with energies above 13.6 eV there are no internal sources inside the cloud, while photons in the energy range 6–13.6 eV are still emitted and are important in the processes of ionization (of some elements), thermal and photochemical balance of both gas and dust. These photons participate in many secondary processes which occur with such intensity that their contribution is obligatory when considering many problems of cloud physics and chemistry, including ice content in dust particles depending on the radius of the cloud. It is interesting to note that the absence of ices outside the clouds where the lifetime of the ice is much shorter than the characteristic time of chemical reactions that transform the ice mixtures into a stable form is due to intense UV radiation in the entire spectrum, while in the inner regions where ices are present, their content is regulated by the UV radiation field mainly at 10 eV. The only significant source of such photons inside the clouds, far from the boundary, is the process of generation of secondary radiation as a result of the excitation of hydrogen molecules by CR (protons with energies of the order of MeV and higher), with subsequent emission of photons in Lyman and Werner bands predominantly at 10 eV. Details of corresponding theory for the first time were considered by (Prasad, 1983) and in subsequent publications of many authors (Ferland et al., 2013) and references therein). Also (Ferland et al., 2013) have implemented it into the Cloudy model and corresponding code.

In this case molecular clouds in the circumnuclear regions of the active galaxy are considered similar to the clouds of our Galaxy, that is interstellar gas-dust objects with a dominant H_2 content

and characteristic values of concentration, size and temperatures of the order of $n_H \sim 10^3 - 10^4 \text{ cm}^{-3}$, $L \sim 30 \text{ pc}$ and $T \sim 10 - 100 \text{ K}$, respectively.

Dust is of the order of less than 1/100 by mass. Dust particles with silicate or graphite cores with sizes of the order of 0.01-0.1 μm have mantles of several 0.1 μm thick, consisting of stable polymers of unknown nature and/or ices of volatile compounds, primarily water, carbon oxides, and other, less abundant molecules. The one-dimensional physicochemical model of the cloud, including the radial dependence of the flux of the electromagnetic radiation field in this work, was calculated by the CLOUDY program (Ferland et al., 2013). The model includes the full calculated ionization atomic-molecular and thermal structures of the gas and dust components, as well as the spectral distribution of the radiated energy, including several million emission lines from the radio to the gamma range.

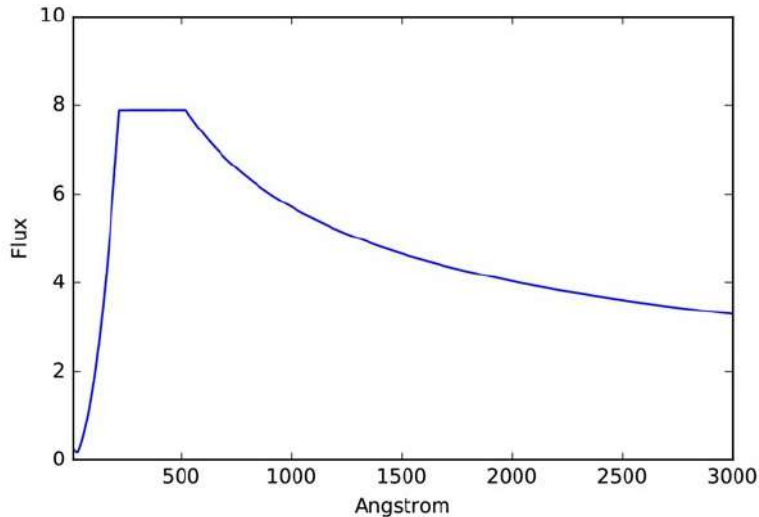


Figure 4: The hard incident radiation in the case of starbursts

The state of the medium, under the influence of external electromagnetic and particle radiation, was assumed to be stationary and homogeneous, with the initial atomic composition of a given metallicity of the first 30 elements, from hydrogen to elements of the iron group. Chemical reactions in the gas and on the surface of the dust particles lead to the kinetic equilibrium between atoms (585 with all ions) and 83 molecules, molecular ions and radicals in the gas, and, specifically, for H_2O , CO and OH species in the solid phase, that is Cloudy calculates their content not only in gas, but also in ice mantle of dust particles. In this case, the program uses the currently most accurate reaction rate coefficients and interaction cross sections between all species including interaction with radiation. It should be noted that the kinetic equations are solved for multilevel models of atoms, ions and molecules, and the effects of radiation transfer in the continuous spectrum and for the most important optically thick spectral lines are taken into account in the approximation known as *escape probability*. This approximation provides the necessary accuracy of calculations in the used static and homogeneous cloud model. Thus, a one-dimensional cloud model with the most complete consideration for all possible elementary processes, was used to calculate the radiation field and ice content along the radius using Cloudy. The cloud distance from the central source in all models was taken to be 15-20 pc, the hydrogen concentration was $10^3 - 10^4 \text{ cm}^{-3}$, and the values of the ionization parameter U , was chosen as $\lg(U) = -2, -3$ (Netzer, 2013). Hydrogen ionization rates by energetic protons with energies of several MeV and higher, ζ , (s^{-1}), corresponds to the our galactic value ($\lg(\zeta) = -16$). The values of hydrogen column densities were chosen according to Fig.3.

As the longest chemical timescale of water and water ice formation is much less ($t \sim 10^9/n_H \sim 10^5 - 10^6$ years) as compared with the NLR clouds timescale of about 10^8 years (a limit following from the condition of exhaustion of the star formation gas (Stasińska et al., 2015)) one can use stationary models for description of the clouds. Thus we model clouds in steady-state conditions with constraints following from observational data.

The spectral energy distribution of radiation sources were chosen corresponding to the AGN mode

of Cloudy obtained by their authors by combining available observations (Ferland et al., 2013). The intensity of the radiation was varied by changing the initial parameters presented in Table 3. The spectral distribution of the radiation incident on the cloud is shown in Fig. 4.

5. On the survivability of ices in the interstellar clouds of active galaxies

Now we turn to the question of the sensitivity of the water ice content to the spectral shape of radiation incident on the cloud.

Ices are sensitive to the presence of direct irradiation by electromagnetic and corpuscular radiation, as well as to the values of the medium parameters determined by these radiations, for example, by the temperature of gas and dust.

Now we present results of our calculated models (Table 3).

Table 3: The calculated column densities of water ice for some models

Model	$\lg(r_0)$	$\lg(n)$	$\lg(U)$	$N(H)$	$N(ice)$
1	19.65	4	-3	3.00E+23	1.00E+20
2	19.65	4	-2	3.00E+23	1.10E+19
3	20.48	3	-2	1.00E+22	2.00E+19
4	20.48	3	-2	9.00E+22	1.20E-01

As we see, the ice content depends on the value of the ionization parameter, and is inversely proportional to its value, as was shown in (Yeghikyan, 2016). It should be noted that first 2 models correspond to the concentration 10^4 cm^{-3} and have hydrogen column densities larger than in Fig. 3. Models 3,4 have the concentration of 10^3 cm^{-3} and smaller hydrogen column densities in accordance with Fig.3.

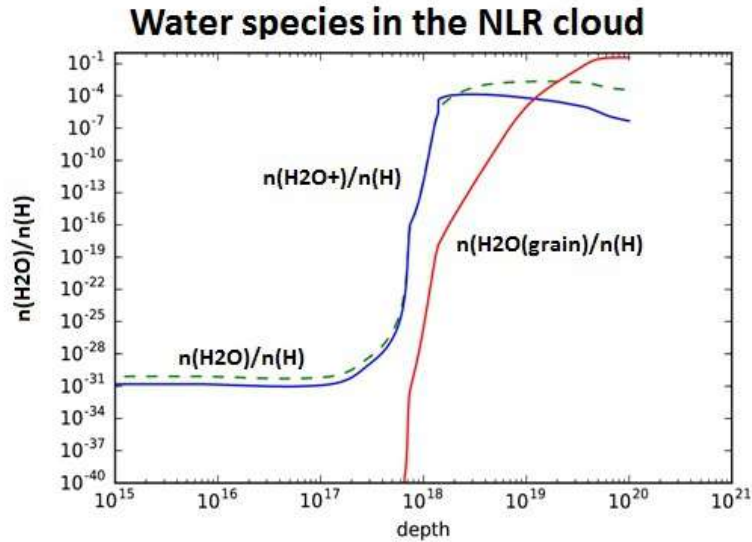


Figure 5: Water ice and related abundances in model 3

It should be underlined that there is a strong difference between shapes of incident radiation for starburst galaxies and AGN. In the case of starbursts it is due to the total amount of thermal radiation of massive and hot stars while AGN have a contribution in the hard part of the spectrum because of an accretion disk radiation. Now we will increase the contribution of hard UV and X-ray radiation as shown in Fig. 6. Results are shown in Table 3.

The hardening of the incident radiation intensity similar to that observed in typical AGN is de-

scribed (in Cloudy) by

$$I_\nu = \nu^{\alpha_{UV}} \exp(-h\nu/kT_{BB}) \exp(-kT_{IR}/h\nu) + a\nu^{\alpha_X}, \quad (5)$$

where $\alpha_{UV} = -0.5$ is the low-energy slope of the continuum at $\approx 1Ryd$ (so-called Big Bump component), $T_{BB} = 1.5 \cdot 10^5 K$ - the temperature of the bump. Also the shape of spectral distribution is regulated by non-thermal parameters, related with UV and X-ray parts, namely by $\alpha_{0X} = -1.4$ and $\alpha_X = -1$, where the 1-st parameter is the X-ray to UV ratio and the 2-nd parameter is the slope of the X-ray component.

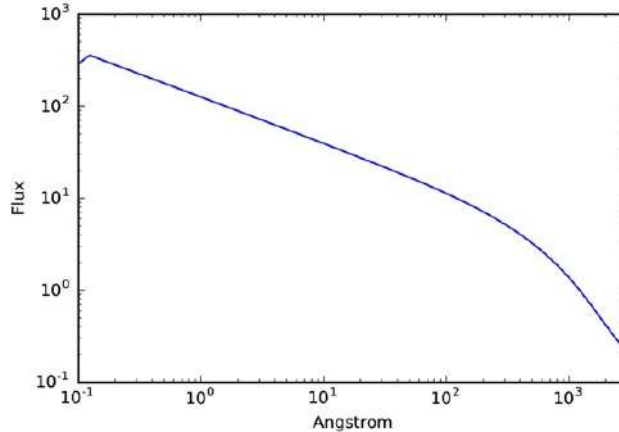


Figure 6: The hard incident radiation from AGN

The calculation results are presented in Table 3 which shows the column densities of water ices for different models. First 2 models are adopted from (Yeghikyan, 2016) and just supported observed column densities of starbursts for typical parameters of circumnuclear clouds. Models 3 and 4 are slightly different and influenced by two type of incident radiation like starburst (model 3) and AGN (model 4). One can easily seen that radiation from the accretion disk of the AGN is enough to completely disrupt water ice wherever it is in the cloud. Also intensity of X-ray and UV part of the incident spectrum should be about 100 times larger then that of in the starburst case.

6. Conclusion

Earlier we have shown (Yeghikyan, 2016) that ices in active galaxies regardless of type of galaxy (starburst or AGN) could not survive if cosmic ray fluxes are about 1000 times larger than in the Galaxy. Now we show that if the X-ray and UV fluxes are about 100 times larger which is typical for AGNs as compared with starbursts water ice is completely absent and could not be observed. In the case of starbursts the incident radiation is much softer and ices are present and even may be close to the observed values. But in Table 1 we have typical AGN or composite galaxies and ices are observed. These are preliminary model calculations and such analysis should be carried out for all other galaxies from Table 1 to be ready for further statistical considerations.

References

- Bohlin R. C., Savage B. D., Drake J. F., 1978, *ApJ*, **224**, 132
- Boogert A. C. A., Gerakines P. A., Whittet D. C. B., 2015, *ARA&A*, **53**, 541
- Cottin H., Moore M. H., Bénilan Y., 2003, *ApJ*, **590**, 874
- Dworkin J. P., Seb Gillette J., Bernstein M. P., Sandford S. A., Allamandola L. J., Elsila J. E., Ryan McGlothlin D., Zare R. N., 2004, *Advances in Space Research*, **33**, 67

- Ferland G. J., et al., 2013, *RMXAA*, [49](#), [137](#)
- Hagen W., Tielens A. G. G. M., Greenberg J. M., 1983, *AAS*, [51](#), [389](#)
- Imanishi M., Dudley C. C., Maloney P. R., 2006, , [637](#), [114](#)
- Kaiser R. Roessler K., 1998, *ApJ*, [503](#), [959](#)
- Kaiser R. I., Roessler K., 1997, *ApJ*, [475](#), [144](#)
- Kaiser R. I., Eich G., Gabrysch A., Roessler K., 1997, *ApJ*, [484](#), [487](#)
- Moroz L. V., Arnold G., Korochantsev A. V., Wäsch R., 1998, *Icarus*, [134](#), [253](#)
- Netzer H., 2013, "The Physics and Evolution of Active Galactic Nuclei", Cambridge, UK: Cambridge University Press
- Osterbrock D. E., Ferland G. J., 2006, "Astrophysics of gaseous nebulae and active galactic nuclei", CA: University Science Books
- Prasad S. Tarafdar S., 1983, *Astrophys. J.*, [267](#), [603](#)
- Roche H. Aitken D., 1984, *MNRAS*, [208](#), [481](#)
- Spoon H. W. W., Keane J. V., Tielens A. G. G. M., Lutz D., Moorwood A. F. M., Laurent O., 2002, *A&A*, [385](#), [1022](#)
- Spoon H. W. W., et al., 2004, *ApJS*, [154](#), [184](#)
- Stasińska G., Costa-Duarte M. V., Vale Asari N., Cid Fernandes R., Sodr e L., 2015, *MNRAS*, [449](#), [559](#)
- Tielens A. G. G. M., 2005, "The Physics and Chemistry of the Interstellar Medium", ISBN 0521826349. Cambridge, UK: Cambridge University Press
- Yeghikyan A., 2016, *ASP Conf. Ser.*, [505](#), [144](#)
- Yeghikyan A., Martirosyan J., 2018, *Communications of the Byurakan Astrophysical Observatory*, [65](#), [303](#)

Acknowledgements

The authors acknowledge the partial support of this work from Ambartsumian research award in 2019

AGN Activity in Brightest Cluster Galaxies (BCGs)

Süleyman Fişek^{*1,2}, Sinan Aliş^{1,2}, E. Kaan Ülgen¹, and F. Korhan Yelkenci¹

¹Istanbul University, Science Faculty, Department of Astronomy and Space Sciences, Istanbul, Turkey

²Istanbul University Observatory Application and Research Center, Istanbul, Turkey

Abstract

The aim of our study is to classify the Brightest Cluster Galaxies (BCG), which are the brightest and most massive galaxies in the universe and to determine fraction of BCGs showing AGN activity. Within the scope of the study, we combine BCGs from galaxy cluster catalogs which presented by Hao et al. (2010) and Wen et al. (2009) constructed from the SDSS (Sloan Digital Sky Survey) data and BCGs identified from CFHTLS (Canada-France-Hawaii Telescope Legacy Survey) Deep fields (Alis, 2009). Our combined sample contains 42490 BCGs. We determine activity types of BCGs by means of BPT diagrams and WISE color-color diagrams. 140 BCGs show AGN activity out of 42490. In addition, we calculated star formation rates (SFR) by using H α emission lines for 5569 BCGs with suitable spectral data and investigated the correlation between SFR and redshift.

Keywords: *Galaxy: AGN - Galaxy: BCG - Galaxy: evolution - Galaxy: star formation*

1. Introduction

BCGs are the brightest and the most massive galaxies in the universe and usually located in the center or near the center of rich galaxy clusters (Jones & Forman, 1984, Smith et al., 2005). Most of the BCGs are red elliptical galaxies and star formation activities are almost stopped (Edwards et al., 2007). The evolutionary processes of BCGs is still not fully understood; galaxy-galaxy interactions and galaxy mergers are thought to be effective for the process of formation of these galaxies where there is intense interactions (Edwards et al., 2007).

As a result of these interactions within the cluster, an increase in the star formation activity of the BCGs can be observed, unlike the other elliptical galaxies in the cluster (Liu et al., 2012, O'Dea et al., 2008, Pipino et al., 2009). Investigating star formation activity in BCGs can help us to understand the evolution of the cluster and environment as a function of redshift.

2. Data

BCGs examined in this study collected from two different datasets. 89 BCGs were determined by Aliş et al. (Alis, 2009, Aliş et al., 2012) constitute our first dataset. These galaxies identified using a set of 159 galaxy cluster identified by Olsen et al. (2007) using five bands (u, g, r, i, z) from the CFHTLS-Deep Survey.

The second dataset used in our study are constructed from Hao et al. (2010) and Wen et al. (2009), where galaxy clusters identified from the SDSS. In the list given by Wen et al. (2009), 39716 galaxy clusters in the range of $0.05 < z < 0.6$ were determined using SDSS DR6 data. Hao et al. (2010) listed 55427 galaxy clusters in the range of $0.1 < z < 0.55$ using DR7 data. When the lists are combined, with overlapping galaxy clusters taken into account, the total number of galaxy clusters become 82164. Merged cluster catalog of CFHTLS and SDSS contains 82253 clusters hence BCGs.

*sfisek@istanbul.edu.tr

In this study, emission line fluxes of $H\alpha$ [6562], $H\beta$ [4861], $OIII$ [5006], OI [6300], NII [6583], SII [6716] and spectroscopic redshifts of BCGs were obtained from the SDSS DR12 (i.e. *emissionLinesPort*) (<http://www.sdss.org/dr12/>). These emission line fluxes are used to determine the activity type of BCGs and also to calculate the star formation rates.

For the 42490 BCGs out of 82253 we could obtain spectroscopic data from SDSS. First we keep fluxes with ($F(H\alpha) > 0$) for SFR calculation. In order to use the most reliable flux measurements, we eliminated the flux values with associated errors very high. For this purpose, we only used flux measurements with a relative error less than 50% for $H\alpha$. Besides flux error we also used signal to noise ratio (S/N) for keeping high quality fluxes. In a similar study [Liu et al. \(2012\)](#) used $S/N > 3$. Therefore, we created two subsamples one is with $S/N > 3$ and the other one is with $S/N > 15$. In both samples we kept the fluxes with relative errors less than 50%.

Among 42490 BCGs with relevant flux measurements, there are 1137 galaxies satisfying the flux error and S/N criteria and only 143 of them can be used in the BPT diagram. When we loose the S/N criteria as $S/N > 3$, 5613 galaxies with appropriate fluxes for SFR calculation and 410 galaxies suitable for BPT diagram remain.

The infrared photometric data used in this study were obtained from the AllWISE catalog, which is the all sky survey by WISE (Wide-field Infrared Survey Explorer) satellite. We obtained W1, W2, W3 and W4 infrared magnitudes for our galaxies from NASA/IPAC Infrared Science Archive (<http://irsa.ipac.caltech.edu/Missions/wise.html>).

3. Method

3.1. Determining Activity Types of Galaxies

In this study, we use two different methods to determine the activity types of BCGs.

BPT Diagram:

The first method is the BPT diagram ([Baldwin et al., 1981](#)). In this diagram, it is possible to classify galaxies according to their activity by using $H\alpha$ [6562], $H\beta$ [4861], $OIII$ [5007], OI [6300], NII [6583], SII [6717] emission line fluxes. In addition, the BPT diagram is a tool used in the literature to determine whether galaxies show star formation activity.

WISE Color - Color Diagram:

From the photometric data obtained by the WISE satellite, the W1 (3.4μ) and W2 (4.6μ) bands are sensitive to the stellar mass of galaxies and the W3 (12μ) band is sensitive to the star formation rates ([Cluver et al., 2014](#), [Fraser-McKelvie et al., 2014](#)).

[Cluver et al. \(2014\)](#) matched the GAMA <http://www.gama-survey.org> Survey and WISE data to examine the infrared properties of more than 110,000 galaxies. Infrared color - color diagrams ($(W2 - W3) - (W1 - W2)$) were created where galaxies with $W2 - W3 > 1.5$ show mostly star formation activity.

3.2. Star Formation Rate (SFR) Calculation

The $H\alpha$ emission flux is one of the most reliable and widely used tool to determine star formation in galaxies. The $H\alpha$ line, seen as an emission in a galaxy spectrum, is an indicator of the star formation activity in galaxies.

In this study, we calculated star formation rates of the galaxies using (1) equation given by [Kennicutt \(1998\)](#).

$$SFR(M_{\odot}/\text{year}) = 7.9 \times 10^{-42} \times L(H\alpha) \text{ (ergs s}^{-1}\text{)} \quad (1)$$

As a first step, emission line fluxes obtained from SDSS needed to be converted to $H\alpha$ luminosity. Thus, we computed the distances of our BCGs using their spectroscopic redshifts. Within the Λ CDM cosmology, we determined the luminosity distances with $\Omega_m = 0.3$, $\Omega_\Lambda = 0.7$ ve $H_0 = 70$ km/s/Mpc (Hogg, 1999). The distance calculations were made using the Python version of Ned Wright's cosmology calculator (<http://www.astro.ucla.edu/~wright/CosmoCalc.html>) (Wright, 2006). This Python program used by adapting it into the SFR script that we developed (Fişek, 2018).

Once the distances are known it is straightforward to obtain $H\alpha$ luminosities by the equation (2):

$$L(H\alpha)(\text{ergs } s^{-1}) = 4 \times \pi \times d^2 \times F(H\alpha) \quad (\text{ergs } cm^{-2}s^{-1}) \quad (2)$$

After calculating the $H\alpha$ luminosity, the star formation rates were calculated for each galaxy by using equation (1).

4. Results

4.1. BCGs by Type

Using by BPT Diagram:

In this study, We show the BPT diagram produced from the spectra with $S/N > 15$ is in Figure 1 for the galaxies we have examined in this study.

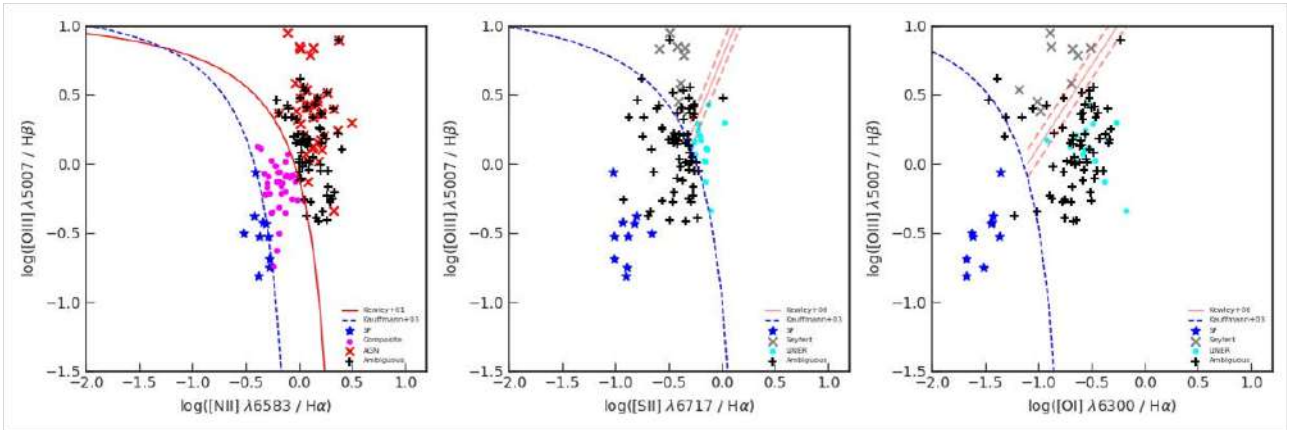


Figure 1. BPT diagram for galaxies with flux error less than 50% and $S/N > 15$. The BPT diagrams show star forming galaxies (blue stars - SF), composite galaxies (pink dots - Comp), AGNs (red crosses), Seyfert Galaxies (gray crosses), LINER Galaxies (turquoise crosses), and "ambiguous" galaxies (black pluses).

Using by WISE Diagram:

Galaxies classified by the BPT diagram are shown in the WISE color - color diagram in Figure 2. 18 galaxies with $S/N > 15$ in the BPT diagram couldn't be used in the WISE color - color diagram since the WISE magnitudes couldn't be measured for these galaxies. In addition, all the galaxies identified as SF in the BPT diagram are also determined as SF according to the WISE color - color diagrams.

4.2. Star Formation Rates of BCGs

SFR of 5569 ($S/N > 3$) and 1136 ($S/N > 15$) galaxies were determined and the distribution of these SFRs are shown in Figure 3a.

Correlation between SFR and Redshift:

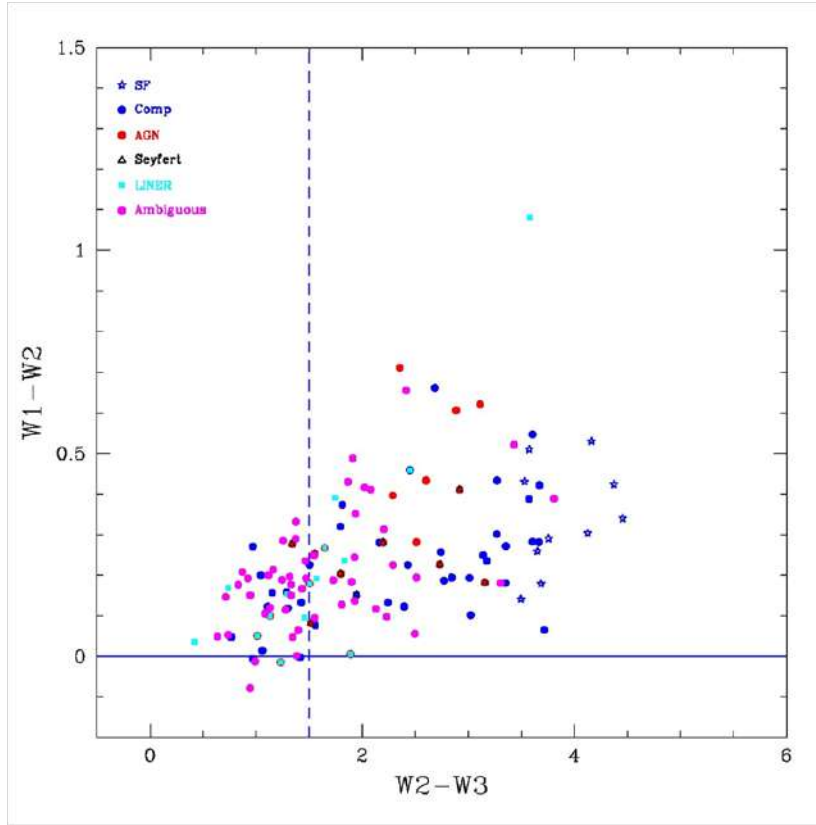


Figure 2. WISE color - color diagram for galaxies with flux error less than 50% and $S/N > 15$. The dashed line indicates $W2 - W3 = 1.5$. In the graph, galaxies are marked according to the BPT classes.

In order to check whether SFRs of BCGs evolve with redshift, we computed the mean SFRs with redshift bins of 0.1. When there are less galaxies than 10 in any bin, corresponding statistical values are not used. Figure 3b shows the SFR as a function of redshift.

5. Discussion and Conclusion

In this study, we investigated star formation activity of BCGs identified from CFHTLS and SDSS.

There is no clear correlation between the SFR of BCGs and their redshift. Similar result was presented by [Cooke et al. \(2014\)](#) in their study of 42 BCGs in the same redshift range as in this study. However, as shown in Figure 3b, it can be seen that the mean SFRs obtained after discarding outliers (i.e. 3σ) decrease towards lower redshifts. This is consistent star formation history of the universe as given by [Madau & Dickinson \(2014\)](#). However, BCGs can be expected to behave differently from this general trend due to their environment. Environment plays an important role especially in the galaxy clusters with cooling cores. There have been studies where BCGs in cooling core clusters show induced star formation activity ([Pipino et al., 2009](#), [Voit, 2005](#)). However, this behaviour is not well understood and needs to be investigated further.

Largest spectroscopic data available so far is the SDSS but with SDSS it is not possible to reach redshifts beyond $z \sim 0.5$. Thus, wide area spectroscopic surveys with larger telescopes are needed in order to understand evolution of these galaxies. It seems this will become possible with the Mauna Kea Spectroscopic Explorer (MSE) in the near future.

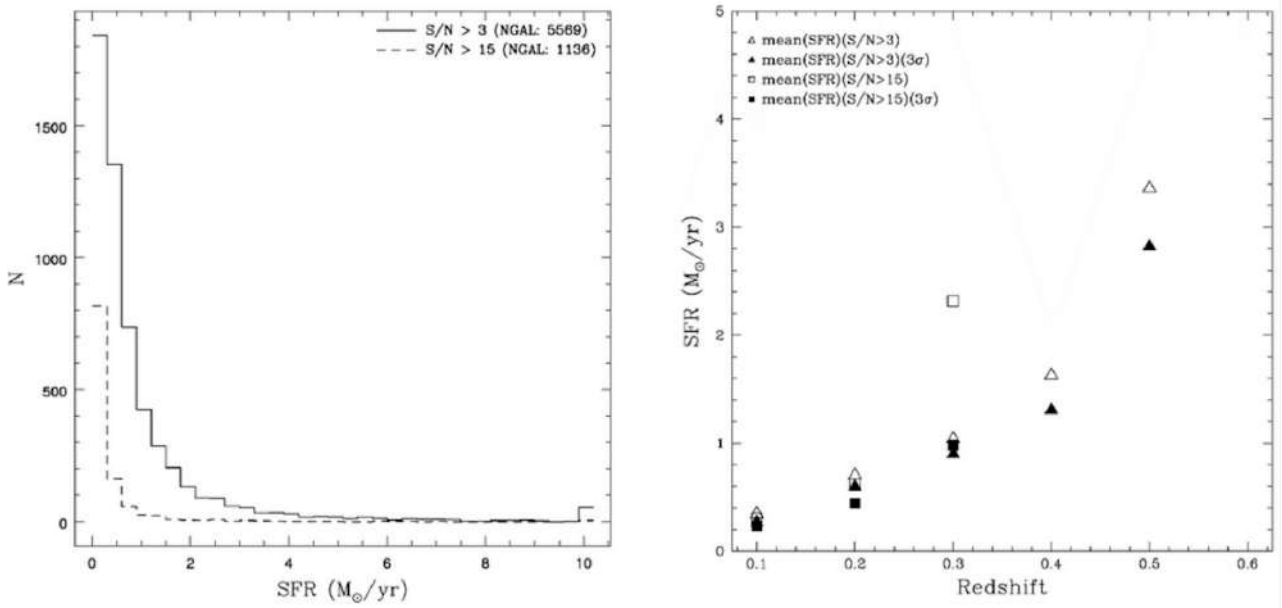


Figure 3. **(a)** Distribution of calculated SFR values (for $SFR < 10 M_{\odot}/\text{year}$). The solid line indicates galaxies with $S/N > 3$ and the dashed line indicates galaxies with $S/N > 15$. **(b)** Variation of the mean SFR of the galaxies with redshift for the galaxies with flux error less than 50% and $S/N > 3$ or $S/N > 15$. Empty triangles represent the mean SFR for galaxies with $S/N > 3$ and empty squares are for galaxies with $S/N > 15$. The filled symbols show values when outliers (i.e. 3σ) are not taken into account.

6. References

References

- Alis S., 2009, Publications de l'Observatoire Astronomique de Beograd, [86](#), [309](#)
- Aliş S., Yelkenci K., Benoist C., Limboz F., 2012, XVIII. National Astronomy Congress of TURKEY Proceedings Book, p. 345
- Baldwin J. A., Phillips M. M., Terlevich R., 1981, Publications of the Astronomical Society of the Pacific, [93](#), [5](#)
- Cluver M. E., Jarrett T. H., Hopkins A. M., et al. 2014, The Astrophysical Journal, [782](#), [17](#)
- Cooke K. C., O'Dea C. P., Baum S. A., et al. 2014, The Astrophysical Journal, [833](#), [10](#)
- Edwards L. O. V., Hudson M. J., Balogh M. L., Smith R. J., 2007, The Astrophysical Journal, [379](#), [100](#)
- Fişek S., 2018, Istanbul University, Graduate School of Engineering and Science, [p. 1](#)
- Fraser-McKelvie A., Brown M. J. I., Pimblet K. A., 2014, Monthly Notices of the Royal Astronomical Society, [444](#), [63](#)
- Hao J., McKay T. A., Koester B. P., et al. 2010, The Astrophysical Journal Supplement Series, [191](#), [254](#)
- Hogg D. W., 1999, arXiv:astro-ph, [5116](#)
- Jones C., Forman W., 1984, The Astrophysical Journal, [276](#), [38](#)
- Kennicutt R. C. J., 1998, Annual Review of Astronomy and Astrophysics, [36](#), [189](#)
- Liu F. S., Mao S., Meng X. M., 2012, Monthly Notices of the Royal Astronomical Society, [423](#), [422](#)
- Madau P., Dickinson M., 2014, Annual Review of Astronomy and Astrophysics, [52](#), [415](#)
- O'Dea C. P., Baum S. A., Privon G., et al. 2008, The Astrophysical Journal, [681](#), [1035](#)
- Olsen L. F., Benoist C., Cappi A., et al. 2007, Astronomy & Astrophysics, [461](#), [81](#)
- Pipino A., Kaviraj S., Bildfell C., et al. 2009, Monthly Notices of the Royal Astronomical Society, [395](#), [462](#)
- Smith G. P., Kneib J. P., Smail I., et al. 2005, Monthly Notices of the Royal Astronomical Society, [359](#), [417](#)
- Voit G. M., 2005, Reviews of Modern Physics, [77](#), [207](#)
- Wen Z. L., Han J. L., Liu F. S., 2009, The Astrophysical Journal Supplement Series, [183](#), [197](#)
- Wright E. L., 2006, The Publications of the Astronomical Society of the Pacific, [118](#), [1711](#)

The MAGNUM survey: a high-resolution study of the complex nuclear environment of local Seyfert galaxies

Mingozzi M.^{*1,2}, Venturi, G.^{†3,2}, Mannucci F.^{‡2}, Marconi A.^{§4,2}, and Cresci G.^{¶2}

¹INAF - Osservatorio Astronomica di Padova, Padova, Italy

²INAF - Osservatorio Astrofisico di Arcetri, Florence, Italy

³PUC - Pontificia Universidad de Chile, Santiago de Chile

⁴Università di Firenze, Dipartimento di Fisica e Astronomia, Firenze, Italy

Abstract

The central regions of Seyfert galaxies, comprising broad and narrow line regions and the inner parts of galaxy disk and bulge, is characterized by a complex interplay among many physical effects. Specifically, it is shaped by the influence of the central black hole, producing ionization by an hard continuum and gas outflows. The integral-field spectrograph MUSE at the ESO VLT allows to carry out a detailed study of these regions to obtain their ionization, dynamical, and metallicity properties. Here we present some highlights of the MAGNUM survey which is designed to study the central regions of a sample of nearby ($D < 50$ Mpc) Seyfert galaxies. We describe the rationale of the survey, the data analysis techniques used to extract information on ionization and dynamics, and the results for one galaxy, Centaurus A.

1. Introduction

A variety of physical processes shape the observed distribution of galaxy properties: some of them account for galaxy growth (e.g., star formation, SF; galaxy merging), while others regulate this growth (e.g., energetic feedback from supernovae, SN and active galactic nuclei, AGN; ultraviolet, UV, radiation background). Indeed the evolution of a galaxy is a matter of synergy among these diverse physical processes. Metal poor gas is accreted from the intergalactic medium (IGM), the dilute reservoir that permeates the space between galaxies (McQuinn, 2016), triggering SF inside the galaxy. However, gas accretion and SF can also be the consequence of major and/or minor mergers. Stellar evolution, via SN explosions and stellar winds, provides chemical enrichment of the gaseous component of galaxies, referred to as the *interstellar medium* (ISM) or the *diffuse matter* (Klessen & Glover, 2016). Part of this enriched gas leaves the galaxy through galactic winds, enriching the circumgalactic medium (CGM), a large gas halo extending by hundreds of kpc in which galaxies are embedded, or the IGM, while the rest is recycled several times, in several stellar generations. Also dust plays a role in the physics of ISM, since it locks and releases metals, being continuously created and destroyed. Finally, the presence of a central AGN can largely influence the properties of the ISM and of the CGM, by heating, compressing and/or removing the gas through AGN-driven winds and jets (feedback). These processes that cause this gas flow in and out of galaxies providing the fuel both for SF and black hole (BH) accretion are known as the *galaxy baryon cycle*. Overall, since the ISM is the primary “repository” of galaxies, the study of its properties can give information on all the processes listed above (Maiolino & Mannucci, 2019).

Here we present the early results of the MAGNUM (Measuring AGN under MUSE microscope) survey (P.I. A. Marconi), using the IFU spectrograph MUSE on ESO/VLT to study the inner regions

*matilde.mingozzi@inaf.it

†gventuri@astro.puc.cl

‡filippo.mannucci@inaf.it, Corresponding author

§alessandro.marconi@unifi.it

¶giovanni.cresci@inaf.it

of a number of local AGNs with the aim of disentangling all these effects. The high spatial resolution obtained by MUSE ($\sim 0.6 - 0.8$ arcsec) and the large spatial coverage (~ 1 arcmin) will allow us to derive a complete picture of these galaxies, in terms of metallicity, ionization properties, dynamical status, and stellar populations.

This contribution is based on a number of published papers, namely [Cresci et al. \(2015b\)](#), [Venturi et al. \(2017\)](#), [Venturi et al. \(2018\)](#), and [Mingozi et al. \(2019\)](#), and on unpublished material from M. Mingozi's Phd Thesis (2019, University of Bologna), and G. Venturi's Phd Thesis (2018, University of Florence).

2. Galaxy sample, observations, and data analysis

MAGNUM galaxies have been selected to be observable from Paranal Observatory and with a luminosity distance $D < 50$ Mpc. In [Venturi et al. \(2020, in prep.\)](#) we present our sample, explaining in detail the selection criteria, data reduction and analysis, and investigating the kinematics of the ionized gas. We observed nine Seyfert galaxies, namely Centaurus A, Circinus, NGC 4945, NGC 1068, NGC 1365, NGC 1386, NGC 2992, NGC 4945 and NGC 5643. Each galaxy was observed for 0.5-1 hours.

The final datacube on each galaxy consists of $\sim 300 \times 300$ spaxels, for a total of over 90000 spectra with a spatial sampling of $0.2'' \times 0.2''$ and a spectral resolution going from 1750 at 4650 Å to 3750 at 9300 Å. The FOV of $1' \times 1'$ covers the central part of the galaxies, spanning from 1 to 10 kpc, according to their distance. The average seeing of the observations, derived directly from foreground stars in the final datacubes, is $\sim 0.6 - 0.8''$. The datacubes were analysed making use of a set of custom python scripts in order to fit and subtract the stellar continuum in each single-spaxel spectrum and fit the emission lines with multiple Gaussian components where needed. Here we summarise the main steps of the data analysis.

3. Stellar continuum fitting

First of all, a Voronoi adaptive binning, that is a technique that allows to obtain bins with different spatial extension but having a minimum signal-to-noise ratio (S/N) ratio in the data, was performed in order to achieve an average S/N per wavelength channel of 50 on the continuum under 5530 Å, where stellar features are more prominent. This threshold allows us to fit also the fainter regions of the FOV, preserving the maximum spatial resolution. In order to fit the stellar continuum and derive the systemic velocity and velocity dispersion of the stellar absorption lines, we applied the Penalized Pixel-Fitting (PPXF; [Cappellari & Emsellem 2004](#)) code on the Voronoi-binned spaxels. Basically, this fast and simple algorithm recovers galaxy stellar kinematics by fitting a template to an observed spectrum, applying the maximum penalized likelihood formalism. We employed as a template a linear combination of [Vazdekis et al. \(2010\)](#) synthetic spectral energy distributions for single stellar population models in the wavelength range 4750 – 7500 Å. Note that at this stage our aim is only to reproduce the shape of the stellar features and derive the bulk velocity and velocity dispersion of the stellar population, and not to get more detailed physical information from the models. Instead, a linear baseline was used to fit the local continuum around the [S III] $\lambda 9069$ emission line, since this line is not contaminated by underlying absorptions. The main emission lines lying in the selected wavelength range (H β - [O III] $\lambda\lambda 4959, 5007$ - [O I] $\lambda\lambda 6300, 64$ - H α - [N II] $\lambda\lambda 6548, 84$ - [S II] $\lambda\lambda 6717, 31$) were included in the fit as well, in order to better constrain the absorption underlying the Balmer lines. Fainter lines and regions affected by sky residuals were masked. The emission lines were fitted with one, two, three, or four Gaussian components according to the shape of the line profile, tying the velocity and width of each component to be the same for all the lines and leaving the intensities free to vary, apart from the [O III], [O I], and [N II] doublets, where an intrinsic ratio of 0.333 between the two lines was used (see e.g. [Storey & Zeippen 2000](#)).

A reduced χ^2 ($\tilde{\chi}^2$) selection to the different fits is made in each spaxel, in order to define where multiple components were really needed to reproduce the observed spectral profiles, with the idea of keeping the number of parameters of the fit as low as possible and using multiple components only in

case of complex non-Gaussian line profiles. This happens mainly in the central parts of the galaxies and in the outflowing cones.

The stellar continuum fit included also a multiplicative and an additive polynomials of degree m and a (with $7 < m < 10$ and $a = 2$) to account for any spectrum deformation not present in the models (e.g. reddening). Finally, the fitted stellar continuum in each Voronoi bin was subtracted spaxel by spaxel, rescaling the modelled continuum emission in each bin to the median of the observed continuum of each spaxel.

NGC 1365 and NGC 2992 host a Seyfert 1 nucleus. For these galaxies we subtracted the contribution from the BLR assumed to be spatially unresolved and spread across the FoV due to the seeing.

4. Emission line fitting

From the continuum-subtracted cube, we generated a spatially smoothed data cube and a Voronoi-binned data cube. The former is obtained by spatially smoothing the cube with a Gaussian kernel having $\sigma = 1$ spaxel (i.e. $0.2''$), without degrading significantly the spatial resolution, given the observational seeing. The latter, produced by applying a Voronoi binning in the range $\sim 4850 - 4870 \text{ \AA}$ in the vicinity of $H\beta$, requiring an average S/N per wavelength channel of at least 3, can be used to make quantitative comparisons among the galaxies.

Finally, in each spaxel (or bin in the Voronoi-binned cube), the gas emission lines ($H\beta$ - $[O\text{ III}]\lambda\lambda 4959, 5007$ - $[O\text{ I}]\lambda\lambda 6300, 6448$ - $H\alpha$ - $[N\text{ II}]\lambda\lambda 6548, 8446$ - $[S\text{ II}]\lambda\lambda 6717, 3128$) were fitted in the same spectral range used for the stellar fitting, while the residual continuum was fitted with a linear baseline, free to vary to account for small deviations of the overall residuals from null value. To do this, we employed the MPFIT procedure (Markwardt, 2009), taking into account one, two, three, or four Gaussians to reproduce the emission line profile, tying the velocity and widths of each component to be the same for all the lines and leaving the intensities free to vary (apart from the $[O\text{ III}]$, $[O\text{ I}]$, and $[N\text{ II}]$ doublets), as described above. Note that the width of all the emission lines was forced to be greater than MUSE spectral resolution ($\sim 65 \text{ km/s}$ at $[O\text{ III}]-H\beta$ wavelengths; $\sim 50 \text{ km/s}$ at $[N\text{ II}]-H\alpha-[S\text{ II}]$ wavelengths). Then, the $[S\text{ III}]\lambda 9069$ emission line fit is performed analogously, fixing the velocity and width of each of its Gaussian components to the values obtained for the other emission lines in the previous fit. The same $\tilde{\chi}^2$ selection described above is applied to choose the best-fit in each spaxel (bin). Finally, the flux of each emission line is the sum of the integrated fluxes of the adopted Gaussians.

5. Kinematic maps

The analysis of MUSE data described above leads to trace the kinematics of the stars and the warm ionized gas. As an example, Fig. 1 shows the kinematic maps of one galaxy of the sample, NGC 1365, that we investigated in detail in Venturi et al. (2018), to visually appreciate the outflow shape and location within the galaxy.

The stellar velocity map (Fig. 1a) has been obtained from the fit of stellar continuum carried out on the Voronoi-binned data cube, and clearly shows the rotation of the stars in the galactic disc, approaching the observer to the NE and receding to the SW direction. The twisted shape in the central region corresponds to the boundary where the velocity changes sign and is likely due to the presence of the bar.

The $[O\text{ III}]$ velocity map (Fig. 1b) instead is the 1st-order moment of the $[O\text{ III}]$ total line profile resulting from the fit of the star-subtracted smoothed data cube. In addition to the rotational field, it shows other complex motions, that can be isolated and highlighted by subtracting spaxel-by-spaxel the stellar rotation (Fig. 1c). This reveals a clumpy double-conical outflow approximately in the SE-NW direction, with the SE and NW cone having approaching and receding velocities, respectively. The shape and structure of the outflow are well-traced by the $[O\text{ III}]$ W70 velocity width (Fig. 1d), that is the difference between the velocities including 85% and 15% of the flux of the total fitted line profile. High W70 values come from the regions of the outflow, composed by the kinematic components belonging to disc, bar and outflow.

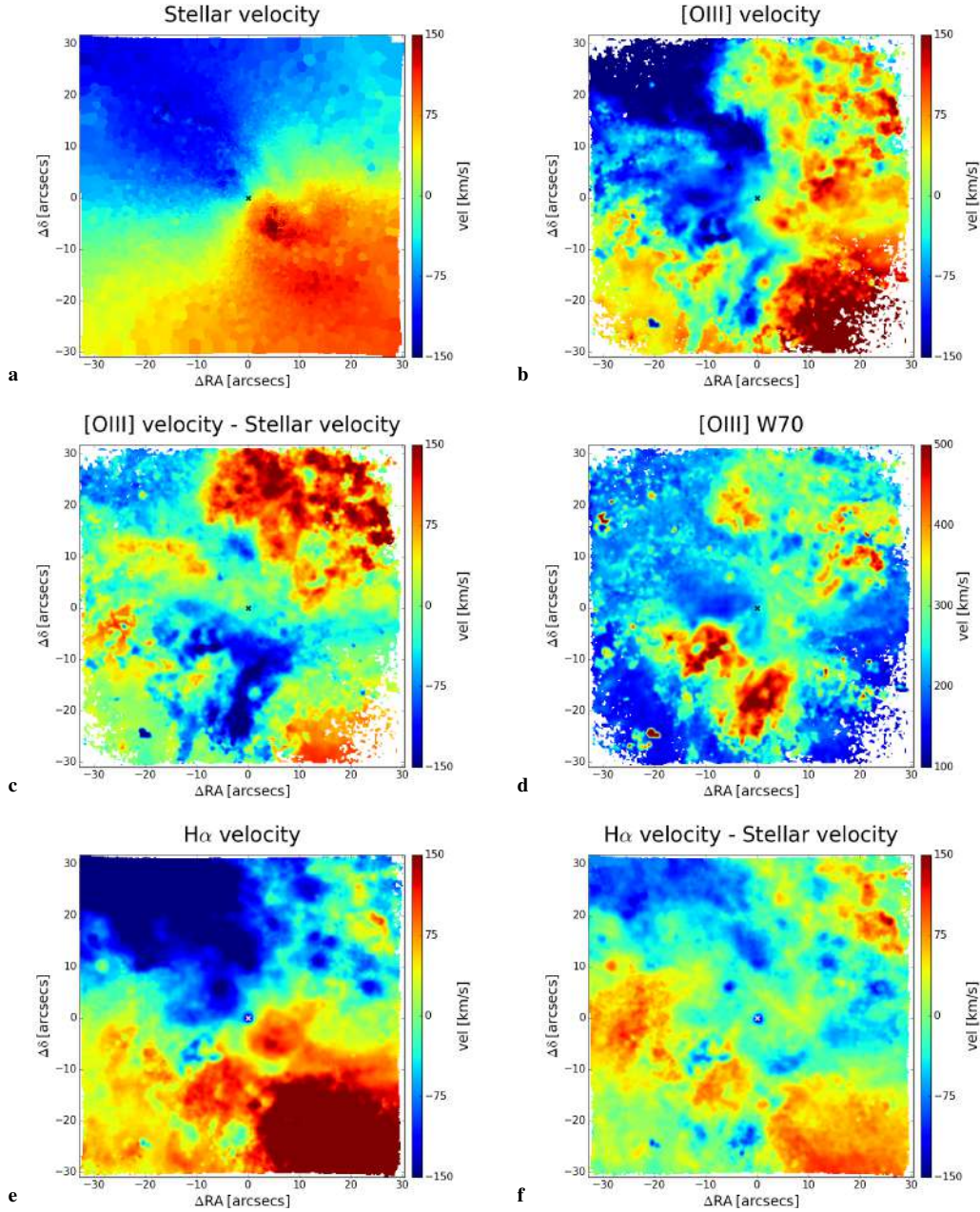


Figure 1. (a) Stellar velocity map of NGC 1365, with respect to the systemic velocity (1630 km s^{-1}). (b) [O III] velocity map with respect to the systemic velocity. This map has been re-smoothed with a $\sigma = 1$ spaxel Gaussian kernel for a better visual output, and a signal-to-noise cut of 3 was applied (this holds for the other maps reported in panels c, d, e, f). (c) [O III] velocity subtracted spixel-by-pixel by the stellar velocity. (d) [O III] W70 (i.e. difference between the 85th-percentile and 15th-percentile velocities of the fitted line profile) map. (e) $\text{H}\alpha$ velocity map with respect to the systemic velocity. (f) $\text{H}\alpha$ velocity map spaxel-by-spaxel subtracted by the stellar velocity. East is to the left. This figure is taken from [Venturi et al. \(2018\)](#).

The kinematics of the ionized gas in the disk can be better inspected from the $\text{H}\alpha$ velocity map (see [Venturi et al. 2018](#) for more details). Fig. 1e and Fig. 1f show the $\text{H}\alpha$ velocity map with respect to the rest frame velocity and to the stellar velocity, respectively. The $\text{H}\alpha$ kinematics is primarily dominated by two thick lanes aligned with the bar in the NE-SW direction, having opposite velocities in excess to stellar rotation. This non-circular motions may indicate an inflow of material along the bar of NGC 1365.

6. Gas properties: disk versus outflow

Excitation and ionization conditions, as well as dust attenuation of the ISM in each MAGNUM galaxy can be investigated through specific emission-line ratios. Thanks to integral field spectrographs (IFUs), we explore the different properties of the disk and the outflow of our galaxies by separating and analysing the different gas components across the MUSE FOV.

Specifically, we define velocity channels of ~ 50 km/s, ranging from -1000 km/s to $+1000$ km/s around the main emission lines ($H\beta$ - [O III] - [O I] - $H\alpha$ - [N II] - [S II] - [S III]), centring the zero velocity to the measured stellar velocity in each spaxel of the MUSE FOV for all the galaxies, since the stellar velocity is generally a good approximation of the gas velocity in the disk. In order to derive the flux in each velocity bin, we integrate the fitted line profile within each velocity channel of the emission lines taken into account. However, Centaurus A is characterised by a strong misalignment between stars and gas (e.g. Morganti 2010), and thus we consider the global systemic velocity ($v_{\text{sys}} = 547$ km/s) as a reference for the gas disk velocity.

We associate the velocity channels close to the core of the lines in the fitted line profile with the disk (hereafter disk component), and the sum of the redshifted and blueshifted channels with the outflow (hereafter outflow component). Specifically, the disk component comprises velocity in the range -100 km/s $< v < 100$ km/s for Circinus, NGC 1365, and NGC 1386, and -150 km/s $< v < 150$ km/s for the other galaxies, while the outflow component is associated with velocities $v > +150$ km/s and $v < -150$ km/s for Circinus, NGC 1365 and NGC 1386, $v > +250$ km/s and $v < -250$ km/s for NGC 1068, and $v > +200$ km/s and $v < -200$ km/s for the other galaxies. These values are chosen after an accurate spaxel-by-spaxel analysis of the spectra in the outflowing regions of the galaxies. Overall, the disk component represents the low-velocity component of the ionized gas, which is rotating similarly to the stars, while the outflow component (i.e. the high-velocity component) is moving faster than the stellar velocity, and is partly blueshifted and partly redshifted with respect to it. Since we are looking at the central regions of AGN galaxies, the narrow line region (NLR) is present in both the disk and in the outflow components.

Because the $H\alpha$ emission is in general dominated by the disc, while the outflow is enhanced in [O III] (e.g. Venturi et al. 2018), in Fig. 2 we show the $H\alpha$ disk component flux maps, superimposing the [O III] λ 5007 outflow component flux contours (not corrected for dust reddening) for all the galaxies, using the method described above to separate the two components. The blueshifted and redshifted outflowing components are indicated in blue and red, respectively. For each velocity bin, we only select the spaxels with a S/N > 5 , computed by dividing the integrated flux in the velocity channels by the corresponding noise. The noise is estimated from the standard deviation of the data-model residuals of the fit around each line (within a range about 60 to 110 Å wide, depending on the line). Looking at Fig. 2, it can be seen that the disk flux maps and the outflow contours are clearly different from each other. The outflow component is often extended in a kpc-scale conical or biconical distribution, as can be clearly seen in Circinus (north-west cone), IC 5063 (north-west and south-east cones), NGC 2992 (north-west and south-east cones), NGC 4945 (north-west and south-east cones), and NGC 5643 (east and west cones). In Centaurus A the outflow component is mainly distributed in two cones (direction north-east and south-west) in the same direction of the extended double-sided jet revealed both in the radio and X-rays (e.g. Hardcastle et al. 2003), and located perpendicularly with respect to the gas in the disk component. Unfortunately, since for this galaxy the stellar velocity cannot be taken as a reference, in some regions we underestimate the gas velocity of the disk component. Consequently, a portion of the disk is still present in the outflowing component. Also in NGC 1365, the outflow component flux map has a biconical shape extended in the south-east and north-west directions, while the disk component appears to be completely different, being dominated by an elongated circumnuclear SF ring and by the bar.

Unfortunately, similar to Centaurus A, a portion of the disk is still present in our outflowing gas selection, because of the high velocity reached by the gas along the bar (see Venturi et al. 2018 for more details). NGC 1068 is almost face-on, allowing us to admire the spiral arms of the disc, traced by the disk component, and preventing the outflowing component from having a clear biconical distribution, but to be broadly extended in all the inner region of the observed FOV. Both the ionized and molecular outflow already observed in this galaxy are observed in the north-east and south-west directions (e.g.

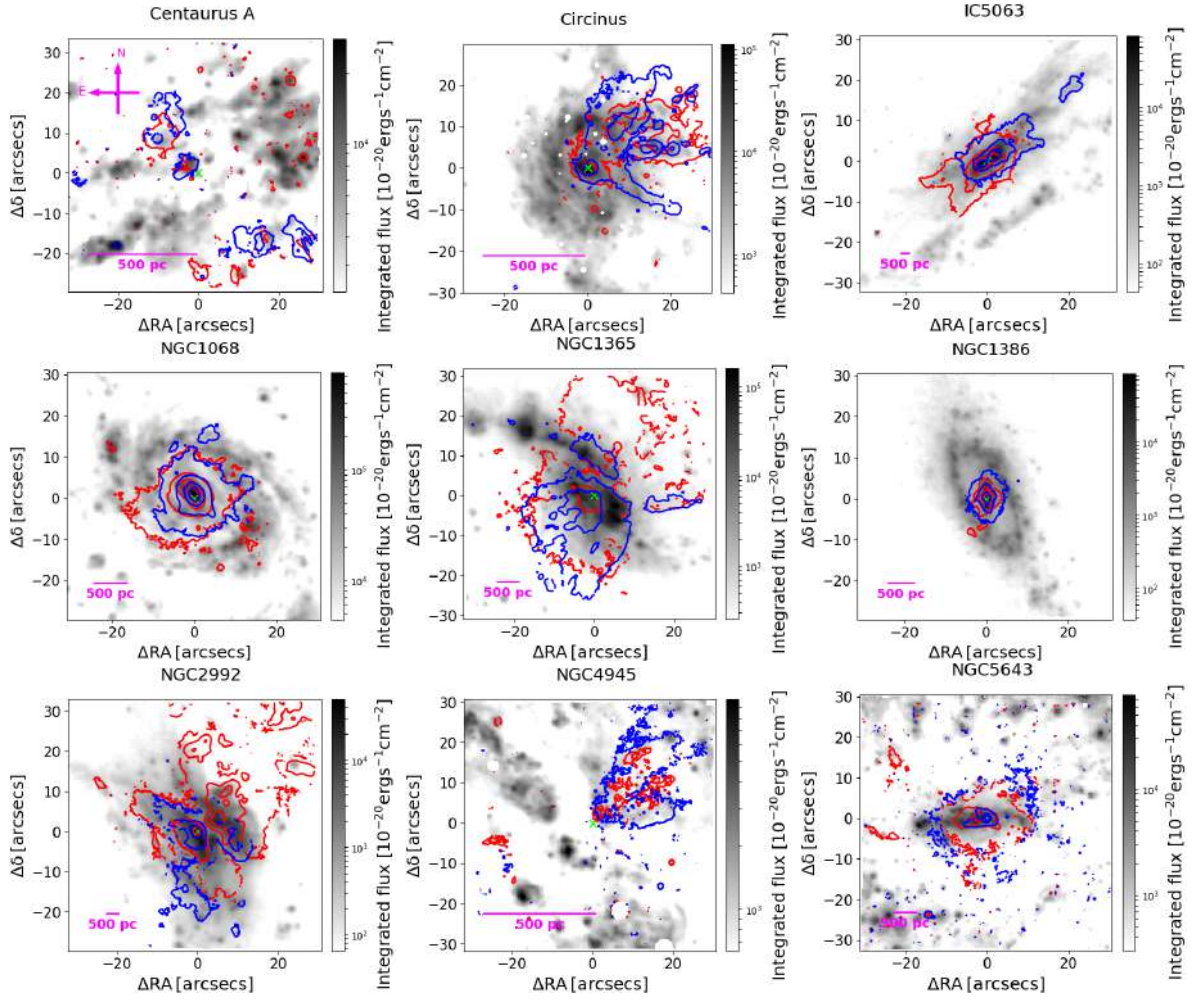


Figure 2. $H\alpha$ disk component flux maps (not corrected for dust reddening) for all the galaxies, namely Centaurus A, Circinus, IC 5063, NGC 1068, NGC 1365, NGC 1386, NGC 2992, NGC 4945, and NGC 5643. $[O\text{III}]\lambda 5007$ outflow component flux contours are superimposed for all the galaxies. The blueshifted and redshifted outflow emission (in blue and red, respectively) is often extended in a kiloparsec-scale conical or biconical distribution. For each velocity bin, we show only the spaxels with a $S/N > 5$. The magenta bar represents a physical scale of ~ 500 pc. East is to the left, as shown in the first image on the left. The white circular regions are masked foreground stars. The cross marks the position either of the Type 1 nucleus (i.e. peak of the broad $H\alpha$ emission), if present, or the peak of the continuum in the wavelength range $6800 - 7000 \text{ \AA}$.

Cecil et al. 2002, García-Burillo et al. 2014). Finally, in NGC 1386 the outflow component does not show a well-defined conical distribution, but appears to be located in the very inner region of the galaxy, with two elongated structures to the north and south of the nucleus, corresponding to nuclear bipolar outflows already revealed by Ferruit et al. (2000) and Lena et al. (2015).

Note that in almost all galaxies the (bi)conical outflow is detected in both its blueshifted and redshifted components, which are often overlapping. For example, this can be clearly seen in NGC 4945, where the north-west cone has approaching velocities at its edges and receding ones around its axis, while the south-east cone has the opposite behaviour, with receding velocities at its edges and approaching ones around its axis. This was already revealed by Venturi et al. (2017) through the kinematic maps of the $[\text{N II}]$ line emission.

7. Spatially and kinematically resolved BPT

Spatially and kinematically resolved Baldwin-Phillips-Terlevich (BPT) diagrams allow us to explore the dominant contribution to ionization in each spaxel in the disk and outflow components

separately (a similar approach has been used by e.g. Westmoquette et al. 2012, McElroy et al. 2015, and Karouzos et al. 2016).

The left and middle panels of Fig. 3 show the [N II]- and [S II]-BPT diagrams of Circinus for the disk and outflow components, respectively. For each velocity bin, we select only the spaxels with a $S/N > 5$, computed by dividing the integrated flux in the velocity channels for each emission line by the corresponding noise. The dashed curve is the boundary between star forming galaxies and AGN defined by Kauffmann et al. (2003) (ka03), while the solid curve is the theoretical upper limit on SF line ratios found by Kewley et al. (2001) (ke01). The dotted line, instead, is the boundary between Seyferts and LI(N)ERs introduced by Kewley et al. (2006) (ke06). The dominant source of ionization is colour-coded: shades of blue for SF, green for intermediate regions in the [N II]-BPT and LI(N)ER in the [S II]-BPT, and red for AGN-like ionizing spectra, as a function of the x-axis line ratios (darker shades means higher x-axis line ratios). The LI(N)ER-like excitation can be due either to shock excitation (e.g. Dopita & Sutherland 1995) or to hard-X radiation coming from AGN and to hot evolved (post-asymptotic giant branch) stars (e.g. Belfiore et al. 2016). The corresponding position on the map of the outflowing gas component, colour-coded based on the different sources of ionization, is shown in the right panels of Fig. 3. In the background of all the pictures (black dots in the BPTs and shaded grey in the corresponding maps), we show the disk and outflow components together to allow us a better visual comparison.

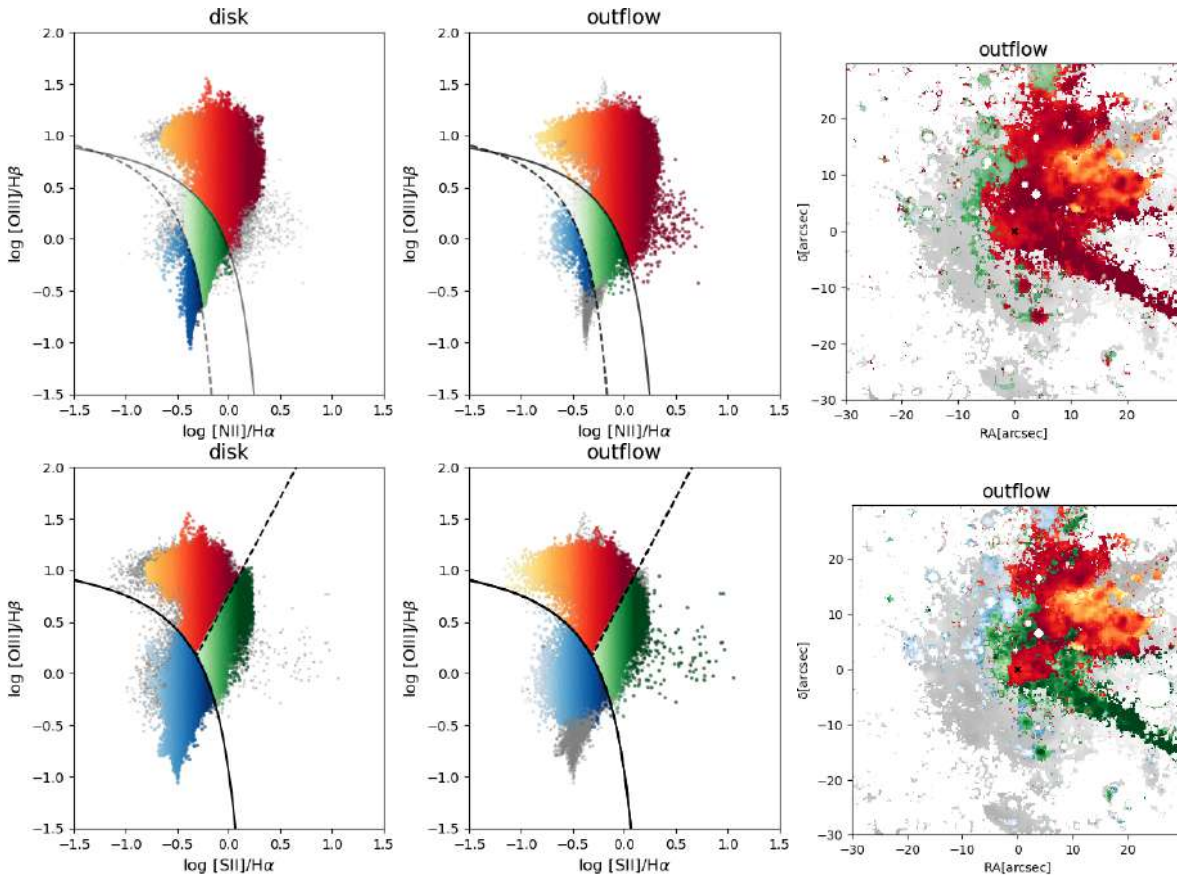


Figure 3. *Left and central panels:* [N II]- and [S II]-BPT diagrams for the disk and outflow components, on the left and on the right respectively, of Circinus. Blue denotes SF-dominated regions, green intermediate regions in the [N II]-BPT and LI(N)ER in the [S II]-BPT, and red AGN-like ionized spectra, colours-coded as a function of the x-axis line ratios (darker shades means higher x-axis line ratios). The black dashed and solid curves, and the black dotted line show the ka03, ke01 and ke06 boundaries, respectively. *Right panels:* [N II]- and [S II]-BPT maps of the outflowing gas component, colour-coded according to BPTs. In the background of all the pictures (grey dots in the BPTs and shaded grey in the corresponding maps), we show the disk and outflow component together. For each velocity bin, we select only the spaxels with a $S/N > 5$ for all the lines involved.

Looking at Fig. 3, we note that the outflow spans a wider range of $[\text{N II}]/\text{H}\alpha$ and $[\text{S II}]/\text{H}\alpha$, including lower and higher values compared to the disk. Specifically, the highest and lowest values of low-ionization line ratios (LILrs; i.e. $[\text{N II}]/\text{H}\alpha$ and $[\text{S II}]/\text{H}\alpha$), displayed in dark red and orange, are prominent in the AGN/LI(N)ER-dominated outflow component, while they are not observable in the disk component. As described in detail in Mingozi et al. (2019), these features are visible in almost all the MAGNUM sample, in which, in general, the highest LILrs trace the inner parts along the axis of the emitting cones, where the $[\text{S III}]/[\text{S II}]$ line ratio is enhanced (i.e. high excitation), while the lowest LILrs follow the cone edges and/or the regions perpendicular to the axis of the outflow, characterised also by a higher $[\text{O III}]$ velocity dispersion.

8. Centaurus A: an ideal local laboratory to study AGN positive feedback

This galaxy is the result of a recent merger between an early-type elliptical and a spiral galaxy (e.g. Israel 1998). Indeed, it is characterised by a stellar-dominated almost circular component and by a dusty and gaseous thick lane approximately in the SE-NW direction, containing the majority of molecular, ionized and neutral atomic gas (Morganti, 2010). Centaurus A galaxy shows a characteristic double-sided jet observed in radio and X-rays (see Morganti 2010 for a review), expanding in a set of radio lobes from ~ 5 kpc up to ~ 250 kpc (e.g. Israel 1998). At the center of Centaurus A there is an accreting supermassive black hole with a mass of $\sim 5 \times 10^7 M_{\odot}$, Israel et al. (2017) discovered an outflow of gas that from the center of Centaurus A extends along an axis close to that of the northern X-ray/radio jet, detected in the neutral gas traced by CO and C I, and in the far-infrared through fine-structure lines. Israel et al. (2017) detected also a less clear southern counterpart to the well-collimated northern outflow. Furthermore, an $[\text{O III}]$ ionization cone of ~ 500 pc along the minor axis, related to AGN or shock activities, is revealed by Bland-Hawthorn & Kedziora-Chudczer (2003). This galaxy is the best example of a radio jet emitted by the central AGN interacting with the ISM, which may have induced star formation in the outskirts of the galaxy (positive feedback). The region where this interaction appears most clearly is characterised by filaments of highly ionized gas, between about 9 and 20 kpc from the nucleus, roughly aligned along the jet direction (Morganti et al., 1991). Interestingly, these filaments are known to contain massive young stars, whose formation was possibly triggered by the interaction of the AGN radio plasma with a cloud of cold gas due to a recent merger, as suggested by the alignment with the jet direction and the kinematics of the gas (e.g. Santoro et al., 2016).

In this context, we investigated the central region of this galaxy, exploiting our approach of disentangling the disk from the outflow component to obtain an independent classification of their excitation properties with the BPT diagrams. The upper and lower panels of Fig. 4 shows the $[\text{N II}]$ and $[\text{S II}]$ BPT maps for the disk (on the left) and the outflow (on the right), with regions dominated by SF, AGN and composite/LI(N)ER activity indicated in blue, red, and green, respectively. The direction of the inner jet, revealed both in the radio and X-rays (see Fig. 5, Hardcastle et al. 2003) and consistent with the location of the bi-conical outflow dominated by LI(N)ER- and AGN-like ionization, is marked by the black arrow.

Looking back at Fig. 4, the SW portion of the galaxy FOV hosts a blob (solid circle, left pictures), characterised by a velocity consistent with the gas disk and by composite and SF dominated ionization ($[\text{N II}]$ - and $[\text{S II}]$ -BPT, respectively), that could be interpreted as SF triggered in the ionization cone due to compression of the galaxy ISM by the jet (as in Cresci et al. 2015a and Santoro et al. 2016). Moreover, a nearby clump appears to have SF like ionization, but velocities consistent with the gas in the outflow (solid square, right pictures), suggesting that in this case new stars could be formed at high velocity directly in the outflow (as in Maiolino et al. 2017). If confirmed, this would be the first example of these two types of positive feedback coexisting in the same object.

Fig. 6 shows the spectrum of the SF blob in the outflow (highlighted by the solid square in Fig. 4), that clearly presents outflow signatures. The asymmetric line profile can be reproduced by a three Gaussian component fit as shown in the figure. Fig. 7 illustrates the $[\text{N II}]$ and $[\text{S II}]$ BPT diagrams of these three components, indicated with the same color used in the previous figure. The redshifted

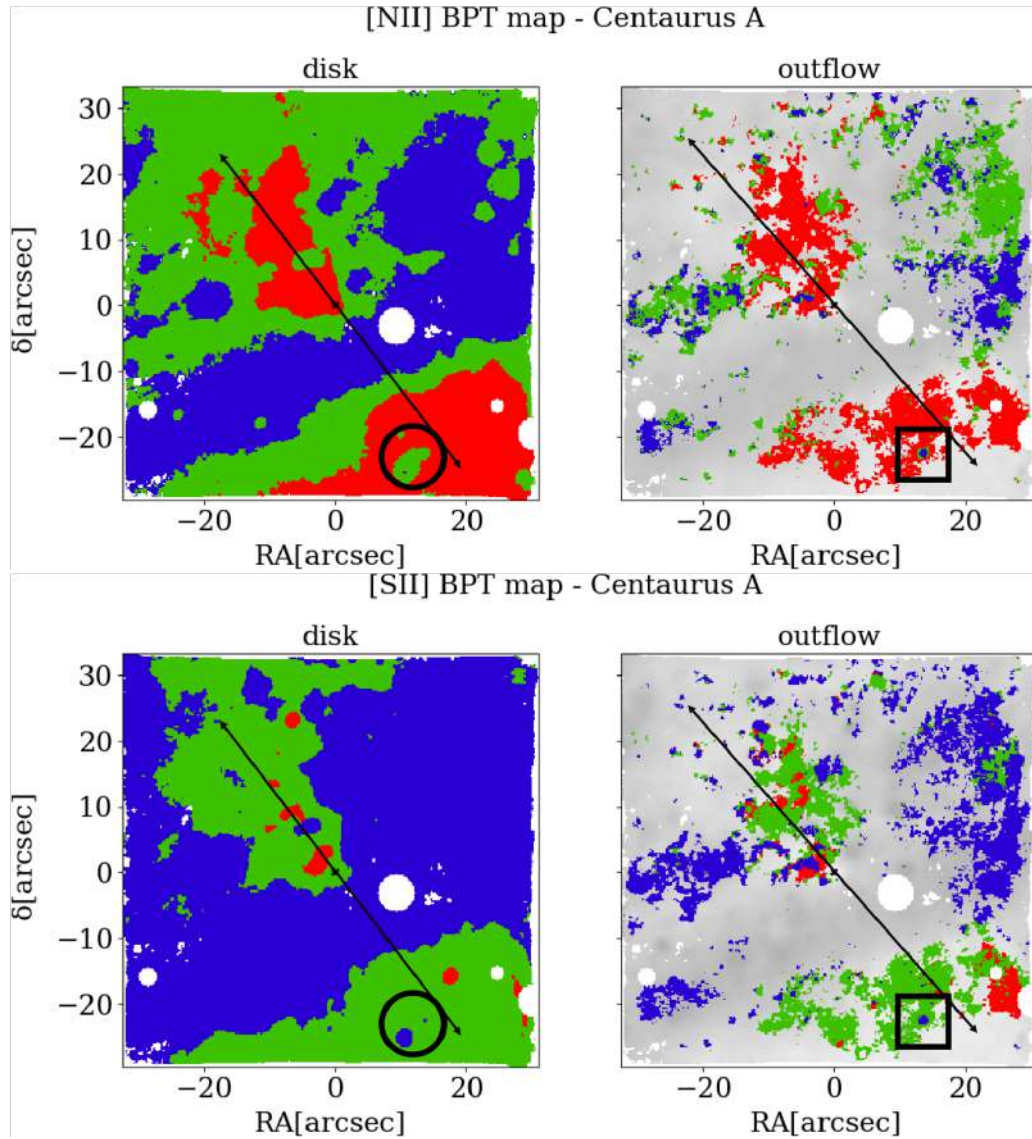


Figure 4. [N II]- (upper panel) and [S II]- (lower panel) BPT maps for the disk and outflow component of Centaurus A. To separate the two components, we divide each line profile in each spaxel of the MUSE FOV in velocity bins, associating to the disk the core of the line ($-150 \text{ km/s} < v < +150 \text{ km/s}$) centred at Centaurus A systemic velocity ($v_{\text{sys}} \sim 547 \text{ km s}^{-1}$), and the sum of the redshifted and blueshifted wings to the outflow ($v > +200 \text{ km/s} - v < -200 \text{ km/s}$). SF, AGN and Composite/LI(N)ER dominated regions are indicated in blue, red and green, respectively. The black arrow indicates the direction of the outflow, while the solid circle and square highlight the position of composite/SF blobs, located in the direction of the outflow.

Gaussian component (dashed red Gaussian) has a very strong $H\alpha$ emission, with $\log([\text{N II}]/H\alpha) \sim -0.6$, $\log([\text{S II}]/H\alpha) \sim -0.5$ and $\log([\text{O III}]/H\beta) \sim 0$ flux ratios, indicating SF ionization, pointing towards a stellar-like ionization source at redshifted velocities consistent with the outflow at the same location. On the other hand, the blueshifted (dashed-dotted blue Gaussian) and disk (dotted green Gaussian) components have AGN and composite/LI(N)ER-like ratios.

We estimate the star formation rate (SFR) of the two star forming blobs using the $H\alpha$ -based calibration taken from Lee et al. (2009). From the extinction-corrected luminosity of the redshifted $H\alpha$ component (shown in red in Fig. 6), we find a $\text{SFR} \sim 8 \times 10^{-3} M_{\odot}/\text{yr}$ in the outflow. Taking into account also the SF blob in the disk (highlighted in the black circle in Fig. 4, left panels), we obtain a total $\text{SFR} \sim 0.01 M_{\odot}/\text{yr}$, which is $\sim 3\%$ of the global value of the galaxy ($\text{SFR} = 0.4 M_{\odot}/\text{yr}$ Diamond-Stanic & Rieke 2012). However, we are observing just a small part of the outflow in Centaurus A,

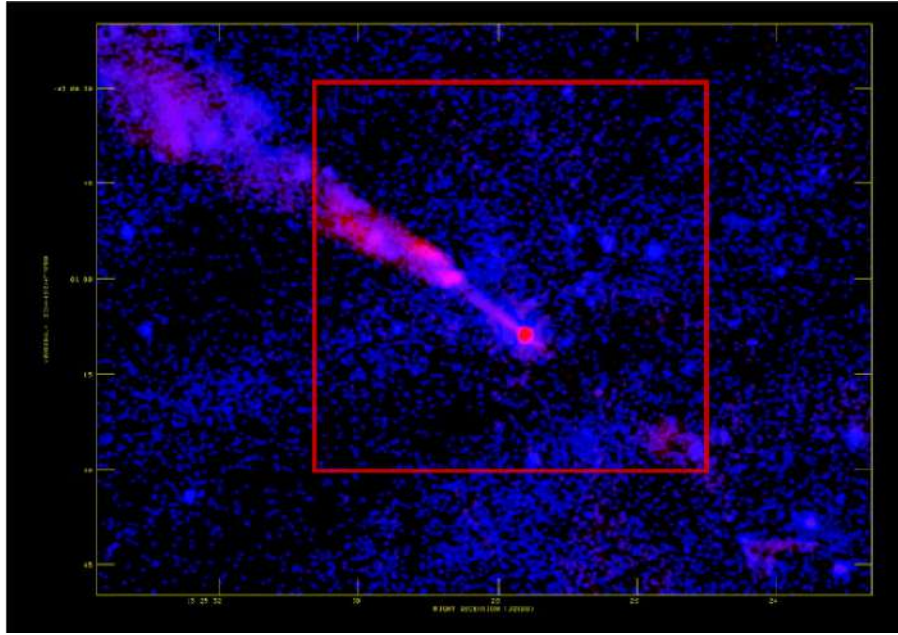


Figure 5. X-ray (0.4 and 2.5 keV, in blue) and radio structure (in red) of the jet in Centaurus A. This image is taken from [Hardcastle et al. \(2003\)](#). The red square superimposed indicates our MUSE FOV.

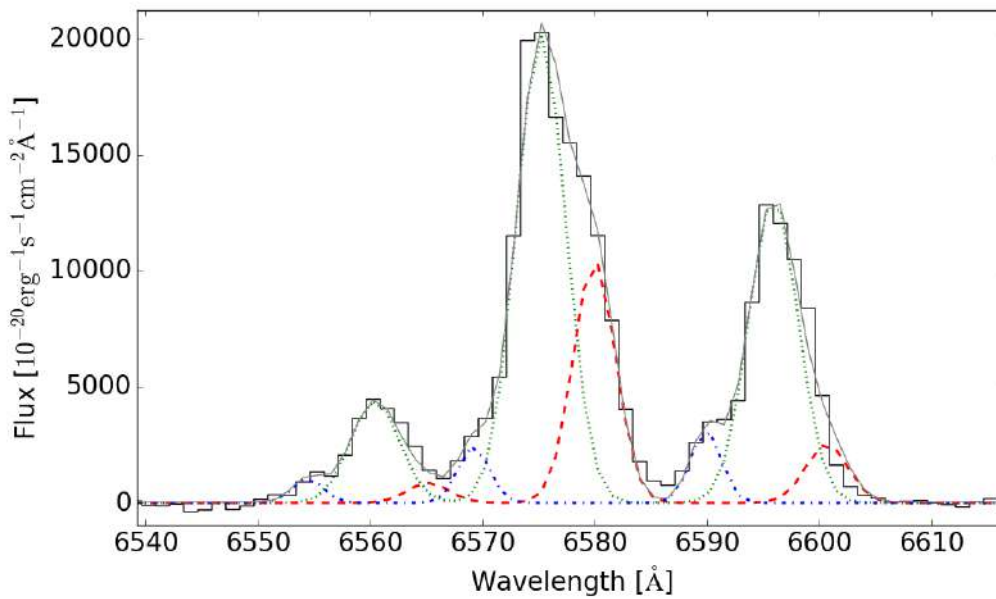


Figure 6. Spectrum of the SF blob in the outflow around $H\alpha$ and $[N II]$. The asymmetric line profile is reproduced by a three Gaussian component fit: blueshifted (dashed-dotted blue Gaussian), systemic (dotted green Gaussian) and redshifted (dashed red Gaussian).

given the dust obscuration and the MUSE limited FOV due to the proximity of the source, which means that there could be many more SF clumps embedded in the outflow. Even if the contribution to the total SFR might seem irrelevant, it remains that Centaurus A may be used as a local test bench to explore in detail the structure and kinematic of the gas, improving our knowledge on positive feedback and possibly confirming that it is not a rare mechanism. Indeed, this phenomenon may play a significant role in the formation of the spheroidal component of galaxies at high redshift, where AGN-driven outflows are more prominent and, possibly, the associated SF inside those very massive outflows much higher ([Gallagher et al., 2019](#)).

Overall, these two blobs could represent the first evidence of the two modes of positive feedback

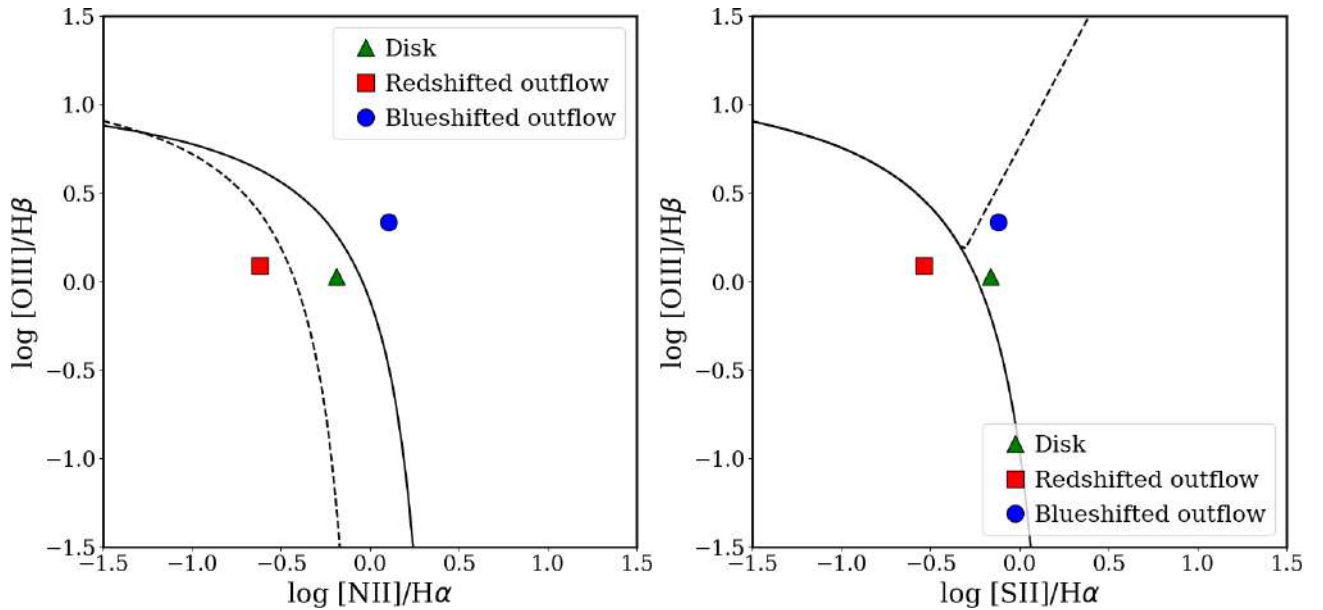


Figure 7. [N II] and [S II]BPT diagrams of the three Gaussian components used to fit the asymmetric line profiles shown in Fig. 6. Note that while the blueshifted (dashed-dotted blue Gaussian) and disk (dotted green Gaussian) components have AGN and Composite/LI(N)ER-like ratios, respectively, the redshifted component (dashed red Gaussian) is SF dominated.

in the nuclear region of this galaxy. However, Maiolino et al. (2017) demonstrated that only the combination of X-Shooter and MUSE data allow to undoubtedly identify the signatures of SF in the outflow. Indeed, X-shooter has a broad-band spectral coverage able to cover IR diagnostics, such as the $[\text{Fe II}]\lambda 1.64\mu\text{m}/\text{Br}\gamma\lambda 2.16\mu\text{m}$ versus the $\text{H}_2(1-0)\text{S}(1)\lambda 2.12\mu\text{m}/\text{Br}\gamma$ and the $[\text{Fe II}]\lambda 1.25\mu\text{m}/\text{Pa}\beta\lambda 1.28\mu\text{m}$ versus $[\text{P II}]\lambda 1.18\mu\text{m}/\text{Pa}\beta$ diagrams (Oliva et al., 2001), that can further discriminate among SF, AGN and shock ionization. Typically, in star forming regions these ratios are expected to be very low, since shocks could enhance the emission of $[\text{Fe II}]$ and H_2 , while the $\text{Br}\gamma$ and the $[\text{P II}]$ are direct tracers of the AGN UV and soft-X ionizing radiation, respectively. Moreover, X-shooter high spectral resolution allows to investigate the presence of young stars formed in the outflow. To do this, the stellar absorption features, such as the Balmer series down to $\lambda \sim 4000 \text{ \AA}$ (tracing young hot O-B-type stars), the Ca II triplet at $\lambda \sim 8500 \text{ \AA}$ (in case of recent SF, dominated by young red supergiants and young asymptotic giant branch stars) and, possibly, the weak absorption feature of $\text{He I}\lambda 4922 \text{ \AA}$ (unambiguous tracer of B-type stars and of young stellar populations) can be taken into account. Hence, we successfully asked for observations with the X-Shooter spectrograph (0102.B-0292(A), P.I. Mingozi). The observations were carried out during the nights of April 1-2 and of August 3-5 2019, making use of the $0.8''$ slit, orientated in order to observe the two SF blob simultaneously, and will be analysed in the next months.

9. Conclusions

The MAGNUM survey is exploring the gas properties and the source of ionization of the outflowing gas in the NLR of the 9 nearby Seyfert galaxies, all characterised by prominent conical or biconical outflows. Exploiting the very high spatial resolution of the optical integral field MUSE spectrograph at VLT, we were able to disentangle the outflow component from the disk component in order to analyse its peculiarities through spatially and kinematically resolved maps. To do this, we divided the main emission lines ($\text{H}\beta$, $[\text{O III}]$, $[\text{O I}]$, $\text{H}\alpha$, $[\text{N II}]$, $[\text{S II}]$ and $[\text{S III}]$) in velocity bins, associating the core of the lines (centred on the stellar velocity in each spaxel) with the disc, and the blueshifted and redshifted wings with the outflow. In the following, we report our main results:

- We have analyzed the ionization state of the NLR of MAGNUM galaxies, by making spatially and kinematically resolved BPT diagrams. We find that the AGN/LI(N)ER-dominated

outflow is characterised by the lowest and highest values of low-ionization line ratios (LILrs, $\log([\text{N II}]/\text{H}\alpha) \sim -1$, $\log([\text{S II}]/\text{H}\alpha) \sim -1$ and $\log([\text{N II}]/\text{H}\alpha) \sim 0.5$, $\log([\text{S II}]/\text{H}\alpha) \sim 0.5$, respectively), which are not observed in the disk. The lowest LILrs mainly come from the innermost regions of the outflowing cone, near the outflow axis. On the other hand, the highest LILr appear to come from the edges of the outflowing cones.

- We discussed the detection of two star-forming blobs embedded in the ionization cone of Centaurus A, that could represent the first evidence of the two modes of positive feedback in act in the nuclear region of this galaxy. We will soon analyse X-shooter data with the aim of unambiguously confirming the presence of positive feedback and fast moving young stars forming in the outflow.

We speculate that the gas in the outflowing cones of our galaxies is set up in clumpy clouds characterised by higher density and ionization parameters with respect to the disk gas. The innermost regions of the cone are optically thin to the radiation, being characterised by high excitation, and are possibly directly heated by the central ionizing AGN. The edges of the cones and the regions perpendicular to the outflow axis could instead be dominated by shock excitation probably because of the interaction between the outflowing gas and the ISM. Alternatively, these regions, generally characterised by low excitation ($[\text{S III}]/[\text{S II}] < 1$) could be impinged by an ionizing radiation filtered by clumpy, ionized absorbers. The next step of our analysis will be a detailed modelling of each MAGNUM galaxy, also making use of the photoionization code CLOUDY (Ferland et al., 2017) to better investigate the different scenarios that we propose to interpret our findings.

References

- Belfiore F., et al., 2016, MNRAS, [461](#), [3111](#)
- Bland-Hawthorn J., Kedziora-Chudczer L., 2003, PASA, [20](#), [242](#)
- Cappellari M., Emsellem E., 2004, PASP, [116](#), [138](#)
- Cecil G., Dopita M. A., Groves B., Wilson A. S., Ferruit P., Pécontal E., Binette L., 2002, ApJ, [568](#), [627](#)
- Cresci G., et al., 2015a, AAP, [582](#), [A63](#)
- Cresci G., et al., 2015b, ApJ, [799](#), [82](#)
- Diamond-Stanic A. M., Rieke G. H., 2012, ApJ, [746](#), [168](#)
- Dopita M. A., Sutherland R. S., 1995, ApJ, [455](#), [468](#)
- Ferland G. J., et al., 2017, RMXAA, [53](#), [385](#)
- Ferruit P., Wilson A. S., Mulchaey J., 2000, ApJS, [128](#), [139](#)
- Gallagher R., Maiolino R., Belfiore F., Drory N., Riffel R., Riffel R. A., 2019, MNRAS, [485](#), [3409](#)
- García-Burillo S., et al., 2014, AAP, [567](#), [A125](#)
- Hardcastle M. J., Worrall D. M., Kraft R. P., Forman W. R., Jones C., Murray S. S., 2003, ApJ, [593](#), [169](#)
- Israel F. P., 1998, AAPR, [8](#), [237](#)
- Israel F. P., Güsten R., Meijerink R., Requena-Torres M. A., Stutzki J., 2017, AAP, [599](#), [A53](#)
- Karouzos M., Woo J.-H., Bae H.-J., 2016, ApJ, [833](#), [171](#)
- Kauffmann G., et al., 2003, MNRAS, [346](#), [1055](#)
- Kewley L. J., Dopita M. A., Sutherland R. S., Heisler C. A., Trevena J., 2001, ApJ, [556](#), [121](#)
- Kewley L. J., Groves B., Kauffmann G., Heckman T., 2006, MNRAS, [372](#), [961](#)
- Klessen R. S., Glover S. C. O., 2016, Saas-Fee Advanced Course, [43](#), [85](#)
- Lee J. C., Gil de Paz A., Tremonti C., Kennicutt Robert C. J., Salim e. a., 2009", ApJ, [706](#), [599](#)
- Lena D., et al., 2015, ApJ, [806](#), [84](#)
- Maiolino R., Mannucci F., 2019, AAPR, [27](#), [3](#)
- Maiolino R., et al., 2017, NAT, [544](#)
- Markwardt C. B., 2009, in Bohlender D. A., Durand D., Dowler P., eds, Astronomical Society of the Pacific Conference Series Vol. 411, Astronomical Data Analysis Software and Systems XVIII. p. 251
- McElroy R., Croom S. M., Pracy M., Sharp R., Ho I.-T., Medling A. M., 2015, MNRAS, [446](#), [2186](#)
- McQuinn M., 2016, ARAA, [54](#), [313](#)
- Mingozi M., et al., 2019, AAP, [622](#), [A146](#)
- Morganti R., 2010, PASA, [27](#), [463](#)
- Morganti R., Robinson A., Fosbury R. A. E., di Serego Alighieri S., Tadhunter C. N., Malin D. F., 1991, MNRAS

Oliva E., et al., 2001, AAP, [369](#), [L5](#)

Santoro F., Oonk J. B. R., Morganti R., Oosterloo T. A., Tadhunter C., 2016, AAP, [590](#), [A37](#)

Storey P. J., Zeppen C. J., 2000, MNRAS, [312](#), [813](#)

Vazdekis A., Sánchez-Blázquez P., Falcón-Barroso J., Cenarro A. J., Beasley M. A., Cardiel N., Gorgas J., Peletier R. F., 2010, MNRAS, [404](#), [1639](#)

Venturi G., Marconi A., Mingozi M., Carniani S., Cresci G., Risaliti G., Mannucci F., 2017, *Frontiers in Astronomy and Space Sciences*, [4](#), [46](#)

Venturi G., et al., 2018, A&A, 619, A74

Westmoquette M. S., Clements D. L., Bendo G. J., Khan S. A., 2012, MNRAS, [424](#), [416](#)

Studies of Active Galaxies in Byurakan: Recent Results

A. M. Mickaelian*, H. V. Abrahamyan, G. M. Paronyan, G. A. Mikayelyan, and M. V. Gyulzadyan

NAS RA Byurakan Astrophysical Observatory (BAO), Byurakan 0213, Aragatzotn Province, Armenia

Abstract

We present the recent results of studies on active galaxies (both AGN and Starbursts) by the Extragalactic group of Byurakan Astrophysical Observatory (BAO) Research Department “Astronomical Surveys”. The research has been carried out in 2017-2019 and the results are published in 2018-2019. These studies are characterized by multiwavelength approach to statistical analysis of large amount of data obtained in different wavelengths; from X-ray to radio. Results on HRC/BHRC sample objects (optical identifications of ROSAT X-ray sources), studies of Markarian galaxies in UV and multiwavelength SEDs, abundance and star formation determinations in Mrk galaxies from SDSS spectra, revised optical classification of “LINERs”, study and classification of SDSS spectra for Byurakan-IRAS Galaxies, summary of observations and study of Byurakan-IRAS Galaxies (BIG objects), discovery of new bright ULIRGs from the IRAS PSC/FSC Combined Catalogue and their spectral classification, radio variable sources at 1400 MHz and their optical variability, classification of BZCAT objects having uncertain types (BZU objects), and optical variability of blazars are presented.

Keywords: *active galaxies, AGN, Starburst Galaxies, quasars, Seyfert galaxies, LINERs, composite spectrum objects, HII, IRAS galaxies, variable sources*

Introduction

Recent results of the Extragalactic group of BAO Research Department “Astronomical Surveys” are related to multiwavelength studies of active galaxies using large amount of data from X-ray, UV, optical, IR and radio ranges, namely large-area or all-sky surveys, with heavy use of cross-correlations, classifications on activity types using our observations and SDSS spectra, building diagnostic diagrams, Spectral Energy Distributions (SEDs), etc. For classification of SDSS spectra, we have used our new approach that is focused on detailed analysis of the most important emission lines and introducing fine details, like subtypes for the main broad-line Seyfert galaxies and narrow-line Seyfert ones. Results on HRC/BHRC sample objects (optical identifications of ROSAT X-ray sources), studies of Markarian galaxies in UV and multiwavelength SEDs, abundance and star formation determinations in Mrk galaxies from SDSS spectra (for spectra having higher signal-to noise ratio), revised optical classification of “LINERs”, study and classification of SDSS spectra for Byurakan-IRAS Galaxies (BIG objects), summary of observations and study of BIG objects, discovery of new bright ULIRGs from the IRAS PSC/FSC Combined Catalogue (compiled earlier by our group) and their spectral classification using SDSS spectra, 6300 radio variable sources at 1400 MHz and their optical variability, classification of BZCAT objects having uncertain types (BZU objects), and optical variability of blazars are given in individual sections. These studies have been carried out during 2017-2019 and the results are published in a number of papers in 2018-2019. Previous results can be found in the review papers by [Mickaelian \(2017\)](#) and by [Mickaelian et al. \(2017\)](#).

*aregmick@yahoo.com, Corresponding author

Activity Types of Galaxies Selected from HRC/BHRC Sample (Paronyan et al. 2018, 2019a,b)

In this study we carry out detailed spectral classification of 371 (173+198) AGN candidates from the Joint HRC/BHRC sample, which is a combination of HRC (Hamburg-ROSAT Catalogue) and BHRC (Byurakan-Hamburg-ROSAT Catalogue). These objects were revealed as optical counterparts for ROSAT X-ray sources; however, spectra for 371 of them are given in SDSS without definite spectral classification. We studied these 371 objects using the SDSS spectra and revealed the detailed activity types for them. Three diagnostic diagrams and direct examination of the spectra were used to obtain more confident classification. We also identified these sources in other wavelength ranges and calculated some of their parameters. In Figure 1 we give examples of SDSS DR15 spectra for some classified HRC-BHRC objects.

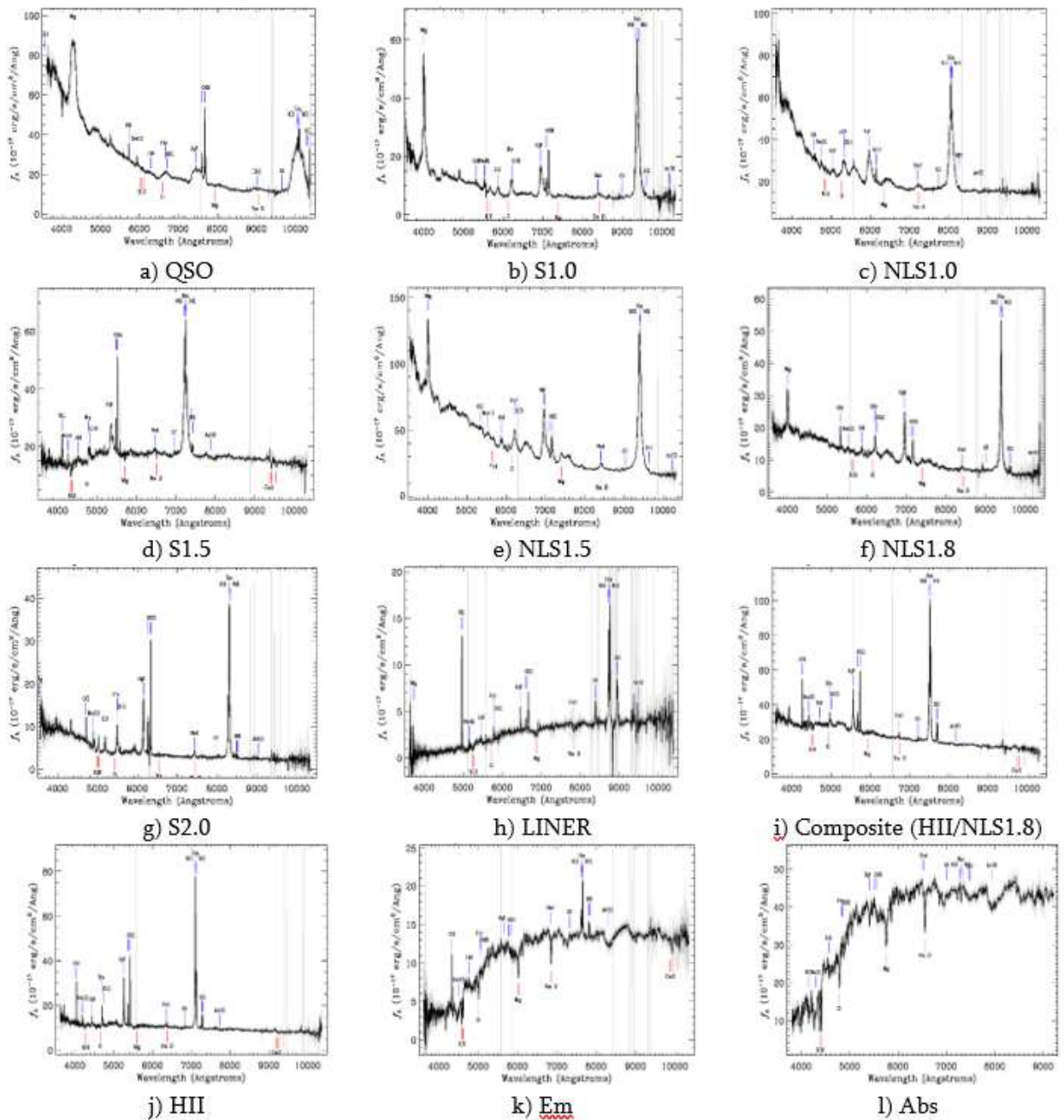


Figure 1. Examples of SDSS DR15 spectra for some HRC-BHRC objects. a) QSO, b) S1.0, c) NLS1.0, d) S1.5, e) NLS1.5, f) NLS1.8, g) S2.0, h) LINER, i) HII/NLS1.8, j) HII, k) Em, l) Abs.

Markarian galaxies in UV and multiwavelength studies (Mickaelian et al. 2018a)

The UV properties of 1152 Markarian galaxies have been investigated based on GALEX data. These objects have been investigated also in other available wavelengths using multi-wavelength data from X-ray to radio. Using our classification for activity types for 779 Markarian galaxies based on SDSS spectroscopy, we have investigated these objects on the GALEX, 2MASS and WISE color-magnitude and color-color diagrams by the location of objects of different activity types and have revealed a number of loci. UV contours overplotted on the optical images revealed additional structures, particularly spiral arms of a number of Markarian galaxies. UV (FUV and NUV) and optical absolute magnitudes and luminosities have been calculated showing graduate transition from AGN to Composites, HIIs and Absorption line galaxies from (average M) -17.56^m to -15.20^m in FUV, from -18.07^m to -15.71^m in NUV and from AGN to Composites, Absorption line galaxies and HII from -21.14^m to -19.42^m in optical wavelengths and from (average L) 7×10^9 to $4 \times 10^8 L_{\odot}$ in FUV, from 1×10^{10} to $5 \times 10^8 L_{\odot}$ in NUV and from AGN to Composites, Absorption line galaxies and HII from 7×10^{10} to 1×10^{10} in optical wavelengths. We give in Figure 2 the distribution of GALEX FUV and NUV magnitudes by redshifts for 1152 Markarian galaxies.

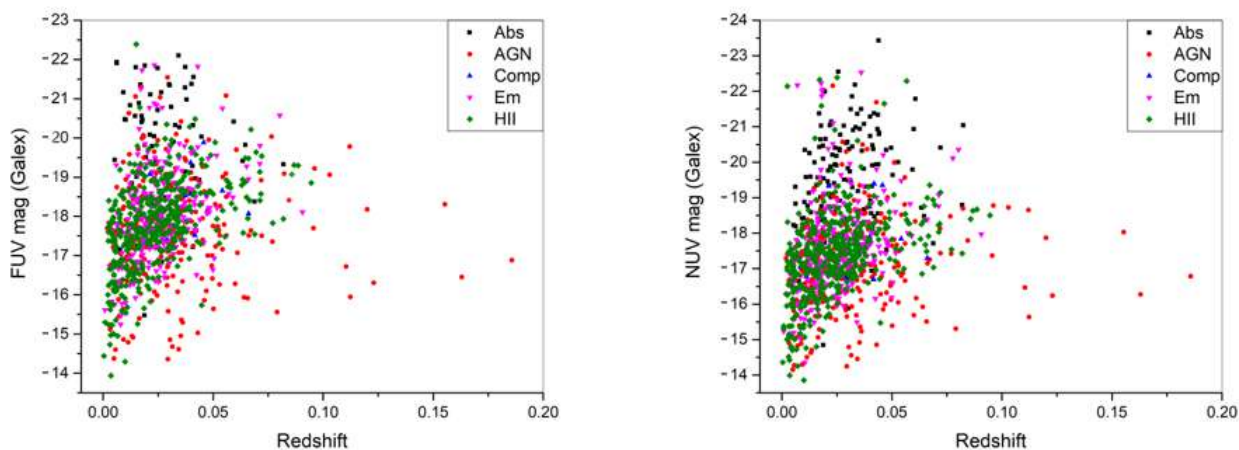


Figure 2. The distribution of GALEX FUV and NUV magnitudes by redshifts for Markarian galaxies. As expected, AGNs and Composites are detected at higher redshifts due to their higher luminosities.

Abundance and Star Formation Determinations in Mrk galaxies from SDSS Spectra (Gyulzadyan et al. 2018)

We analyze the oxygen and nitrogen abundance and specific star formation rates (sSFR) in Markarian galaxies from SDSS spectra. The Data Release 7 (DR7) of SDSS contains photometric data for more than 1000 and spectral information for more than 700 Markarian objects. The Mrk sample has played a central role in the task of distinguishing between the astrophysical different types of phenomena that occur in AGNs. In the course of the Markarian survey, more than 200 Seyfert galaxies, and hundreds of starbursts, blue compact, and H II galaxies were discovered. The Markarian survey remains perhaps the best-known source of such objects in the local universe. We have measured their line fluxes and derived the O and N abundances using recent calibrations. We have compared the oxygen and nitrogen abundances derived from global emission-line Sloan Digital Sky Survey (SDSS) spectra of galaxies using (1) the Te method and (2) two recent strong-line calibrations: the ON (Oxygen-Nitrogen) and NS (Nitrogen-Sulfur) calibrations. The behaviour of the $[N/H]$ ratio in under abundant regions gives strong support to a partially primary origin of nitrogen. The star formation rate (SFR) is one of the main parameters used to analyze the evolution of galaxies through time. In the local Universe, the $H\alpha$ luminosity derived from IFS (Integral Field Spectroscopy) observations can

be used to measure SFR, at least in statistically significant, optically-selected galaxy samples, once stellar continuum absorption and dust attenuation effects are accounted for.

Revised optical classification of “LINERs” (Abrahamyan et al. 2018a)

This work is dedicated to reclassification of LINERs. For our investigation we use the catalogue Véron-Cetty & Véron 13th edition. In this catalogue 926 LINERs are included. Cross-correlation of these sources with SDSS DR14 gives 176 objects which have spectra in SDSS. Having medium-resolution spectra from SDSS we have done reclassification of these sources. As a result, 54% of these sources have changed their classification. We give in Figure 3 the dependence of absolute magnitude vs. redshift for LINERs.

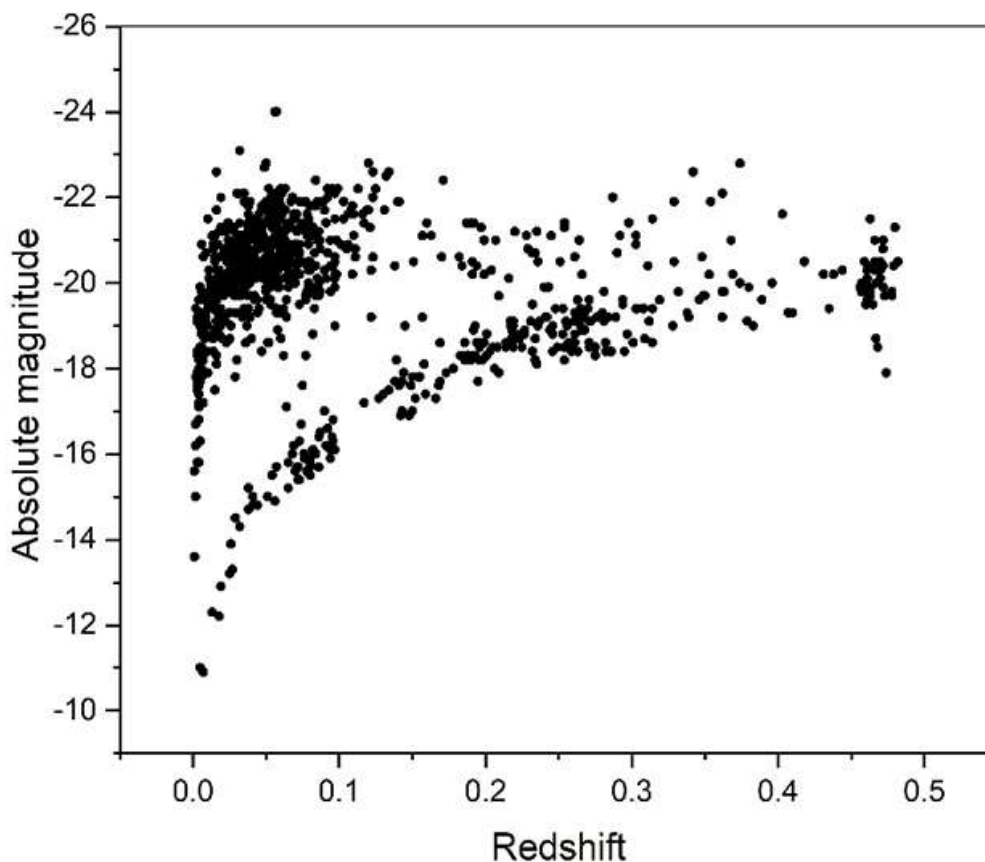


Figure 3. Absolute magnitude vs. redshift for LINERs.

Study and Classification of SDSS Spectra for Byurakan - IRAS Galaxies (Mickaelian et al. 2018b)

The sample of Byurakan-IRAS galaxies (BIG) has been created based on optical identifications of IRAS Point Source Catalog (PSC) at high galactic latitudes. As a result, 1178 galaxies have been identified. 172 of them have been observed spectroscopically with Byurakan Astrophysical Observatory (BAO, Armenia) 2.6 m, Special Astrophysical Observatory (SAO, Russia) 6m and Observatoire de Haute Provence (OHP, France) 1.93 m telescopes. Later on, spectra were obtained for more 83 BIG objects in Sloan Digital Sky Survey (SDSS). We have extracted and studied these spectra, classified

them and measured spectral features. Diagnostic diagrams have been built to distinguish starbursts (SB), LINERs and Seyfert galaxies. Cross-correlations were made for these objects with multiwavelength (MW) catalogues and their physical properties were studied. Among these 83 objects, 55 HII, 8 Seyfert galaxies, 2 LINERs, 4 other AGN, 6 composite spectrum objects, and 8 other emission-line galaxies have been revealed. Three of these objects are Ultra-Luminous InfraRed Galaxies (ULIRG). We give in Figure 4 the dependence of L_{ir} and L_{fir} vs. redshift.

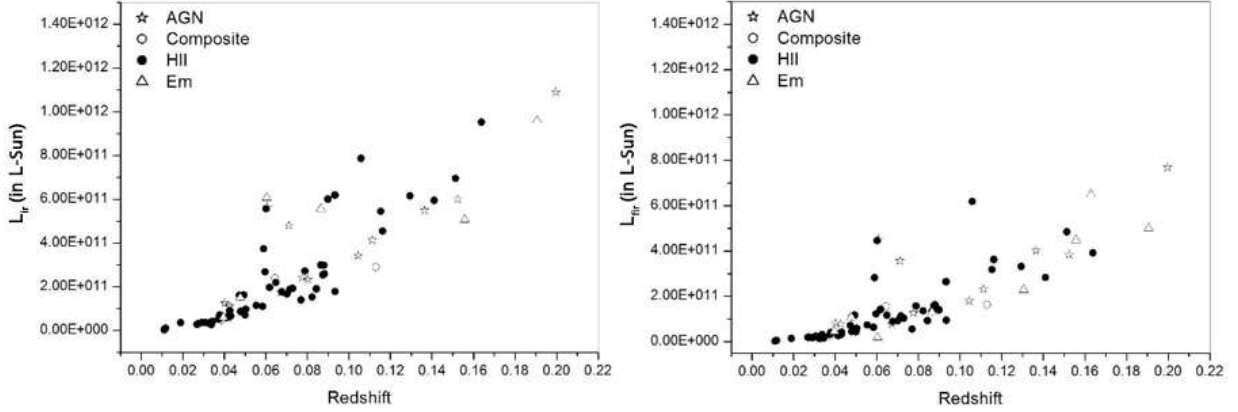


Figure 4. The dependence of L_{ir} and L_{fir} (in L_{\odot}) vs. redshift

Observations and study of Byurakan-IRAS Galaxies were summarized (Mikayelyan et al. 2019a)

A general analysis of optical spectroscopic data on 257 Byurakan-IRAS Galaxies (BIG objects) obtained with the BAO 2.6m, SAO 6m, OHP 1.93m telescopes and taken from SDSS spectroscopic database was carried out. 149 star-formation regions (SB) galaxies, 42 galaxies with active nuclei (AGN), and 28 galaxies with a composite spectrum were identified. The spectra of 21 galaxies show signs of emission, but without the possibility of more precise determination of their activity type (we assign them as Em), 13 galaxies appear to have star formation rates that do not exceed normal (we assign them as HII), and 3 are absorption galaxies (we assign them as Abs). We give in Table 1 the the distribution of 257 BIG objects by activity types.

Table 1. The distribution of 257 BIG objects by activity types.

Activity type	Number of objects	%	Activity type	Number of objects	%
HII	149	58.0	AGN	13	5.1
Composite	22	8.6	Em	21	8.2
HII / LINER	4	1.5	Norm	13	5.1
HII / Sy	2	0.8	Abs	3	1.1
LINER	12	4.6	Unknown	1	0.4
Sy	17	6.6	All	257	100.0

Discovery of new bright ULIRGs from the IRAS PSC/FSC Combined Catalogue (Mikayelyan et al. 2018)

High-luminosity IR galaxies (LIRGs, ULIRGs, and HLIRGs) are important for studies related to star-formation processes in the early Universe, as their luminosity allows to detect them at large distances. High IR indicates active star-formation and often starburst processes, which is typical to HII (starburst, SB) and AGN. An interesting question is whether the starburst triggers AGN or vice versa

or there is no direct impact. Considering that very often such objects manifest double and multiple structure, it is also interesting to investigate the interrelationship between the SB, nuclear activity and interactions or merging. We have analyzed the IRAS PSC/FSC Combined Catalogue for search for new bright ULIRGs. By means of the SDSS DR14 data, namely redshifts for those objects having spectroscopic data, we have calculated the IR luminosities and have found 114 very high-luminosity IR galaxies; 107 ULIRGs and 7 HLIRGs. Among them, 48 new ULIRGs and 7 new HLIRGs have been discovered. These objects have been studied by SDSS color-color, luminosity-redshift and other diagrams. Further studies will include the content of the sample for activity types and other available data. We give in Figure 5 SDSS u-g vs. g-r color-color diagram and in Figure 6, the IR luminosity vs. redshift for 114 newly revealed ULIRGs and HLIRGs.

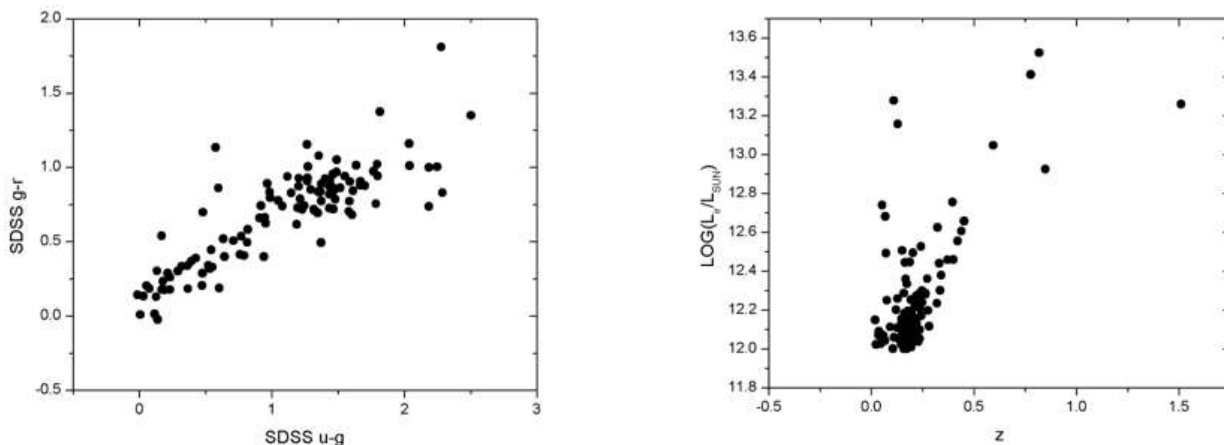


Figure 5. SDSS color-color diagram for 114 newly revealed ULIRGs and HLIRGs.

Figure 6. IR luminosity vs. redshift for 114 newly revealed ULIRGs and HLIRGs.

Spectral Classification of ULIRGs from IRAS PSC/FSC Combined Catalogue (Mikayelyan et al. 2019b)

High-luminosity IR galaxies (LIRGs, ULIRGs, and HLIRGs) are important for studies related to star-formation processes in the early Universe, as their luminosity allows to detect them at large distances. High IR indicates active star-formation and often starburst processes, which is typical to HII (starburst, SB). In many cases high IR indicates an Active Galactic Nuclei (AGN). An interesting question is whether the starburst triggers AGN or vice versa or there is no direct impact. Considering that very often such objects manifest double and multiple structure, it is also interesting to investigate the interrelationship between the SB, nuclear activity and interactions or merging. As a result of cross-correlation of the IRAS PSC/FSC Combined catalogue with SDSS DR14, 114 ULIRGs were separated and classified by the activity types. 1 BLL, 2 quasars, 29 Seyferts of types 1.0-1.8, 5 Seyferts of type 2, 14 LINERS, 36 HII, 14 objects with a composite spectrum (Composite) were identified. Among the type 1 Seyfert galaxies there are many objects with narrow lines. We give in Figure 7 typical examples of SDSS spectra for each activity type.

Radio variable sources at 1400 MHz and their optical variability (Abrahamyan et al. 2018b)

In the present study we have cross-correlated NVSS and FIRST radio catalogues having radio flux measurements at the same 1.4 GHz frequency. This way we benefit from repeated observations from both catalogues, as they give more accurate positions and fluxes and more important, reveal large differences between the two measured fluxes, thus allowing to establish radio variability. As

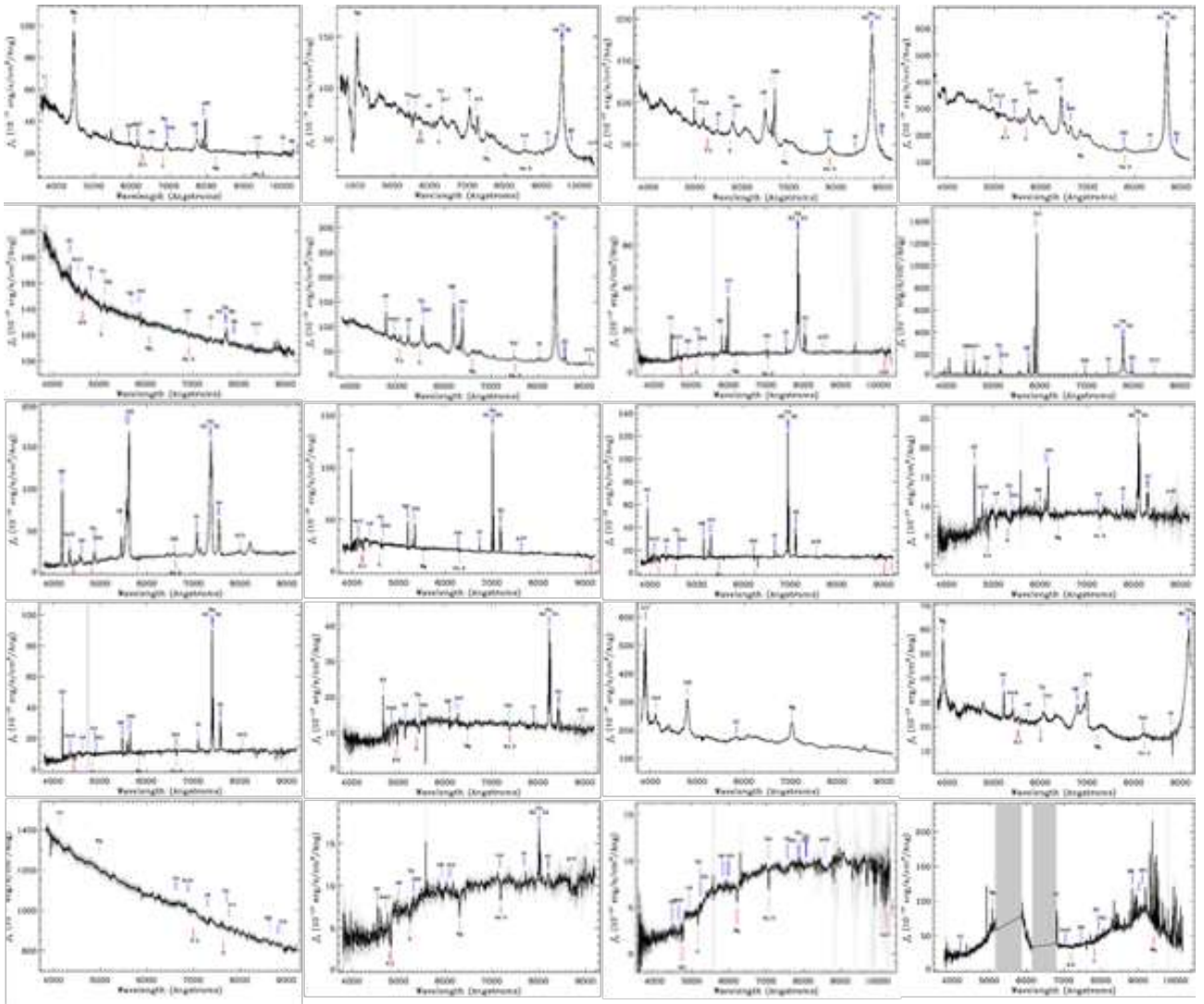


Figure 7. Typical examples for each activity type (from left to right and from top to bottom): S1.0, NLS1.0, S1.2, NLS1.2, S1.5, NLS1.5, S1.8, S2.0, LINER, HII, S1.9/HII, S1.9/LINER, LINER/HII, NLAGN, QSO, NLQSO, BL Lac, Em, Abs, Unkn.

a result, 79,382 radio variables have been revealed, including 6301 with flux differences at 1.4 GHz larger than 15 mJy, 1917 with flux differences > 45 mJy and 260 with flux differences > 200 mJy. By using a special technique (Mickaelian & Sinamyan 2010, Mickaelian et al. 2011), 2425 optically variable objects out of 6301 radio sources have been revealed. 2425 radio sources with both high radio and optical variability into four categories have been divided. 1206 (19%) out of 6301 radio sources have activity types from available catalogues and 619 (25.5%) out of 2425 radio sources with at the same time radio and optical variability have activity types from available catalogues. In addition, 279 radio sources out of 2425 have high variability in optical range. We have established their activity types when available. The IR fluxes and colors for the 6301 variable radio sources have been studied. Color-color diagrams show that most of the "unknown" sources are galaxies. The activity types for 110 (42%) out of 260 extremely high variable radio sources also have been retrieved. We give in Table 2 the distribution of the activity types of 6301 radio sources having radio variability and in Table 3, the distribution of the activity types of 2425 radio sources having both radio and optical variability.

Table 2. Activity types of 6301 radio sources having radio variability.

No.	Activity type	Numbers
1	Blazar (BZB, BZG, BZQ, BZU)	308
2	QSO	639
3	Sy 1.0 / Sy 1	19
4	Sy 1.2	2
5	Sy 1.5	6
6	Sy 1.9	2
7	Sy 2.0 / Sy 2	9
8	AGN	97
9	Starburst	1
10	FSS (Flat-Spectrum radio source)	87
11	USS (Ultra-Steep-Spectrum radio source)	36
	Known (total)	1206 (19%)
	Unknown	5095 (81%)
	Total	6301 (100%)

Table 3. Activity types of 2425 radio sources having both radio and optical variability.

No.	Activity type	Numbers
1	Blazar (BZB, BZG, BZQ, BZU)	176
2	QSO	333
3	Sy 1.0 / Sy 1	9
4	Sy 1.5	6
5	Sy 2.0 / Sy 2	5
6	AGN	45
7	FSS (Flat-Spectrum radio source)	41
8	USS (Ultra-Steep-Spectrum radio source)	4
	Known (total)	619 (25.5%)
	Unknown	1806 (74.5%)
	Total	2425 (100%)

Classification of BZCAT objects having uncertain types ([Abrahamyan et al. 2019a](#))

Classification of BZCAT objects having uncertain types was aimed at understanding some optical properties of blazars having uncertain types (BZU) in BZCAT Catalogue v5. Cross-correlation with SDSS revealed 43 BZU objects that have spectra in SDSS out of the total 227 BZU ones. We have carried out spectral re-classification for these 43 blazar candidates for activity types. As a result, 37 (86%) objects out of 43 changed their previous type. We give in Table 4 the new classification of former BZU objects and in Table 5, spectral classification of these objects for activity types using SDSS spectra.

Table 4. New classification of BZU objects.

No.	Old	New	Numbers
1	BZU	BZB	1 (2%)
2	BZU	BZG	14 (33%)
3	BZU	BZQ	22 (51%)
4	BZU	BZU	6 (14%)
	All		43 (100%)

Table 5. Spectral classification using SDSS spectra.

No.	Activity Type	Numbers
1	Abs	1
2	BLL	1
3	Em	4
4	LINER	2
5	NLQSO	1
6	QSO	17
7	QSO 1.2	3
8	QSO 1.5	1
9	Sy 1.2	1
10	Sy 1.5	2
11	Sy 1.8	1
12	Sy 2.0	3
13	Unknown	6
Total		43

Optical variability of blazars (Abrahamyan et al. 2019b)

The analysis of blazars' parameters from BZCAT leads to a conclusion that they do not have the same properties. The preliminary criterion to include an object in the catalog was the strong radio emission; however, two type of radio sources were selected: BL Lacertae (BLL) objects and Flat Spectrum Radio Quasars (FSRQ). As a number of properties are typical of blazars (strong radio emission, optical variability, continuum optical spectra, polarization, high luminosity, etc.), using the optical data, we investigate them to clarify which property plays the most significant role in their classification as blazars. We found that 60% of blazars have optical variability. We use a technique developed based on POSS1 and POSS2 photometry and group the variability into extreme, strong, medium, and low classes. In the optical range, 51 blazars have powerful variability (extreme variables), and 126 are high variables. In addition, 63% of blazars have detected radiation in X-ray and 28% have detected radiation in gamma rays. We give the average statistical characteristics of blazars based on our analysis and calculations. Here we give in Figure 8 absolute magnitude vs. redshift for BZCAT blazars.

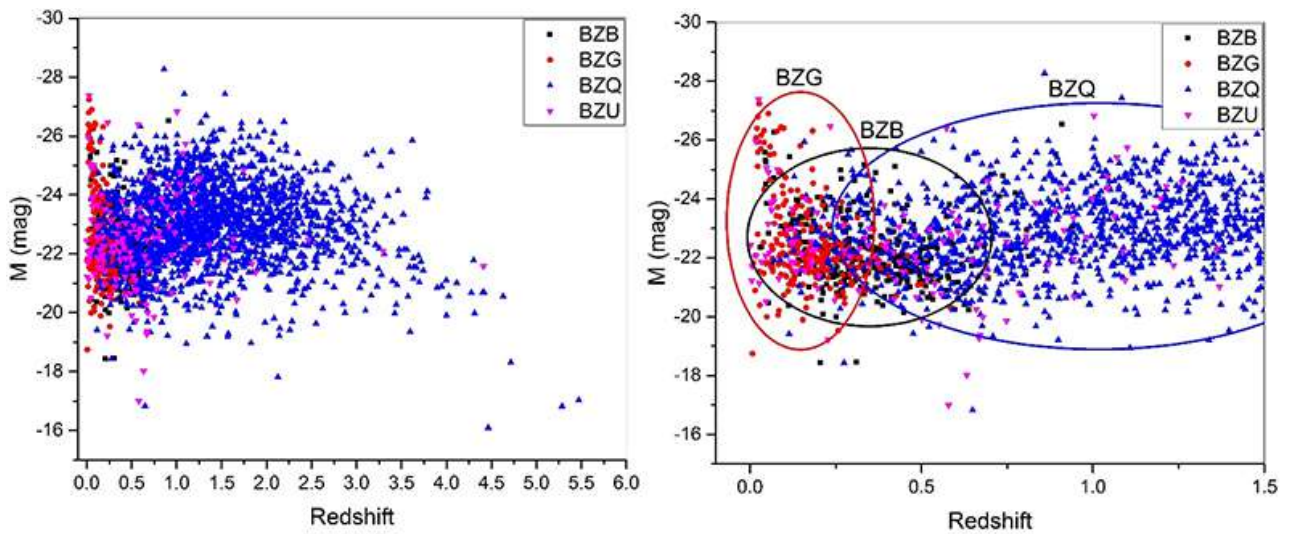


Figure 8. Absolute magnitude vs. redshift for BZCAT blazars.

Summary

A number of interesting results have been obtained in the field of multiwavelength studies of active galaxies, including X-ray, IR and radio sources identified with AGN and Starbursts. Among the important results one could mention:

- Study of SDSS spectra of 371 optical identifications of HRC/BHRC Sample ROSAT X-ray sources (Paronyan et al. 2018, 2019a,b). These sources were also identified in other wavelength ranges and some of their parameters were calculated.
- The UV properties of 1152 Markarian galaxies were investigated based on GALEX data (Mickaelian et al. 2018a). Using our classification for activity types for 779 Markarian galaxies based on SDSS spectroscopy, we have investigated these objects on the GALEX, 2MASS and WISE color-magnitude and color-color diagrams by the location of objects of different activity types and have revealed a number of concentrations.
- Abundance and Star Formation Determinations in more than 700 Markarian galaxies from SDSS Spectra (Gyulzadyan et al. 2018). We have measured their line fluxes and derived the O and N abundances using recent calibrations. The behavior of the [N/H] ratio in under-abundant regions gives strong support to a partially primary origin of nitrogen.
- Revised optical classification of objects classified as “LINERs” in the Catalogue Véron-Cetty & Véron 13th edition (Abrahamyan et al. 2018a), where 926 LINERs are included. We found 176 objects having spectra in SDSS DR14. The re-classification of these objects led to 54% of them to change their activity type classifications.
- Study and classification of SDSS spectra for Byurakan-IRAS Galaxies (Mickaelian et al. 2018b). To the previously observed 172 BIG objects (with BAO, SAO and OHP telescopes) 83 BIG objects were added having spectra in SDSS. Among them, 55 HII, 8 Seyfert galaxies, 2 LINERs, 4 other AGN, 6 composite spectrum objects, and 8 other emission-line galaxies have been revealed. Three of these objects are ULIRGs. The observations and study of 257 Byurakan-IRAS Galaxies were summarized in Mikayelyan et al. (2019a).
- Discovery of new bright ULIRGs from the IRAS PSC/FSC Combined Catalogue (Mikayelyan et al. 2018). By means of the SDSS DR14 data, namely redshifts for those objects having spectroscopy, we have calculated the IR luminosities and have found 114 very high-luminosity IR galaxies; 107 ULIRGs and 7 HLIRGs. Among them, 48 new ULIRGs and 7 new HLIRGs have been discovered. Spectral classification of these ULIRGs were carried out (Mikayelyan et al. 2019b). 1 BLL, 2 quasars, 29 Seyferts of types 1.0-1.8 (including narrow-line), 5 Seyferts of type 2, 14 LINERs, 36 HII, 14 objects with a composite spectrum (Composite) were identified.
- Radio variable sources at 1400 MHz were studied and their optical variability was revealed (Abrahamyan et al. 2018b). As a result, 79,382 radio variables have been revealed, including 6301 with flux differences at 1.4 GHz larger than 15 mJy. By using a special technique (Mickaelian & Sinamyanyan 2010, Mickaelian et al. 2011), 2425 optically variable objects out of 6301 radio sources have been revealed.
- Classification of BZCAT objects having uncertain types was carried out (Abrahamyan et al. 2019a). 43 BZU objects were found to have SDSS spectra and as a result, 37 (86%) objects changed their previous type.
- Optical variability of blazars was studied (Abrahamyan et al. 2019b). We found that 60% of blazars have optical variability. In the optical range, 51 blazars have powerful variability (extreme variables), and 126 are high variables. In addition, 63% of blazars have detected radiation in X-ray and 28% have detected radiation in gamma rays.

List of Used Abbreviations

2MASS - 2 Micron All-Sky Survey
AGN - Active Galactic Nucleus
BAO - Byurakan Astrophysical Observatory (Armenia)
BIG - Byurakan-IRAS Galaxy
BLL - BL Lacertae object
BZCAT - Roma Blazars Catalogue
BZG - BZCAT Galaxy
BZQ - BZCAT Quasar
BZU - BZCAT Uncertain type object
DR - Data Release
FIRST - Faint Images of the Radio Sky at Twenty-centimeters
FSC - Faint Source Catalogue
FSRQ - Flat Spectrum Radio Quasars
FSS - Flat Spectrum radio Source
FUV - Far UltraViolet
GALEX - Galaxy Explorer
HBRC - Hamburg-Byurakan-ROSAT Catalogue
HLIRG - Hyper-Luminous InfraRed Galaxy
HRC - Hamburg-ROSAT Catalogue
IFS - Integral Field Spectroscopy
IRAS - InfraRed Astronomical Satellite
LINER - Low Ionization Nuclear Emission-line Region
LIRG - Luminous InfraRed Galaxy
NUV - Near UltraViolet
NVSS - NRAO/VLA Sky Survey
OHP - Observatoire de Haute Provence (France)
POSS1 - Palomar Observatory Sky Survey 1
POSS2 - Palomar Observatory Sky Survey 2
PSC - Point Source Catalogue
SAO - Special Astrophysical Observatory (Russia)
SB - StarBurst galaxy
SDSS - Sloan Digital Sky Survey
SED - Spectral Energy Distributions
SFR - Star Formation Rate
ULIRG - Ultra-Luminous InfraRed Galaxy
USS - Ultra Steep Spectrum radio Source
WISE - Wide-field Infrared Survey Explorer

References

- Abrahamyan H. V., Mickaelian A. M., Mikayelyan G. A., Paronyan G. M., 2018a, *ComBAO*, 65, 1
- Abrahamyan H. V., Mickaelian A. M., Paronyan G. M., Mikayelyan G. A., Gyulzadyan M. V., 2018b, *Astronomy & Computing*, 25, 176
- Abrahamyan H. V., Mickaelian A. M., Paronyan G. M., Mikayelyan G. A., Gyulzadyan M. V., 2019a, *ComBAO*, 66, 1
- Abrahamyan H. V., Mickaelian A. M., Paronyan G. M., Mikayelyan G. A., 2019b, *AN*, 340, 437
- Aguado D. S., Romina A., Andrés A., et al. 2019, *ApJS*, 240, id. 23
- Bianchi L., Herald J., Efremova B., et al. 2011, *Ap&SS*, 335, 161
- Bird A. J., Bazzano A., Bassani L., et al. 2010, *ApJS*, 186, 1
- Condon J., Cotton W., Greisen E., et al. 1998, *AJ*, 115, 1693
- Gyulzadyan M. V., Mickaelian A. M., Abrahamyan H. H., Mikayelyan G. A., Paronyan G. M., 2018, *ComBAO*, 65, 392
- Helfand D. J., White R., Becker R. H., 2015, *ApJ*, 801, id. 26
- IRAS 1988, Joint IRAS Science W.G., IRAS Catalog of Point Sources, Version 2.0
- Massaro E., Alessandro M., Cristina L., et al. 2015, *Ap&SS*, 357, id. 75
- Mickaelian A. M., 2017, *ComBAO*, 64, 15
- Mickaelian A. M., Sinamyanyan P. K., 2010, *MNRAS*, 407, 681
- Mickaelian A. M., Hovhannisyanyan L. R., Engels D., Hagen H.-J., Voges W., 2006, *A&A*, 449, 425
- Mickaelian A. M., Mikayelyan G. A., Sinamyanyan P. K., 2011, *MNRAS*, 415, 1061
- Mickaelian A. M., Gyulzadyan M. V., Abrahamyan H. V., Paronyan G. M., Mikayelyan G. A., 2017, “Non-Stable Universe: Energetic Resources, Activity Phenomena, and Evolutionary Processes”, *Proc. Intl. Symp. dedicated to 70th anniv. of Byurakan Astrophysical Observatory (BAO), held in Yerevan and Byurakan, Armenia 19-23 September 2016*. Eds. A. M. Mickaelian, H. A. Harutyunian, E. H. Nikoghosyan. *ASP Conf. Ser.*, 511, 149
- Mickaelian A. M., Abrahamyan H. V., Gyulzadyan M. V., Paronyan G. M., Mikayelyan G. A., 2018a, *Ap&SS*, 363, id. 237
- Mickaelian A. M., Harutyunyan G. S., Sarkissian A., 2018b, *Astronomy Letters*, 44, 351
- Mikayelyan G. A., Mickaelian A. M., Abrahamyan H. V., Paronyan G. M., 2018, *ComBAO*, 65, 13
- Mikayelyan G. A., Mickaelian A. M., Abrahamyan H. V., Paronyan G. M., Gyulzadyan M. V., 2019a, *ComBAO*, 66, 31
- Mikayelyan G. A., Mickaelian A. M., Abrahamyan H. V., Paronyan G. M., Gyulzadyan M. V., 2019b, *Ap*, 62, 503
- Moshir M., Copan G., Conrow T., et al. 1989, *IRAS Faint Source Catalog, Version 2.0*, NASA
- Paronyan G. M., Mickaelian A. M., Abrahamyan H. V., Mikayelyan G. A., 2018, *ComBAO*, 65, 412
- Paronyan G. M., Mickaelian A. M., Harutyunyan G. S., Abrahamyan H. V., Mikayelyan G. A., 2019a, *Ap*, 62, 147

Paronyan G. M., Mickaelian A. M., Abrahamyan H. V., Mikayelyan G. A., 2019b, *Ap*, in press

Véron-Cetty M. P., Véron P., 2010, *A&A*, 518, A10

Voges W., Aschenbach B., Boller T., et al. 1999, *A&A*, 349, 389

Voges W., Aschenbach B., Boller T., et al. 2000, MPE, Garching. The ROSAT Faint Source Catalogue

Zickgraf F.-J., Engels D., Hagen H.-J., Reimers D., Voges W., 2003, *A&A*, 406, 535

Investigations of the extended extragalactic radio sources: The quasars 1502+10 and 0923+39 and their environment

M.A.Hovhannisyan^{*1}, R.R.Andreasyan^{†2}, G.M.Paronyan^{‡2}, and H.V.Abrahamyan^{§2}

¹NAS RA Institute of Applied Problems of Physics, Armenia

²NAS RA V. Ambartsumian Byurakan Astrophysical Observatory (BAO), Armenia

Abstract

It was studied the environment of quasars 1502+10 and 0923+39. The investigation of the region with radius of 360 arcmin around these extended extragalactic radio sources shows that distribution of extragalactic objects around them is mainly homogeneous. This study is carried out in the framework of a large project, to find large regions with deficit of extragalactic sources around extragalactic radio sources with very large linear sizes, as it is in the case of DA240, NGC315 radiogalaxies.

Keywords: *galaxy, radio galaxy, quasar*

1. Introduction

The extended radio sources were studied in all electromagnetic wavelength region and their research is ongoing. These objects are interesting because of their very large luminosity as well as their large sizes (Waggett et al. (1977), Algaba & Lo (2016), Mingo et al. (2014)). A part of these objects are galaxies, another part are quasars. The investigation of the environment of extended extragalactic radio sources shows that distribution of extragalactic objects around them is mainly homogeneous. But around some of them this distribution is extremely different from the homogeneous.

2. The quasar 1502+10 and its environment

The 1502+10 is one of extended extragalactic radio sources and it is well known quasar. For the investigation of this quasar and extragalactic sources in his environment is dedicated this paragraph. It was studied the quasar and his environment in the region with radius of 360 arcmin. We use the data from the site of NASA (<https://ned.ipac.caltech.edu>). As the density ρ of galaxies is very large for the analyses of galaxies we use only the objects in the 60 arcmin environment.

The density ρ of galaxies in the regions R_{\min} - 10, 20, 30, 40, 50, 60 arcmin is almost the same. In average there are 3.241 galaxies in the region of one square minute. As it is seen from the Table 1 the number of galaxies in the error limits is practically the same.

In the Table 2 we bring GP(galactic pairs), GT(galactic triples), GG(galactic groups), GC(clusters of galaxies), QSO(quasars). QG(quasar groups), GL(gravitational lenses), ABLs(sources with absorption lines), EMLS(sources with emission lines), and number of objects in the regions with radius R_{\min} - 60, 120, 180, 240, 300, 360 arcmin respectively.

The density of these objects almost three orders of magnitude lower than the density of galaxies. In some cases, this difference reaches four orders of magnitude.

*martin@bao.sci.am, Corresponding author

†randrasy@bao.sci.am

‡paronyan.gurgen@yahoo.com

§abrahamyanhayk@gmail.com

Table 1. Galaxies

R_{\min}	N_{gal}	Ring ($R_i - R_{i-1}$)	N_{Ring}	ρ_R	ρ_{Ring}
10	1012	100	1012	3.221	3.221
20	3804	300	2792	3.027	2.962
30	9014	500	5210	3.188	3.318
40	16160	700	7146	3.371	3.249
50	25945	900	9785	3.303	3.461
60	37703	1100	11758	3.334	3.402

Table 2. Number of objects in the region

R_{\min}	GP	GT	GG	GC	QSO	QG	GL	ABLS	EMLS
60	61	0	33	81	61	0	0	3	0
120	255	1	153	307	224	0	0	6	0
180	498	5	369	744	478	0	0	26	0
240	729	16	711	1270	901	0	0	28	0
300	1051	29	1095	2069	1388	0	3	47	0
360	1235	380	1564	2980	2023	0	5	49	1

In Table 3 we bring the number and density of Super Nova. These data we bring additional to show that our data is very close to the real data and each Super Nova is used to determine the distances of the quasars because the quasars are behind the Super Nova.

Table 3. SN

R_{\min}	N	ρ_R	Ring	ρ_{Ring}
30	0	0	900	0
60	1	0.884×10^{-4}	2700	1.179×10^{-4}
120	11	2.432×10^{-4}	10800	2.947×10^{-4}
180	29	2.849×10^{-4}	18000	3.183×10^{-4}
240	53	2.929×10^{-4}	25200	3.032×10^{-4}
300	92	3.254×10^{-4}	32400	3.832×10^{-4}
360	131	3.217×10^{-4}	39600	3.135×10^{-4}

In the Tables 4 and 5 we bring the data of extragalactic radio sources and quasars. The density of radio sources is nearly the same in everywhere, but is three time more than the density of quasars.

Table 4. Radio sources

R_{\min}	N	ρ_R	Ring	ρ_{Ring}
60	239	21.132×10^{-3}	3600	21.132×10^{-3}
120	783	17.374×10^{-3}	10800	16.034×10^{-3}
180	1801	17.694×10^{-3}	18000	18.002×10^{-3}
240	3214	17.761×10^{-3}	25200	17.848×10^{-3}
300	5091	18.006×10^{-3}	32400	18.440×10^{-3}
360	7390	18.151×10^{-3}	39600	18.480×10^{-3}

The analyses of data from Tables 1 - 5 suggest that the density of quasars around the 1502 + 10 are not very different, as is in the case for other type sources.

In the Fig. 1 we bring the distribution of quasars from the distances. From the figure 1 it is clear that the distribution of quasars from the redshift in the neighborhood of quasar 1502+10 is close to homogeneous distribution as in many other domains.

Table 5. QSO

R_{\min}	N	ρ_R	Ring	ρ_{Ring}
60	61	5.394×10^{-3}	3600	5.394×10^{-3}
120	224	4.951×10^{-3}	10800	4.804×10^{-3}
180	478	4.696×10^{-3}	18000	4.492×10^{-3}
240	901	4.979×10^{-3}	25200	5.343×10^{-3}
300	1388	4.909×10^{-3}	32400	4.784×10^{-3}
360	2023	4.969×10^{-3}	39600	5.104×10^{-3}

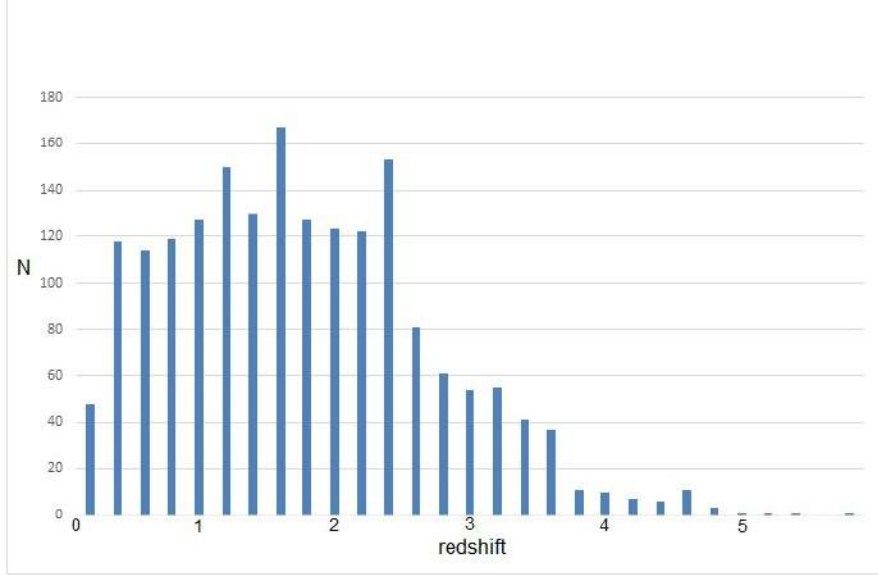


Figure 1. Quasars distribution by their redshifts (by 0.2 intervals) around the quasar 1502+10.

3. The quasar 0923+39 and its environment

In all the Tables 6-10 and Fig. 2 in this paragraph we bring similar data as are given in Tables 1-5 and Fig. 2.

Table 6. Galaxies

R_{\min}	N_{gal}	Ring ($R_i - R_{i-1}$)	N_{Ring}	ρ_R	ρ_{Ring}
10	644	100	644	2.050	2.050
20	2804	300	2164	2.231	2.296
30	6520	500	3716	2.304	2.366
40	11514	700	4994	2.291	2.271
50	21032	900	9518	2.678	3.366
60	37682	1100	16650	3.332	4.818

Table 7. Number of objects in the region

R_{\min}	GP	GT	GG	GC	QSO	QG	GL	ABLS	EMLS
60	1	3	25	94	68	0	0	0	0
120	8	9	145	444	254	0	0	0	0
180	17	28	327	842	565	0	5	0	1
240	23	47	503	1142	1051	0	5	2	3
300	37	70	754	1516	1630	0	5	2	3
360	46	100	1068	2004	2370	0	6	2	5

Table 8. SN

R_{\min}	N	ρ_R	Ring	ρ_{Ring}
40	0	0	1600	0
60	2	1.768×10^{-4}	2000	3.183×10^{-4}
120	6	1.327×10^{-4}	10800	1.179×10^{-4}
180	17	1.670×10^{-4}	18000	1.957×10^{-4}
240	27	1.492×10^{-4}	25200	1.261×10^{-4}
300	48	1.670×10^{-4}	32400	0.970×10^{-4}
360	72	1.768×10^{-4}	9600	1.929×10^{-4}

Table 9. Radio sources

R_{\min}	N	ρ_R	Ring	ρ_{Ring}
60	347	30.682×10^{-3}	3600	30.682×10^{-3}
120	1476	32.627×10^{-3}	10800	33.275×10^{-3}
180	3538	34.759×10^{-3}	18000	36.464×10^{-3}
240	5974	33.014×10^{-3}	25200	30.770×10^{-3}
00	9020	31.902×10^{-3}	32400	29.925×10^{-3}
60	12773	31.372×10^{-3}	39600	30.167×10^{-3}

Table 10. QSO

R_{\min}	N	ρ_R	Ring	ρ_{Ring}
60	68	6.013×10^{-3}	3600	6.013×10^{-3}
120	254	5.615×10^{-3}	10800	5.482×10^{-3}
180	565	5.551×10^{-3}	18000	5.500×10^{-3}
240	1051	5.808×10^{-3}	25200	6.139×10^{-3}
300	1630	5.765×10^{-3}	32400	5.688×10^{-3}
360	2370	5.821×10^{-3}	39600	5.948×10^{-3}

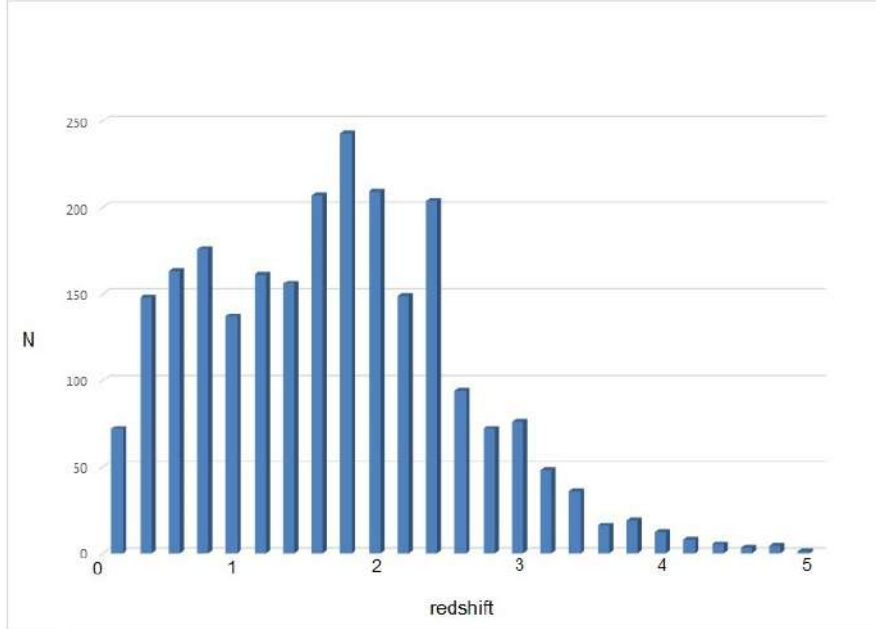


Figure 2. Quasars distribution by their redshifts (by 0.2 intervals) around the quasar 0923+39.

The comparisons of the results suggest that the data surrounding these two quasars are identical to the distribution of such sources in space, similar to the NGC6251 and 3C219 radio galaxies (Hovhannisyan et al. (2018), Hovhannisyan et al. (2019)). This is not the case with DA240 NGC315

radioactivity ([Artyukh & Ogannisyan \(1988b\)](#), [Artyukh & Ogannisyan \(1988a\)](#)).

4. Conclusions

The distribution of extragalactic sources around the quasars 1502 + 10 and 0923+ 39 shows that these universe domains are homogeneous for all types of sources. In future work it is necessary to obtain the distribution of extragalactic sources across all domains, where it cannot be said that the universe is homogeneous in those regions. Such regions already are found (see for example [Artyukh & Ogannisyan \(1988b\)](#), [Artyukh & Ogannisyan \(1988a\)](#)).

References

- Algaba J.-C., Lo W.-P., 2016, *ApJ*, 833, 288
- Artyukh V. S., Ogannisyan M. A., 1988a, *Soviet Astronomy Letters*, 14,4, 301
- Artyukh V. S., Ogannisyan M. A., 1988b, *Soviet Astronomy Letters*, 14,5, 377
- Hovhannisyan M. A., Andreasyan R. R., Paronyan G. M., 2018, *ComBAO*, 2(LXV), 398
- Hovhannisyan M. A., Andreasyan R. R., Mahtesyan A. P., Paronyan G. M., Abrahamyan H. V., Sargsyan A. V., Aghadjanyan H. S., 2019, *Physical Science & Biophysics*, inpress
- Mingo B., Hardcastle M. J., Croston J. H., et al. 2014, *MNRAS*, 440, 269
- Waggett P. C., Warner P. J., Baldwin J. E., 1977, *MNRAS*, 181, 465

Space Activities in Armenia: past, present and future

A. M. Mickaelian* and G. A. Mikayelyan[†]

NAS RA Byurakan Astrophysical Observatory (BAO), Byurakan 0213, Aragatzotn Province, Armenia

Abstract

A review about Space related activities in Armenia is given, particularly in the Byurakan Astrophysical Observatory (BAO, Armenia), including the first Space Astronomy projects by Grigor Gurzadian in 1960s-1970s (Orion and Orion-2 UV observatories), research projects with USA (NASA) and European (ESA) Space observatories (IRAS, ROSAT, Hubble, Spitzer, WISE, etc.) by BAO scientists, Armenian participation in International Virtual Observatory Alliance (IVOA), International Planetary Data Alliance (IPDA), and UN Committee on the Peaceful Users of the Outer Space (COPUOS), “Roscosmos” station in Byurakan established in 2014 for monitoring of Space debris, Armenian participation in NASA Space Apps Hackathons, Armenian participation in the European H2020 project, including the Space field, organization of Space related meetings and schools in Byurakan, etc. Armenia with its astronomical and other related background has great potential in establishing collaborations and promoting Space Sciences and Space Technologies.

Keywords: *Space, Space observatories, Virtual Observatories, COPUOS, NASA, H2020 Space*

Introduction

At present Armenia is a small country with limited economy (by area it is on the 143rd position in the world, by population it is on the 134th position and by budget it is on the 130th position), however with a high level of science and technologies. Though Space activities are mainly carried out by big countries (like USA – NASA, Japan – JAXA) or by a group of countries (e. g. 22 European countries – European Space Agency, ESA), Armenia has been and is involved in many Space related projects and collaborations, including Space Astronomy research projects by the Byurakan Astrophysical Observatory (BAO), Space Astronomy instrument making by BAO and Garni Space Astronomy Institute, participation in international space-related organizations, organization of international meetings and schools, etc.

Armenia with its astronomical and other related background has great potential in establishing collaborations and promoting Space Sciences and Space Technologies. In this article we give an overview of past, present and possible future activities developed in Armenia related to Space.

Space Astronomy and Space related science at BAO in 1960s-1980s

Grigor Gurzadyan (1922-2014) was the pioneer of Space Astronomy in Armenia and one of the pioneers in the USSR. In 1960s, using ballistic rockets R-5, he directed the UV and X-ray observations of the Sun and stars (the first launch was on February 15, 1961 from Kapustin-Yar base). His paper “*A Powerful X-ray Flare on the Sun*”, published in Communications of Armenian SSR Academy of Sciences in 1966 is among the earliest papers on Space Astronomy. Then Gurzadyan moved to design Space orbital observatories; ultraviolet (UV) Orions were the most famous ones. In April, 1971 the first space station Salyut 1 carried **Orion 1** onto the orbit, the first Space telescope with an objective prism. But the highlight was **Orion 2**, which was operated onboard the spacecraft Soyuz 13 in December, 1973. Here are the comparative specifications of Orion 1 and Orion 2 (Table 1).

*aregmick@yahoo.com, Corresponding author

[†]gormick@mail.ru

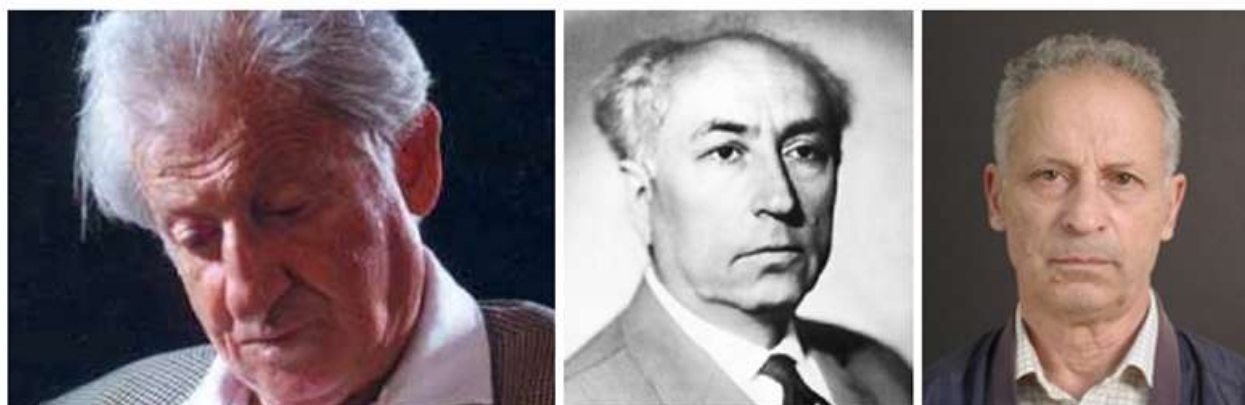
Technical parameters	Orion 1	Orion 2
Optical system	Mersenne	meniscus, Cassegrain (-Maksutov) system
Spectrograph	Wadsworth	objective prism; 2 additional sidereal spectrographs
Diameter of primary mirror	280 mm	300 mm
Focal length	1400 mm	1000 mm
Field of view		5°
Spectral range	2000–3800 Å	
Spectral resolution	5 Å at 2600 Å	8-29 Å at 2000-3000 Å
Film	UFSH 4, width 16 mm, range sensitivity: 4000–2500 Å, resolution better 130 lines/mm	KODAK 103UV, diameter: 110 mm
Cartridge capacity	12 m	
Stabilization	two-stage, inertial; first stage: three-axis inertial stabilization of station Salyut 1	2-star sensor sets: each containing a two-coordinate star sensor coaxial to telescope and one-coordinate one, in 45° to telescope axis
Fine guidance	via a star with accuracy 15 arcsec on each axis	3-axes guidance system accuracy: better than 5 arcsec on two cross-sectional axes of telescope (via star A), and better than 30 arcsec at optical axis (star B)
Star sensor	of semi-disk (diameter of input: 70 mm; focal length: 450 mm), limiting stellar magnitude 5 ^m	input apertures: 80 and 60 mm; focal lengths: 500 and 240 mm; limiting stellar magnitudes: 3.5 ^m and 3.0 ^m
Mass	170 kg	240 kg (telescope 205 kg)
Mass returned to Earth (cartridges)		4.3 kg
Installation onboard	Salyut 1	Soyuz 13
Observer cosmonaut	Viktor Patsaev	Valentin Lebedev
Operational	June 1971	Dec 1973

Spectra of thousands of stars to 13th stellar magnitude, the first satellite UV spectrogram of a planetary nebula were obtained revealing spectral lines of aluminum and titanium – elements not previously observed in planetary nebulae, two-photon emission from nebula was directed for the first time. For comparison, the US Skylab’s UV telescope, which was on the orbit at the same time, could only observe stars down to 7.5th magnitude. The obtained results were published in the most important astronomical journals, including 3 articles in “Nature” (Gurzadyan 1974, Gurzadyan & Ohanesyan 1972, Gurzadyan & Rustambekova 1975).

In the **Byurakan Astrophysical Observatory (BAO)**, the Space Astronomy Research Department was operating in 1964-1968; then The Space Research branch was established and was operating in 1968-1973; later Space Astronomical Laboratory was opened in Garni and was operating in 1973-1978, the Extra-Atmospheric Astronomical Laboratory was operating in Byurakan in 1978-1992, and the Garni Institute of Space Astronomy headed by G. Gurzadyan was operating in 1992-2004. In 1967-1973 Gurzadyan headed BAO branch of space researches, in 1973-1978 he headed Garni Astronomy Laboratory, in 1978-1992 he was the Head of Extra-atmospheric Astronomy Laboratory of BAO, in 1992-2004 he was the Head of Garni Space Astronomy Institute. Since 1979 he established and was the Head of the Chair of Space Instrument-Making of Yerevan Polytechnic Institute as well.

Gurzadyan published books related to Space flights and Space dynamics (Gurzadyan 1992, 1996, 2002).

Special Schools for Soviet astronauts (pre-flight training) were organized in BAO and in Garni in 1960s-1990s, where almost 40 future astronauts had obtained astronomical knowledge.



Grigor Gurzadyan, Norayr Sisakyan and Hrant Tovmassian

BAO researchers were engaged in other Soviet Space projects as well. **Hrant Tovmassian** (b. 1929) worked on the Space ultraviolet telescope **Astron** (Crimean Astrophysical Observatory; Boyarchuk et al. (1984)). Tovmassian's team made the guiding system. An offset guidance was proposed, which was made by the relatively bright star located nearby to the observed object on sky. It was made at the Granit Special Construction Bureau (SCB). The head of the project and the manufacturing was Marat Krmoyan. The telescope was launched to the orbit in 1984.

Later on, Tovmassian initiated the project of the Space Ultraviolet Telescope **Glazar** for study of the far UV emission of OB type stars in stellar associations. The space telescope Glazar was projected and constructed in the Granit SCB in Garni. The diameter of the telescope mirror was 40 cm. The Ritchey-Cretien optical system provided 1.3 deg field of view. Observations were made at 1640Å wavelength. The used optic-electronic detector transferred 1640Å image of the observed field to a visual light, magnified it, and photographed at the ordinary film. The high-quality Kodak films were provided by the Geneva observatory (Switzerland). The telescope was launched to the orbit and attached to the Mir Space Station in 1987 (Tovmassian et al. 1988). Observations have been carried out by cosmonauts by commands from the center of the space communications at Energia near Moscow. Cosmonauts brought to the Earth the exposed films upon their return from the orbit. Usually the exposed films remain at the orbit for about one year. A number of scientific results were obtained, including the study of OB associations, discovery of dust envelopes around some distant B type stars, etc. In 1990, the Space Ultraviolet Telescope **Glazar-2** was constructed and launched to the orbit and attached to the Mir Space Station. It differed from the first Glazar by higher sensitivity achieved by using the better ultraviolet filter. However, it did not work due to problems after the crash of the Soviet Union.

In 1990 at the Granit SCB we started the the projection and construction of the fully reflecting 1m Astrophysical Schmidt Orbital Telescope (**ASchOT**) (Tovmassian et al. 1991). It was planned to perform an image and a spectral sky survey at 1500Å. However, in the result of the collapse of the Soviet Union, the works on manufacturing the ASchOT were ceased.

Academician **Norayr Sisakyan** (1907-1966) was one of the founders of Space Biology and Space Medicine (Space Biomedicine). Sisiakyan was the Vice-President of the International Academy of Astronautics. For some new directions of biochemistry, we owe Sisakyan, who was more interested in cosmic biology. The scientist was convinced that the universe needed to look for life and organism, without doubt that there should be microorganisms at all. Thus, the scientific basis was based on the development of gravitational biology, the study of dimension and, as a consequence, the scientific principles of selection and preparation of cosmonauts, as well as the environmental, astronauts' survival and security issues. He did not doubt that Gagarin's flight would succeed, and he thought modestly

that he had his scientific contribution to that success.

Telecommunication systems of Venus landing module were designed in NAS RA institutions, namely Institute of Radiophysics and Electronics (led by Radik Martirosyan), and experiments on microbes were developed on Soviet spacecrafts (led by Evrik Afrikyan).

Space Astronomy and Space related science at BAO in 2000s-2010s

A number of astrophysical research projects were carried out by BAO scientists with USA (NASA) and European (ESA) Space observatories. Some of the BAO scientists participated in American and European space astronomy programs, in particular Artashes Petrosian participated in the **Hubble Space Telescope (HST)** programs (Hayes et al. 2005, Kunth et al. 2010, Mas-Hesse et al. 2009) in collaboration with STScI in Baltimore, USA, and Areg Mickaelian's observational project on study of high-luminosity IR galaxies and IR excess galactic stars were carried out on IR **Spitzer Space Telescope (SST)** in collaboration with Cornell University (Ithaca, N.Y.) team (Hovhannisyan et al. 2009, Sargsyan et al. 2008). Mickaelian's **Astronomical Surveys research department** at BAO extensively uses space multiwavelength data for astrophysical research. Most important space telescopes that are used for multiwavelength analysis are IRAS, ROSAT, HST, SST, WISE, Herschel, etc.

In addition, the **Digitized First Byurakan Survey (Markarian's Survey)**, the project of digitization of astronomical plates (Massaro et al. 2008, Mickaelian et al. 2007) was carried out due to collaborations with NASA and other several international organizations in 2002-2007. This survey and its digitized version are included in UNESCO's "Memory of the World" Documentary Heritage International Register.

NAS RA Byurakan Astrophysical Observatory has signed a contract with the Russian Space Agency "Roscosmos" in 2014, according to which **monitoring of space artificial fragments (space debris)** is carried out in Byurakan. Every year, some 200 observing nights are being used for some 400,000 measurements and some 600,000 orbits for artificial satellites are being recovered. There is a team of 8 BAO observers that support the observations. BAO Applied Astronomy Department is in charge for this project and Haik Harutyunian is the PI from the Armenian part.



Applied Astronomy Department in Byurakan Astrophysical Observatory (BAO), Armenia, where joint project with Russians on monitoring of cosmic junk is being implemented.

In 2005, based on the Digitized First Byurakan Survey (DFBS or Markarian Survey), Areg Mickaelian created the **Armenian Virtual Observatory (ArVO)** project (Mickaelian 2006, 2007, Mickaelian et al. 2006), which joined the **International Virtual Observatory Alliance (IVOA)** in the

same year. Virtual observatories use all data accumulated in astronomy, from both ground-based and Space telescopes, by all observational methods, at all wavelength ranges and in all epochs, which gives a huge advantage in sense of overall and complete studies compared to individual observations and studies. Mickaelian is IVOA Executive Committee member since 2005. Later on, in 2013, Armenia joined **International Planetary Data Alliance (IPDA)** as an associate member and Mickaelian became IPDA Steering Committee member. IPDA unifies space agencies of most important countries and communities (US National Aeronautics and Space Administration (NASA), European Space Agency (ESA), Japan Aerospace Exploration Agency (JAXA), China National Space Administration, Indian Space Research Organisation (ISRO), UK Space Agency (UKSA), German Aerospace Center – Deutsches Zentrum für Luft- und Raumfahrt e.V. (DLR), French National Centre for Space Studies – Centre National d'Études Spatiales (CNES), Italian Space Agency – Agenzia Spaziale Italiana (ASI), Russian Space Research Institute – Институт Космических Исследований (ИКИ), United Arab Emirates Space Agency and Armenia is represented by the Armenian Astronomical Society, ArAS). IPDA creates database for all planetary data (Sarkissian et al. 2016) and the DFBS project has contributed in it by data related to known asteroids and by search for new asteroids (Berthier et al. 2009, Mickaelian et al. 2019, Sarkissian et al. 2012).

Organization of Space related meetings and schools in Byurakan

In May 1964 (Tovmassian 1965) and Sep 1971 (Sagan 1973) conferences on extraterrestrial civilizations were held in Byurakan. The meeting of 1971 was the **First international symposium on the problem of Extraterrestrial Civilizations and Communication with them (CETI)**. Many prominent scientists, including astronomers, physicists, chemists, biologists, philosophers, and specialists of other related fields participated in the symposium. 32 Soviet and 19 American scientists, as well as representatives from UK, Hungary, and Czechoslovakia participated in the works of the symposium, including the 3 Nobel Prize Winners: biologist F. Crick (UK) and physicists F. W. Dyson and C. Towns (USA). Prominent scientists F. Drake, T. Gold, C. E. Sagan, D. Heesch, K. Kellermann (USA), F. Morrison (UK) and others also took part in the symposium. Many aspects of the problem of extraterrestrial intelligence were discussed at the ten scientific sessions of the symposium. Questions of plurality of planetary systems in the Universe, origin of life on the Earth and its possibility on other cosmic objects, rise and evolution of intelligent life, rise and development of technological civilization, problems of search for signals of extraterrestrial civilizations and traces of astroengineer activity, problems of establishment of communication with extraterrestrial intelligence, as well as their possible consequences were discussed in details.

A Conference for Young Astronomers was held in Nov 2011 (Mickaelian et al. 2012): **50 years of Cosmic Era: Real and Virtual Studies of the Sky**. This was a Conference of young scientists from FSU countries, dedicated to the 50th anniversary of Yuri Gagarin flight to the Space. The main goal of the Conference was to gather young scientists from FSU countries to familiarize them with the latest developments of Astrophysics and Space Physics, including the using of the latest technology and techniques. Within three days for the young scientists were organized lectures and practical exercises on various areas of Astrophysics and Space Research, as well as them was provided the opportunity to present their works.



“Relation of Astronomy to other Sciences, Culture and Society” (RASCS, Harutyunian et al. (2015)) meeting was devoted to the role of astronomy in science, culture and other fields of human activity and development of these fields due to the knowledge obtained from the Universe. In

modern era, astronomy is probably the field of science, which plays a leading role in the formation and development of interdisciplinary sciences. The meeting was aimed at the development of problems of interdisciplinary sciences in Armenia and preparation of a basis for further possible collaborations by means of presentations of available modern knowledge in various areas by experts from different professions and by joint discussions. Particularly, talks on life in the Universe, extraterrestrial intelligence, space flights, space hazards and space ecology were presented.

Orion-Byurakan school for young astronauts was organized jointly with Roscosmos and was held both in BAO and in Physics and Mathematics specialized school after A. Shahinyan (Yerevan State University) in 2017 for students mainly from Russia, and Armenian students joined as well. But the main initiative to activate Space Sciences and Technologies in Armenia and to prepare corresponding staff was the **Regional Summer School on Space Sciences and Technologies** held on 2-6 Sep 2019 in Byurakan (<https://www.bao.am/meetings/meetings/SST/>). It aimed at attracting beginner astronomers and related MSc and PhD students to the field of scientific research, teaching the principles of scientific work. Thanks to these, BAO plays a leading role in this region and offers opportunities for young people in the region to participate in high-level lectures and practical courses as there are not many opportunities for participating in European and American schools. Students in the region also have a wide range of opportunities to communicate, to make new acquaintances, which is very useful for their further advancement. Experts from ESA, LATMOS, “Roskosmos” and other important organizations were invited as lecturers. Several tutorials were also given.



Armenian participation in Space related international organizations

Armenia has joined the international **Committee on Space Research (COSPAR)**, established by ICSU in 1958. Ashot Chilingaryan (Alikhanyan National Laboratory, ANL) is the Representative from Armenia. Among COSPAR’s objectives are the promotion of scientific research in space on an international level, with emphasis on the free exchange of results, information, and opinions, and providing a forum, open to all scientists, for the discussion of problems that may affect space research. These objectives are achieved through the organization of symposia, publication, and other means. COSPAR has created a number of research programs on different topics, a few in cooperation with other scientific Unions.

Armenia is a member of the **United Nations Office for Outer Space Affairs (UNOOSA)**. It works to promote international cooperation in the peaceful use and exploration of space, and in the utilization of space science and technology for sustainable economic and social development. The Office assists any UN Member States to establish legal and regulatory frameworks to govern space activities and strengthens the capacity of developing countries to use space science technology and applications for development by helping to integrate space capabilities into national development programs. UNOOSA is the UN office responsible for promoting international cooperation in the peaceful uses of outer space. UNOOSA serves as the secretariat for the General Assembly’s only committee dealing exclusively with international cooperation in the peaceful uses of outer space: **United Nations Committee on the Peaceful Uses of Outer Space (COPUOS)**, 87 member states), where Armenia became a member in 2014. The **Armenian Space Agency (ArSA)** has been formally created, which was an interdepartmental commission under the authority of the Ministry of Transport, Communication and Information Technologies. The current main objective of the Armenian Space Agency is having an Armenian own satellite.

Armenia joined EC **Horizon 2020 (H2020)** project as an associate member in 2016. H2020 has 25 fields, including the **Space**. Areg Mickaelian and Aram Saharian are H2020 Space Program Committee (PC) members from Armenia, and Gor Mikayelyan and Hripsime Mkrtchyan are National Contact Points (NCPs). Armenian H2020 activities include many areas (<http://h2020.sci.am/>). Armenian scientists participated in H2020 COST Action TD1403 BigSkyEarth (Big Data Era in Sky and Earth Observation) and participate in H2020 COST Action CA18104 MW-Gaia (Revealing the Milky Way with Gaia). Areg Mickaelian was/is Management Committee (MC) member in both projects. A number of conferences and training schools were organized during 2015-2019.

Armenian Space related current activities and legislative steps

“The Space” sector has been included in the list of priority directions in the framework of interstate agreement between Armenia and Russia. The Governments of the Republic of Armenia and India have signed a Memorandum of Understanding on Peaceful Uses of Outer Space in 2017.

RA Security Council has been involved in **Space Security** field since 2018; “The Space development will lead the country towards more ensured security, furthermore it will encourage the growth of national potential to endure modern challenges. Future discussions will be directed to the regulation of the relevant legislative dimension, to the launch of the Armenian Space Project including also the possibility of having Armenia’s own artificial satellite”, said the Secretary of RA Security Council Armen Grigoryan. He officially visited BAO in 2018 and had discussions with BAO Director Areg Mickaelian. The possible opportunity of having Armenia’s own satellite was also discussed. The Government of Armenia has been working on legislative amendments related to Space Transport since 2018 and RA **Law on Space Activities** (discussed and prepared in March 2019; <https://www.e-draft.am/projects/1568/about>) is now ready for acceptance by the RA National Assembly.

Other space related activities in Armenia

Michael Keziryan, the Director of the **International Space Safety Foundation (ISSF)** visited BAO in 2018 and discussed future possible collaboration with BAO Director Areg Mickaelian. Narine Knajyan, one of NASA’s administrative directors, visited BAO and delivered a seminar on the topic of “NASA’s Cassini mission to Saturn” in 2017. NASA’s Ambassador Elena Semerjyan visited the “AYAS” Armenian Aerospace Society in 2018, and presented NASA’s future projects and plans. **ARM-SAT Armenian satellite project** has been prepared with French partners (LATMOS, University of Versailles Saint Quentin, UVSQ). British, Belgian and Swiss scientists (PI from Armenia: Areg Mickaelian) have also participated in the process of the development of the project. The possible organization of a regional summer school on “Space Technologies” was discussed with French partners (LATMOS, UVSQ). The Space Security Project has been discussed between BAO’s director Areg Mickaelian and Aram Saharian, Head of Scientific policy department of the State Committee of Science (SCS) of the Ministry of Education and Science of the RA. The Ministries of Defense and Emergency Situations, NAS RA and other governmental units are also planned to be included in the project.

“The Space Club” (now: **“AYAS” Armenian Aerospace Society NGO**, RA Ministry of Education and Science) was established by Avetik Grigoryan (President of “AYAS”, Co-founder at Armenian Rocket Modeling Society) in 1988, where space flights and technology, or other related field courses are being taught. Avetik Grigoryan as the head of the theoretical research bureau has participated in creation of missile defense facilities for Armenia in the framework of Military-Industrial complex from 1990 to 2000. He has published a science-popular book *“From the Depth of Centuries to Space”* in 2013, the last two chapters of which are devoted to space flight theory, rocket engineering and space observation. The book was distributed to the schools in Armenia and Artsakh. “AYAS” has proposed to create a working group that will develop a mini-satellite (CubSat) project, will generate it, conduct its work tests and prepare for the dissemination (it is also recommended to involve university and school students) by integrating the professional resources of the Aerospace Society’s and other organizations. The launch will be carried out by a foreign CubeSater orbit launching servicing company. It will become the first satellite in Armenia, which will be launched into an orbit around the Earth, as

an easier, faster and low-price satellite. It will conduct a technological scientific experiment directed to solving the urgent problem with the space junk and consequently it will encourage the Armenian society and will bring a new prestige to Armenia.

Space museum was established on Grigor Gurzadyan's initiative on 27 June 2001 in Garni, and later on 28 Nov 2015 it was moved to Yerevan by his son Vahagn Gurzayan's efforts (<http://garni-cosmos.com>). The exposition of the museum includes unique items of early space epoch created in Armenia: a genuine landing capsule returned from space, other items operated in space, replica of space observatory ORION-2 being exhibited in EXPO-2000, Hanover, other devices operated at space experiments. Also, the exhibition includes remarkable documents associated to early space research and space flights, handwritten documents by Soviet cosmonauts, designers of spacecrafts VOSTOK, SOYUZ and scientists, as well as of NASA astronaut and the designer of American spacecraft.



The Space Museum in Yerevan, Armenia

Armenia has started to participate in **NASA's Space Apps Hackathons** since 2016 (Organizer: Arman Atoyan, Head of X-Tech and ARLOOPA companies). Among the organizers, there are X-Tech, FAST (Foundation for Armenian Science and Technology), LOCATOR, BAO, and other companies.



NASA Space Apps Hackathons in Armenia

An idea and design to create a *“Center for Innovative Space Technology Research and Development”*

in Byurakan, attached to BAO, as well as a space station, was developed by architect student Narek Petrosyan, as a diploma thesis at the National University of Architecture and Construction of Armenia. This idea shows that the Armenian young people are eager to develop Space sciences and technologies and build a modern space-oriented society.



Byurakan Center for Space Technology Research and Development

References

- Berthier J., Sarkissian A., Mickaelian A., Thuillot W., 2009, Proc. European Planetary Science Congress, p. 526
- Boyarchuk A. A., Gershberg R. E., Granitskij L. V., Kovtunenkov V. M., Krmoyan M. N., Cruvellier P., Courtes G., Pronik V. I., Severnij A. B., Tovmassian H. M., Khojayants Y. M., Hua C. T., 1984, ARep, 10, 163
- Gurzadyan G. A., 1974, Nature, 250 (5463), 204
- Gurzadyan G. A., 1992, Theory of Interplanetary Flights, Moscow (in Russian)
- Gurzadyan G. A., 1996, Theory of Interplanetary Flights, London, "Gordon and Breach"
- Gurzadyan G. A., 2002, Space Dynamics, "Francis and Taylor"
- Gurzadyan G. A., Ohanesyan J. B., 1972, Nature, 239 (5367), 90
- Gurzadyan G. A., Rustambekova S. S., 1975, Nature, 254 (5498), 311
- Harutyunian H. A., Mickaelian A. M., Farmanyan S. V., (Eds.) 2015, Relation of Astronomy to Other Sciences, Culture and Society, Proceedings of a Meeting held on 7-10 October 2014 in Byurakan, Armenia. Yerevan, Arm. National Acad. Sci. "Gitutyun" Publ. House, 460 p. (Arm)
- Harutyunian H. A., Nikoghosyan E. H., Melikian N. D., et al. 2017, ComBAO, 64, 116
- Hayes M., Östlin G., Mas-Hesse J. M., Kunth D., Leitherer C., Petrosian A., 2005, A&A, 438, 71
- Hovhannisyan L. R., Mickaelian A. M., Weedman D. W., Le Flo'ch E., Houck J. R., Soifer B. T., Brand K., Dey A., Jannuzi B. T., 2009, AJ, 138, 251
- Kunth D., Atek H., Östlin G., Hayes M., Mas-Hesse M., Leitherer C., Petrosian A., Schaerer D., 2010, ASSP, 15, 203
- Mas-Hesse J. M., Kunth D., Atek H., Östlin G., Leitherer C., Petrosian A., Schaerer D., 2009, Ap&SS, 320, 35
- Massaro E., Mickaelian A. M., Nesci R., Weedman D., 2008, The Digitized First Byurakan Survey (book)
- Mickaelian A. M., 2006, RoAJ, 165, 23
- Mickaelian A. M., 2007, HiA, 14, 594
- Mickaelian A. M., Grigoryan A. E., 2015, RASCS Conference, p. 148
- Mickaelian A. M., Sargsyan L. A., Mikayelyan G. A., Erastova L. K., Sinamian P. K., 2006, Virtual Observatory: Plate Content Digitization, Archive Mining and Image Sequence Processing, Proc. of iAstro workshop, Sofia, Bulgaria, 2005, p. 82
- Mickaelian A. M., Nesci R., Rossi C., Weedman D., Cirimele G., Sargsyan L. A., Erastova L. K., Gigoyan K. S., Mikayelyan G. A., Massaro E., Gaudenzi S., Houck J., Barry D., D'Amante L., Germano P., 2007, A&A, 464, 1177
- Mickaelian A. M., Malkov O. Y., Samus N. N., (Eds.) 2012, 50 years of Cosmic Era: Real and Virtual Studies of the Sky; Proceedings of the Conference of Young Scientists of CIS Countries held on 21-25 Nov 2011 in Yerevan, Armenia. Yerevan, "EditPrint" Publishing House, 252 p. (Rus, Eng)
- Mickaelian A. M., Sarkissian A., Berthier J., Meftah M., Thuillot W., Vachier F., 2019, Icarus, 330, 5
- Nikoghosyan E. H., 2017, ComBAO, 64, 126

- Sagan C., 1973, Communication with Extraterrestrial Intelligence (CETI); Proc. International Conference held in Byurakan on September 6-11, 1971, Cambridge
- Sargsyan L., Mickaelian A., Weedman D., Houck J., 2008, ApJ, 683, 114
- Sarkissian A., Arzoumanian E., Mickaelian A. M., Berthier J., Thuillot W., Vachier F., 2012, Proc. Young Scientists Conference, p. 56
- Sarkissian A., Gopala Krishna B., Crichton D. J., Beebe R., Yamamoto Y., Arviset C., Di Capria M. T., Mickaelian A. M., 2016, The International Planetary Data Alliance (IPDA): Overview of the Activities, ASPC, 505, 29S
- Tovmassian H. M., 1965, Extraterrestrial Civilizations; Proc. All-Union Conference held in Byurakan on May 20-23, 1964. Publishing House of the Armenian Academy of Sciences, Yerevan, 152 p. (Rus, Eng)
- Tovmassian H. M., Khojayants Y. M., Krmoyan M. N., Kashin A. L., Zakharian S. Z., Hovhannessian R. K., Mkrtchian M. A., Tovmassian G. H., Huguenin D., Bootov V. V., Romanenko Y. V., Laveikin A. I., Aleksandrov A. P., 1988, AZh, 14, 291
- Tovmassian H. M., Lorenz H., Priebe A., Richter G. M., Schmidt K.-H., Khodjayants Y. M., Krmoyan M. N., Isajanian R. V., Zakharian A. Z., 1991, Astron. Nachr., 312, 281
- Tovmassian H. M., Navarro S. G., Cardona O., 1996, AJ, 111, 306